MONTHLY NOTICES

OF THE

ROYAL ASTRONOMICAL SOCIETY

Vol. 101 No. 5–6

MEETING OF 1941 JUNE 13

Professor S. Chapman, President, in the Chair

The election by the Council of the following Fellows was duly confirmed:—

Clements Markham Colbeck, 38 Glen Drive, Stoke Bishop, Bristol, 9;
George Macfarlan Sisson, M.A., 4 Archbold Terrace, Jesmond, Newcastle-on-Tyne; and
H. E. Krumm, Sonnenschein, Leeuwendal Crescent, Cape Town, S. Africa.

The following candidate was proposed for election as a Fellow of the Society, the name of the proposer from personal knowledge being appended:—

Alan William James Cousins, 27 Exmouth Avenue, Upper Glenwood, Durban, S. Africa (proposed by H. Knox-Shaw).

Thirty-three presents were announced as having been received since the last ordinary meeting.

The President announced that as the Council had not yet succeeded in obtaining a resident porter, it had been resolved to renew the appeal for volunteers to sleep on the premises, in a rota, at least at the week-ends, until such time as a resident porter was appointed. It was hoped to obtain at least six names so that the duty for each would only occur once in three weeks. The President outlined the duties, and emphasised the fact that no actual fire-watching would be required, but that volunteers would only be asked to join the fire-fighting team for the building if an emergency call were received from the roof spotters. Sleeping quarters and an exceptionally strong refuge room were available in the basement.

THEORY OF A POLARISATION EFFECT IN FRAUNHOFER LINES DUE TO OSCILLATOR SCATTERING

H. Zanstra
(Radcliffe Travelling Fellow in Astronomy)

(Received 1941 April 3)

1. *Introduction.*—In dealing with problems of scattering within absorption lines in stellar atmospheres, the simplification is generally introduced that the re-emission occurs evenly in all directions, and, though this is not explicitly stated, that the light emitted is unpolarised. Nevertheless it is realised that this does not, or does not always, correspond to the actual situation. In particular, in the case where the atom behaves like a classical oscillator, the emitted light has the intensity distribution $1 + \cos^2 \phi$, where ϕ is the angle made by it with the direction of incidence. The light scattered in the direction of incidence is then unpolarised, but that scattered perpendicular to this direction is linearly polarised. It is the purpose of the present paper to pursue certain consequences of this assumption that an atom in a stellar atmosphere behaves like a classical oscillator, especially where it might lead to observable effects. By a classical oscillator is meant an electron which is attracted towards a fixed position by a force proportional to the displacement, the factor of proportionality being independent of the direction of the displacement.

If one considers the fact that a few scatterings in succession generally occur in different directions, it would appear that for multiple scattering there is but little difference between oscillator and isotropic scattering. The case of single scattering gives more promise of yielding new results: it is for the first re-emission that considerable anisotropy and polarisation may occur. So it is this mathematically simpler case of faint lines, or the wings of strong lines, that calls for treatment.

Fortunately a method to deal with this case has been devised by Unsöld.* When the absorption in a line, or in a line wing, is small, one may calculate the radiation emerging from a scatterer as if this scatterer were submitted to the radiation of the continuous spectrum outside the line. The intensity within the line then follows in the well-known way by one integration (in our case equation (26)). This principle, originally used for an isotropic scatterer, applies equally well to an oscillator. However, in the latter case one first requires not only the light emitted by the oscillator for the given radiation field, but also its polarisation and directional distribution, and this is done by using a general formula due to Schuster (section 2), involving, for each polarised component, one integration over the angle of incidence.

So much for the method of derivation. Its main result is the prediction of a polarisation effect which comes within the reach of observation. How this effect comes about physically may be seen from the following simple consideration. For the continuous spectrum free from absorption lines there generally are no theoretical reasons for expecting a polarisation of light (see section 4). But consider now a faint absorption line or wing. If it is observed at the centre of the solar disc, there is no polarisation of the light within the line, since there is axial symmetry about the direction of emission, which is normal to the Sun. If it is observed very near the limb, the situation is as follows. In that case the angle made by the line of sight with the normal to the stellar surface is very nearly 90°, which means that only very superficial layers of the Sun come into play, and that the

* A. Unsöld, *Zeitschr. f. Astrophys.*, 4, 339, 1932.

oscillators are exposed to the radiation that is present at the surface of the Sun. If there were no limb darkening, the incident intensity on the scatterer would be constant over a hemisphere, and, on re-emission, there would be no polarisation. Actually, however, the limb darkening means that the radiation incident on the scatterer is more concentrated towards the normal to the solar disc. This produces a polarisation of the scattered light with the electron vibrating parallel to the solar surface. *On the assumption of oscillator scattering, the light within the line observed near the limb should therefore show partial polarisation with the electric vector along the limb, that is with the plane of polarisation perpendicular to the limb.* The effect should increase with the *limb darkening*.

Abbot's observations of limb darkening for the Sun's continuous spectrum may be represented empirically by a linear law for the intensity, $I_0 = \text{const.}\,(1 + \beta \cos\theta)$, if θ is the angle made by the direction of flow with the normal. One seems justified in using this law, provided one does not attach to β a higher accuracy than 10 or 20 per cent.* All our derivations have been made assuming this linear law for the continuous spectrum, and so our results should only be applied in practice with this limitation on the accuracy of β. The polarisation effect can then be predicted likewise with an accuracy of 10 or 20 per cent. This appears good enough for practical purposes, since an eventual observation of it by present means could hardly be done with a higher accuracy.†

On the classical theory every spectral line would be produced by a harmonic oscillator, and hence, if present in absorption in the Sun, should show the polarisation effect. It is quite different for the quantum theory. The type of polarisation for various atoms in the quantum theory was discussed by Öhman ‡ on the basis of Heisenberg's theory for the polarisation and with a view to astrophysical applications. Heisenberg's § treatment is based on the artifice of introducing a magnetic field parallel to the electric light vector of the incident beam. The Zeeman effect for the particular atom and line gives then the intensity and polarisation of each of the components into which the line is split up. From this one may derive the polarisation of the light without magnetic field, where the Zeeman components have merged into one. The Zeeman effect, on the other hand, depends entirely on the inner quantum number j for the initial and final states, and so it is clear that the degree of polarisation of the re-emitted light is determined by these numbers. In particular the combination $j = 0$ and 1 gives 100 per cent. polarisation perpendicular to the incident beam, like the classical oscillator, and $j = \frac{1}{2}$ and $\frac{1}{2}$ gives no polarisation, like the isotropic scatterer. For observations of the Sun, the line λ 4226·73, $4^1S_0 - 4^1P_1$, of neutral calcium, seems the most promising line of the oscillator type for investigating the polarisation effect, and the theoretical prediction for this line is given in fig. 3, to be discussed in sections 3 and 6. On the other hand, lines like the D_1 line of sodium λ 5895·93, $3^2S_{\frac{1}{2}} - 3^2P_{\frac{1}{2}}$, and the K line of Ca^+ presumably act like isotropic scatterers and give no polarisation. The majority of the lines occurring in practice are of a type intermediate between pure oscillator and isotropic scatterer.

Öhman has pointed out that polarisation of light from spectral lines might be expected in comets and high prominences. He did not call attention to the effect we are dealing with, since he did not consider limb darkening. His observation on $H\gamma$ in β Lyræ, ‖ probably the only case of observed polarisation within an absorption line, must have a different explanation from the effect we are considering.

* Compare the crosses and the dots in fig. 2. It seems preferable to use an empirical value rather than a theoretical one, which is generally on the low side. Compare, *e.g.*, Unsöld's Table 25 in *Physik der Sternatmosphären* with our fig. 2.

† A more refined treatment involving what amounts to a non-linear law of darkening might perhaps be carried out by Minnaert's method (M. Minnaert, *Zeitschr. f. Astrophys.*, **12**, 313, 1936), which is equivalent to that of Unsöld, but better adapted to this non-linear case. For the main result, the polarisation effect, this however seems hardly worth while.

‡ Y. Öhman, *M.N.*, **89**, 479, 1929.

§ W. Heisenberg, *Zeitschr. f. Phys.*, **31**, 617, 1925.

‖ Y. Öhman, *Nature*, **134**, 534, 1934.

Schuster's formula for the polarisation and intensity distribution of the light scattered by an oscillator in a given radiation field is given in section 2. By means of it, following Unsöld's method, the intensity within a weak absorption line and the corresponding line depth are derived in section 3 for the Schuster-Schwarzschild model. The derived difference in intensity for the two components of polarisation along and perpendicular to the limb constitutes the polarisation effect. Thus the reader will obtain a fair idea of this effect and its physical background from the first three sections.

The Schuster-Schwarzschild model, though undoubtedly giving the order of the effect, is, however, not a likely one, and for this reason it is desirable to examine other models. One needs then, for substitution in Schuster's formula, the intensity of the continuous spectrum, not only at the solar or stellar surface, but also below it. The required formulæ for this intensity, producing at the surface a linear limb darkening, have not thus far been given explicitly, and they are therefore derived in section 4, after

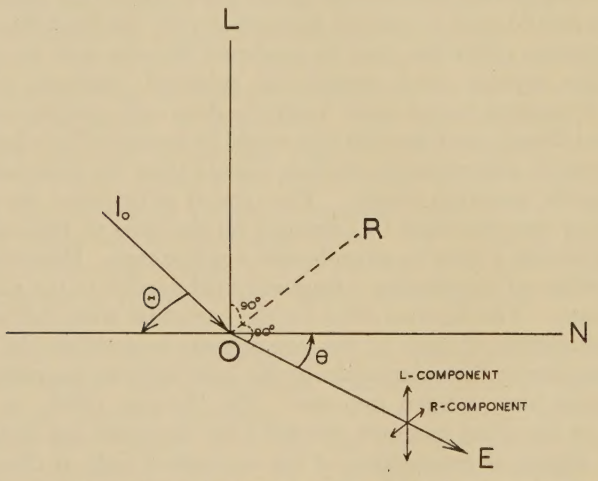

FIG. 1.—*Scattering of incident light of intensity I_0 by an oscillator.*

a brief examination of the production of this continuous spectrum, setting forth more in detail why this spectrum, outside sunspots at any rate, should be unpolarised. The substitution of this intensity into Schuster's formula is made at the end of the section. Unsöld's method is then again applied to the general model in section 5, yielding line depth and polarisation effect. Section 6 deals with the Milne-Eddington model, which is most conveniently derived as a special case of the general model. Since the formulæ are rather complicated, the line depth and polarisation effect for the Milne-Eddington model are represented graphically in fig. 3 as a function of the position on the disc, and for various coefficients of darkening β. Finally, section 7 gives the intensity and corresponding line depth for the light integrated over the disc of a non-rotating star, for each of the three models.

2. *Schuster's Formula.*—In fig. 1, a volume element of the scattering medium is considered to be situated at O. The radiation incident on this volume element is assumed to be unpolarised (see section 4) and to have axial symmetry about the line ON, which therefore, in our case, is the normal to the solar surface. Its intensity, per cm.^{2} per sec. per unit solid angle per frequency unit, is I_0, the suffix o indicating that, to a sufficient approximation, it is that of the continuous spectrum outside the absorption line, according to Unsöld's principle for weak lines or wings. It is a function of both the optical depth for the continuous spectrum τ at O and the angle Θ of the incident direction with the axis. Radiation scattered from the unit of volume in the direction OE has the

intensity ϵ, expressed in the above unit. The vibrations of the light take place perpendicular to the direction of the ray OE, and the two components of polarisation are ϵ_r along OR in the plane EON, and ϵ_l along OL perpendicular to this plane, so that $\epsilon = \epsilon_r + \epsilon_l$. The emergent ray OE makes the angle θ with the axis ON.

The two polarised components of intensity are then given by

$$\epsilon_r = \tfrac{3}{16}\sigma \int_{\Theta=0}^{\pi} I_0(\tau, \Theta)(1+\cos^2\Theta) d(-\cos\Theta), \tag{1}$$

$$\epsilon_l = \tfrac{3}{16}\sigma \int_{\Theta=0}^{\pi} I_0(\tau, \Theta)[(1+\sin^2\theta)+\cos^2\Theta(1-3\sin^2\theta)] d(-\cos\Theta). \tag{2}$$

These are Schuster's formulæ in the form given by Minnaert.* As is customary, the plane of polarisation is that perpendicular to the direction of vibration of the electric light vector. For observations of a certain point on the Sun's disc, it will be seen that ϵ_l represents the component parallel to the limb, and ϵ_r the radial component, which is normal to the limb.† For a narrow beam incident on a cube of side 1 cm. the above formulæ readily yield the result that the fraction σ of the incident energy is scattered over all directions, so that σ represents the scattering coefficient per cm. Since, in general, the point O is within the solar surface, the integration extends over a whole sphere, as the limits show. If O is at the solar surface, the ingoing radiation has intensity zero, and so one may then take $\Theta = 0$ and $\pi/2$ as limits.

3. *Schuster-Schwarzschild Model. Expected Polarisation within Lines.*—In the Schuster-Schwarzschild model the body producing the continuous spectrum is surrounded by the atmosphere in which the line scattering takes place. Throughout the scattering atmosphere the intensity I_0 of the continuous spectrum outside the spectral line is the same as at the surface of this body, viz. at $\tau = 0$. For this intensity the linear approximation in $\cos\theta$ will be used

$$I_0(0, \theta) = I_c \frac{1+\beta\cos\theta}{1+\beta} = \mathcal{J}(0)(1+\beta\cos\theta). \tag{3}$$

In this expression, the coefficient of darkening β is a constant for a given λ. For the other constant, either I_c, the central intensity, for which $\theta = 0$, or $\mathcal{J}(0)$, the intensity at the limb, where $\theta = \pi/2$, may be used, the notation for the latter quantity being in conformity with section 4.

Fig. 2 represents β as a function of λ, as obtained from Abbot's observations of limb darkening for the Sun.‡ The crosses are obtained from the observed ratios of intensity at $\cos\theta = 1$ and 0·312, through which the curve is drawn. The accuracy of the linear approximation is about 10 or 20 per cent. in the value of β, as may be judged from the dots in the figure, which represent the values of β following from the intensity ratios at $\cos\theta = 1$ and 0·661.

The angle with the normal has been designated by θ if the radiation is emerging, and by Θ if the radiation is considered incident, so that when (3) represents the incident radiation on the volume element of the scattering atmosphere, one should replace θ by Θ. The value for $I_0(0, \Theta)$ from (3) is substituted in (1) and (2) and the integration carried out, using 0 and $\pi/2$ for integration limits, the I_0 being zero for the other hemisphere. This

* A. Schuster, *M.N.*, **40**, 35, 1879; M. Minnaert, *Zeitschr. f. Astrophys.*, **1**, 209, 1930, equation (2). The two papers deal with the solar corona. The former contains a number of slips, although none of a fundamental nature, which were corrected by Minnaert.

† Instead of the plane of polarisation, one may also use the plane of vibration of the electric light vector, which is perpendicular to it. This is done by Minnaert, and his tangential component g_t is therefore our radial component ϵ_r, whereas his radial component g_r is our tangential component ϵ_l. His ω is our Θ and his χ our θ.

‡ From A. Unsöld, *Physik der Sternatmosphären* (Springer, 1938), p. 34, Table 3.

yields for the intensities of the two polarised components emitted per unit volume in the direction θ:

$$\epsilon_r = \tfrac{1}{2}\mathcal{J}(0)\sigma(\tfrac{1}{2} + \tfrac{9}{32}\beta), \tag{4}$$

$$\epsilon_l = \tfrac{1}{2}\mathcal{J}(0)\sigma(\tfrac{1}{2} + \tfrac{9}{32}\beta - \tfrac{3}{32}\beta \sin^2\theta), \tag{5}$$

holding for any point in the scattering atmosphere.

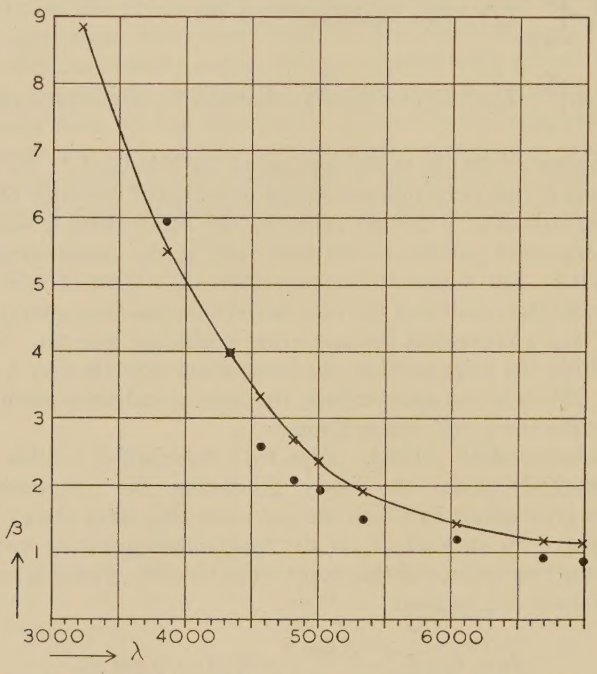

FIG. 2.—*The coefficient of darkening β for the Sun as a function of the wave-length (Abbott). Crosses from cos θ = 1 and 0·312. Dots from cos θ = 1 and 0·661.*

Outside the spectral line, the radiation emerging from the atmosphere is that of the unpolarised (see section 4) continuous spectrum (3), whose two polarised components are

$$I_{0r} = I_{0l} = \tfrac{1}{2}I_0(0, \theta) = \tfrac{1}{2}\mathcal{J}(0)(1 + \beta\cos\theta). \tag{6}$$

The scattering atmosphere of height h has a total optical depth s_1. At a point x, measured inwardly, the optical depth is s. These two quantities are defined by

$$s_1 = \int_{\xi=0}^{h} \sigma d\xi, \qquad s = \int_{\xi=0}^{x} \sigma d\xi. \tag{7}$$

Inside the line the r component of emerging radiation is

$$I_r = I_{0r}e^{-s_1\sec\theta} + \int_{x=0}^{h} \epsilon_r e^{-s_1\sec\theta} dx \sec\theta, \tag{8}$$

and the l component I_l is given by the same expression, replacing r by l.

Since both ϵ_r (4) and ϵ_l (5) are independent of x, equation (8) reduces to

$$I_r = I_{0r}\left[e^{-s_1\sec\theta} + \frac{\epsilon_r}{\sigma I_{0r}}(1 - e^{-s_1\sec\theta})\right], \tag{9}$$

and the corresponding expression for I_l, replacing r by l. In this, (7) has been made use of in the form $ds = \sigma dx$.

Substituting (4) and (5) in (9), and using (6), we obtain the desired expressions for I_r and I_l, or the corresponding expressions for the two components of the depth of the line:

$$D_r = \frac{I_{0r} - I_r}{I_{0r}} = (1 - e^{-s_1 \sec\theta}) \left[1 - \frac{\frac{1}{2} + \frac{9}{32}\beta}{1 + \beta \cos\theta} \right], \tag{10}$$

$$D_l = \frac{I_{0l} - I_l}{I_{0l}} = (1 - e^{-s_1 \sec\theta}) \left[1 - \frac{\frac{1}{2} + \frac{9}{32}\beta - \frac{3}{32}\beta \sin^2\theta}{1 + \beta \cos\theta} \right]. \tag{11}$$

This result only holds for *weak lines* or *wings*, by which is meant that the intensity of incident radiation is sufficiently close to I_0, which *condition* is satisfied if $s_1 << 1$. When approaching the limb, sec θ becomes indefinitely large, and for this reason no limitation

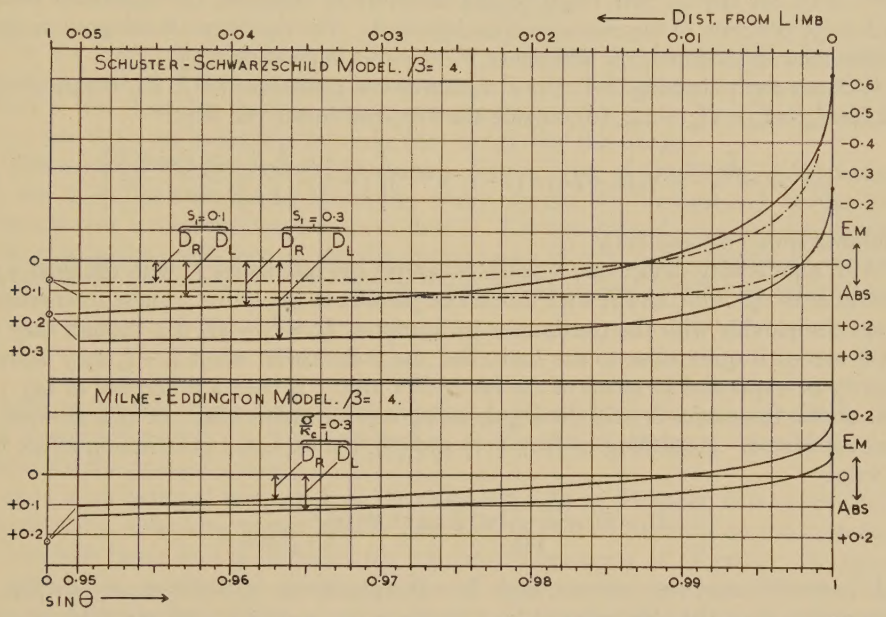

FIG. 3.—*The two polarised components D_l and D_r (planes of polarisation parallel to and perpendicular to the limb) as functions of the distance from the limb expected for the line λ 4227 of calcium on the Sun. For the S.-S. Model, s_1 is the vertical optical depth. For the M.-E. Model, σ/κ_e is the ratio of scattering coefficient to the general coefficient of continuous absorption.*

has been imposed on the order of s_1 sec θ in the previous derivation. Nearer the centre, however, sec θ is of order unity, and then the formulæ are simplified by putting $1 - e^{-s_1 \sec\theta} \simeq s_1 \sec\theta$. At the limb itself this quantity becomes unity, so that there the values of D_r and D_l are independent of s_1.

Fig. 3 gives an application of these formulæ. In the introduction it has been seen that the line λ 4227 of neutral calcium is of the oscillator type and appears to be most promising for investigating the polarisation effect in the Sun. From fig. 2 follows a value of β of somewhat more than 4 for this wave-length region in the Sun. The value $\beta = 4$, substituted in (10) and (11), should therefore give the expected line depths taken with a polarising device perpendicular to or along the limb. This is done for two points of the line wing corresponding to $s_1 = 0{\cdot}1$ and $0{\cdot}3$. For $s_1 = 0{\cdot}3$ the approximation becomes a little doubtful, but yet one should get a reasonable estimate of the effect (the terms left out are of order $s_1^2 \simeq 0{\cdot}1$ as compared with the terms considered of order $s_1 = 0{\cdot}3$). The result is shown in the upper portion of fig. 3 (Schuster-Schwarzschild Model, $\beta = 4$), where the quantities D_r and D_l, indicated by the double pointed arrows,

are plotted against $\sin\theta$ for the range $\sin\theta = 0{\cdot}95$ to 1 (lower scale), the chain lines referring to $s_1 = 0{\cdot}1$, and the full drawn lines to $s_1 = 0{\cdot}3$. The corresponding range in the distance from the limb $1 - \sin\theta$ is from 0 to 5 per cent. of the solar radius (upper scale), which is the region presumably of importance for observation. The values of $D_r = D_l$ have also been given for the centre of the disc, $\sin\theta = 0$, by the circles to the left.

If one selects a point of depth $D_r = D_l = 0{\cdot}17$ on the contour observed at the centre of the disc, the vertical optical depth for this wave-length should be $s_1 = 0{\cdot}3$, and at 2 per cent. from the limb, a point which can be reached in practice, one should have $D_r = 0{\cdot}07$ and $D_l = 0{\cdot}23$, as is read from the full drawn curves. One expects therefore in this case a difference of the two polarised components amounting to 16 per cent. of the continuous background, which should be easy to measure. At the limb itself, $D_r = -0{\cdot}62$, and $D_l = -0{\cdot}25$, for any s_1, both negative and therefore in emission, the difference being as much as 37 per cent. of the continuous background. For the Milne-Eddington model, to be discussed in section 6, the difference is, however, a good deal less.

Without any polarising device one measures the intensities $I = I_r + I_l$ within the line, and $I_0 = I_{0r} + I_{0l} = 2I_{0r} = 2I_{0l}$ (6) outside the line, and hence the depth

$$D = \frac{I_0 - I}{I_0} = \tfrac{1}{2}(D_r + D_l) = (1 - e^{-s_1 \sec\theta})\left[1 - \frac{\frac{1}{2} + \frac{9}{3\,2}\beta - \frac{3}{6\,4}\beta\sin^2\theta}{1 + \beta\cos\theta}\right], \tag{12}$$

as follows from (10) and (11).

With a polarising device one actually measures the intensities I_r with the device perpendicular to the limb, and I_l with the device parallel to the limb. These intensities are always comparable with the continuous background, $I_{0r} = I_{0l} = \frac{1}{2}I_0$ (6), though they may rather exceed it quite close to the limb, and the polarisation effect $I_r - I_l$ may therefore properly be expressed in terms of the latter as a unit. If then a difference of say 3 per cent. of the intensities is still distinguishable, a polarisation effect of this amount can also be detected. According to (10), (11) and (6), the expected polarisation effect * has the value

$$D_l - D_r = \frac{I_r - I_l}{\frac{1}{2}I_0} = (1 - e^{-s_1 \sec\theta})\frac{\frac{3}{3\,2}\beta\sin^2\theta}{1 + \beta\cos\theta}. \tag{13}$$

It is seen that at the extreme limb $D_l - D_r$ approaches $\frac{3}{3\,2}\beta$ for any s_1, so that, for instance, for $\beta = 4$ the effect should be 37·5 per cent., agreeing with the value obtained above from fig. 2. At 2 per cent. from the limb, $\sin\theta = 0{\cdot}98$, and then (13) yields an effect of 15·6 per cent., likewise in agreement with fig. 2.

In order to examine how far processes of true absorption within the line can play a part, the Schuster-Schwarzschild model for scattering and true absorption will now be considered. Let the true scattering coefficient be σ', the true absorption coefficient κ. The sum is our old scattering coefficient, as, for instance, might be calculated from the wave mechanics, and which we continue to denote by σ. Putting $\kappa = f\sigma$, we have

$$\sigma = \sigma' + \kappa, \qquad \kappa = f\sigma, \qquad \sigma' = (1 - f)\sigma. \tag{14}$$

In the formulæ subsequent to (15), f will be assumed constant.

For the present purpose local thermodynamical equilibrium is assumed (the assumption in section 4 is somewhat more general). The re-emission per unit volume subsequent on true absorption has then the intensity $\mathcal{J}(0)f\sigma$, by Kirchhoff's Law, where $\mathcal{J}(0)$ is the intensity of black-body radiation at $\tau = 0$, which is also the intensity of the continuous spectrum at the limb. It is unpolarised, so that each polarised component is $\frac{1}{2}\mathcal{J}(0)f\sigma$. The re-emission due to true scattering is obtained by replacing σ by σ' in (4) and (5), and is therefore $(1 - f)\epsilon_r$ and $(1 - f)\epsilon_l$. In equations (8) and (9) for I_r, the quantity ϵ_r

* This is not the degree of polarisation. The latter is $(I_r - I_l)/(I_r + I_l)$, or about one-half of what we call the polarisation effect.

should therefore now be replaced by

$$\tfrac{1}{2}\mathcal{J}(0)f\sigma+(1-f)\epsilon_r, \tag{15}$$

where ϵ_r has the value (4).

Doing this, one obtains, instead of (10),

$$D_r=(1-e^{-s_1\sec\theta})\left[1-\frac{f}{1+\beta\cos\theta}-(1-f)\frac{\frac{1}{2}+\frac{9}{3\,2}\beta}{1+\beta\cos\theta}\right]. \tag{16}$$

Equation (11) for D_l is correspondingly modified, and the difference constitutes the expected polarisation effect

$$D_l-D_r=(1-e^{-s_1\sec\theta})\frac{\frac{3}{3\,2}\beta\sin^2\theta}{1+\beta\cos\theta}(1-f). \tag{17}$$

From the observed intensities of the centres of various Fraunhofer lines it follows that κ/σ, or f, rarely if ever exceeds the value 0·06.* So the influence of absorption on the effect is less than this fraction, if one compares (13) with (17). Practically one can therefore use the pure scattering formulæ (10) to (13) for the wings.

4. *Discussion of the Continuous Spectrum. Linear Law of Darkening. Expressions for* ϵ_l *and* ϵ_r.—The continuous spectrum, which forms the background of the line spectrum, is now to be considered more in detail. Let this general continuous spectrum have the absorption coefficient κ_c, the absorption being distributed continuously over all depths below the photosphere. The optical depth of this general continuous spectrum is

$$\tau=\int_{\xi=0}^{x}\kappa_c d\xi. \tag{18}$$

In addition to this, there might be the optical depth of the continuous spectrum due to true absorption within the line, referred to at the end of section 3, but this is not considered in the present section.

If there is an external field, such as the magnetic field in sunspots, it is conceivable that, statistically, absorbing atoms may be oriented, so that κ_c depends on the direction of the incident beam and is different for the two components of vibration, the latter factor introducing polarisation in the continuous spectrum let through. We have no evidence at present that outside sunspots there is any important field orientating the atoms. The radiation has a preferential direction (limb darkening) but it does not appear likely that this could orientate the atoms to an appreciable extent, the more so since collisions between atoms, ions and electrons make for arbitrary orientation. Outside sunspots therefore the κ_c should be the same for any direction of incidence and any component of vibration, and processes of absorption should not introduce any polarisation.

Now consider the emission of the continuous spectrum by a volume element. According to present views, this mainly occurs by capture of electrons by ions or atoms (Wildt), and to a less extent by electron switches.† At a temperature of 5000°, the effective area of capture of an electron by a proton is of the order 10^{-20} cm.^{2}, according to Kramers, and that by a hydrogen atom of the order 10^{-22} cm.^{2}, according to Jen ‡ or Massey. § The effective area for an elastic collision of an electron with a proton or another electron giving a large deflection is of order 10^{-13} cm.^{2} for this temperature, that is a factor 10^7 or 10^9 higher than the capture areas. Even allowing for the fact that the concentrations of neutral atoms may be a few powers of ten higher than that of electrons, one may safely

* A. Unsöld, *Phys. d. Sternatm.*, pp. 244, 308, 309. Strictly speaking, this statement applies to the Milne-Eddington model.

† An exception should be made for very high stellar temperatures, around 20,000°, where electron scattering begins to play a part, which should introduce some polarisation in the continuous spectrum.

‡ K. C. Jen, *Phys. Rev.*, 43, 540, 1933, fig. 2. § *Cf.* R. Wildt, *Ap. J.*, 90, 612, 1939.

conclude that an electron in the Sun suffers many elastic collisions before it is captured. This will destroy any preferential orientation of velocities the electrons might show just after being freed photo-electrically; in fact, on account of the many elastic collisions, one may be confident that the distribution of electron velocities is Maxwellian.* Accordingly the light due to these spontaneous captures should be emitted evenly in all directions and be unpolarised. The forced captures, on the other hand, are presumably not very important at solar temperature, but since they behave like negative absorptions, they might be taken into account completely by slightly diminishing the κ_c in (18). To us it is most important that, because of the arbitrary orientation of electron velocities, such a negative absorption, just like the positive absorption discussed above, does not give rise to a polarisation of the continuous spectrum outside sunspots. Thus neither the original emission nor the absorption introduces polarisation, and the continuous spectrum in the absence of a magnetic field should be unpolarised. Nevertheless it would seem wise to eliminate a possible polarisation of the continuous spectrum by always comparing the intensity in the wing with that immediately outside in each polarised component, and this actually is done if the depths D_r and D_l are observed.

The energy of the continuous spectrum emitted per second per frequency unit per unit solid angle by the unit of volume will be denoted by $\kappa_c \mathcal{J}(\tau)$ †, and from the above considerations it follows that this quantity, as well as κ_c and $\mathcal{J}(\tau)$ by themselves, should be independent of direction.

The outgoing radiation of the continuous spectrum is then, at any τ (18), given by

$$I_0(\tau, \theta) = \int_{\tau_1=\tau}^{\infty} \mathcal{J}(\tau_1) e^{-(\tau_1-\tau)\sec\theta} d\tau_1 \sec\theta, \qquad 0 \leqslant \theta \leqslant \frac{\pi}{2}, \qquad (19)$$

and the ingoing radiation by

$$I_0(\tau, \theta) = -\int_{\tau_1=0}^{\tau} \mathcal{J}(\tau_1) e^{-(\tau_1-\tau)\sec\theta} d\tau_1 \sec\theta, \qquad \frac{\pi}{2} \leqslant \theta \leqslant \pi. \qquad (20)$$

As in section 3, the linear law of darkening is assumed

$$I_0(0, \theta) = \mathcal{J}(0)(1 + \beta \cos\theta), \qquad (3)$$

as a fair representation of the observed continuous spectrum.

From this law and (19) follows

$$\mathcal{J}(\tau) = \mathcal{J}(0)(1 + \beta\tau). \qquad (21)$$

In fact, (21) and (19) lead to (3), and since there is only one solution $\mathcal{J}(\tau)$ for any assigned $I_0(0, \theta)$, as Plaskett has shown in a simple way ‡, expression (21) represents this solution.

Substituting (21) in (19) and (20), one obtains, for the out- and ingoing radiations

$$I_0(\tau, \theta) = \mathcal{J}(0)(1 + \beta \cos\theta + \beta\tau), \qquad 0 \leqslant \theta \leqslant \frac{\pi}{2}, \qquad (22)$$

$$I_0(\tau, \theta) = \mathcal{J}(0)\{1 + \beta \cos\theta + \beta\tau - e^{+\tau\sec\theta}(1 + \beta\cos\theta)\}, \qquad \frac{\pi}{2} \leqslant \theta \leqslant \pi, \qquad (23)$$

* The above orders of magnitude apply likewise to nebulæ and show that the distribution of electron velocities must be Maxwellian, assuming capture according to Kramers and elastic collision by Coulomb's Law.

† This is meant as the definition of $\mathcal{J}(\tau)$, and so the special assumption of local thermodynamic equilibrium has not been made. By emission is meant the spontaneous emission, whereas the forced emissions are properly looked upon as negative absorptions, also included in the κ_c. In practice we can probably confine ourselves to positive absorptions for κ_c, and make the assumption of local thermodynamic equilibrium with local temperature equal to the electron temperature, and then $\mathcal{J}(\tau)$ is the intensity of black-body radiation for this temperature. This, however, is not done in the text.

‡ H. H. Plaskett, *M.N.*, **96**, 418–420, 1936; *Comm. Univ. Obs. Oxford*, No. 6.

as rigorous consequences of the assumptions made. In particular, the ingoing radiation (23) vanishes at $\tau = 0$ for any θ.

The formula (23) for the inward I_0 is rather complicated. To use a simpler approximate form, however, would not be advisable: the polarisation effect is very sensitive to the distribution of I_0 as a function of θ, and a simplification might make its calculation entirely untrustworthy.

The light scattered in the wings of a line now follows by first replacing θ by Θ in (22) and (23), and then substituting these expressions for the incident $I_0(\tau, \Theta)$ in the Schuster formulæ (1) and (2), using (22) for the portion of the integral from $\Theta = 0$ to $\pi/2$, and (23) for the portion from $\pi/2$ to π. The two components of emission within the line for any τ thus become

$$\epsilon_l = \tfrac{1}{2}\sigma\mathcal{J}(0)(1+\beta\tau) - \tfrac{3}{16}\sigma\mathcal{J}(0)(1+\sin^2\theta)(K_2 - \beta K_3) - \tfrac{3}{16}\sigma\mathcal{J}(0)(1-3\sin^2\theta)(K_4 - \beta K_5), \quad (24)$$

where

$$K_n = K_n(\tau) = \int_{w=+1}^{\infty} \frac{e^{-\tau w}}{w^n} dw \quad (24a)$$

and

$$\epsilon_r = \text{the same without the } \sin^2\theta \text{ terms.} \quad (25)$$

The portion involving the integrals K_n is entirely due to the $e^{+\tau \sec\Theta}$ term of the ingoing radiation (23), whereas $\sec\Theta$ has been replaced by the variable of integration w.

5. *Expected Polarisation within Lines for General Model with* $\sigma << \kappa_c$.—With the assumptions of the preceding section, the radiation emerging at the surface, $\tau = 0$, at any angle θ, has the components

$$I_{0l} = I_{0r} = \tfrac{1}{2}\mathcal{J}(0)(1+\beta\cos\theta) \quad (6)$$

outside the spectral line.

Let a spectral line be due to pure scattering. The emission of the unit volume, per second per frequency unit per unit solid angle, due to scattering, is then $\epsilon_r + \epsilon_l$, and its two components are ϵ_r (25) and ϵ_l (24). To this should be added the emission of the general continuous spectrum which is $\kappa_c\mathcal{J}(\tau)$, whereas its two components are $\tfrac{1}{2}\kappa_c\mathcal{J}(\tau)$ each, since this emission is unpolarised (section 4).

The radiation within the line wing emerging from the solar or stellar surface has therefore the l component

$$I_l = \int_{x=0}^{\infty} (\tfrac{1}{2}\kappa_c\mathcal{J}(\tau) + \epsilon_l) e^{-u\sec\theta} dx \sec\theta, \quad (26)$$

where

$$u = \int_{\xi=0}^{x} (\kappa_c + \sigma) d\xi, \quad (26a)$$

and $\mathcal{J}(\tau)$ and ϵ_l stand for the expressions (21) and (24).

The r component I_r is obtained by replacing l by r, and then ϵ_r stands for (25).

If $\sigma << \kappa_c$, the intensity is always close to that of the continuous background, and we certainly are dealing with wings or weak lines.* We shall make this assumption, and therefore retain only first order terms in σ/κ_c. Then (26*a*) leads to

$$\left.\begin{aligned} d\tau = \kappa_c dx = \frac{\kappa_c}{\kappa_c + \sigma} du = \left(1 - \frac{\sigma}{\kappa_c}\right) du, \\ ds = \sigma dx = \frac{\sigma}{\kappa_c + \sigma} du = \frac{\sigma}{\kappa_c} du. \end{aligned}\right\} \quad (27)$$

* Not *vice versa*! In the Schuster-Schwarzschild model, $\kappa_c = 0$ in the atmosphere, so that $\sigma >> \kappa_c$, yet we are in the wings if $s_1 << 1$. For this reason, and also since $s_1 \sec\theta \to \infty$ at the limb, we have treated this case separately in section 3.

The expression (26) for I_l, with the substitutions mentioned, then reduces to *

$$\frac{I_l}{\frac{1}{2}\mathcal{J}(0)} = 1 + \beta\cos\theta - \int_{u=0}^{\infty} [\beta\cos\theta + \tfrac{3}{8}(1+\sin^2\theta)(K_2 - \beta K_3) + \tfrac{3}{8}(1 - 3\sin^2\theta)(K_4 - \beta K_5)]\frac{\sigma}{\kappa_c} e^{-u\sec\theta} du \sec\theta, \quad (28)$$

and

$$\frac{I_r}{\frac{1}{2}\mathcal{J}(0)} = \text{the same without the } \sin^2\theta \text{ terms.} \quad (29)$$

The quantities K_n under the integral sign are functions of τ by (24*a*), and so it is better to change over from u to τ for the variable of integration. By (27), $du = (1+\sigma/\kappa_c)d\tau$, where σ/κ_c is small of the first order, so that we may likewise put $u = (1+\Delta)\tau$ where Δ is of the first order, and so changing over from u and du to τ and $d\tau$ only introduces quantities of the second order in (28). We therefore may replace u by τ under the integral sign, and have $\tau = 0$ and ∞ as integration limits.

From (28), (29) and (6) one easily obtains, as in section 3, the two components of the depth of the line

$$D_l = \frac{I_{0l} - I_l}{I_{0l}} = (1+\beta\cos\theta)^{-1}\int_{\tau=0}^{\infty} [\beta\cos\theta + \tfrac{3}{8}(1+\sin^2\theta)(K_2 - \beta K_3) + \tfrac{3}{8}(1 - 3\sin^2\theta)(K_4 - \beta K_5)]\frac{\sigma}{\kappa_c} e^{-\tau\sec\theta} d\tau \sec\theta, \quad (30)$$

and

$$D_r = \text{the same without the } \sin^2\theta \text{ terms,} \quad (31)$$

where now u has been replaced by τ for the reason just given. The difference $D_l - D_r$ constitutes the polarisation effect. (See section 3.)

In this general model, σ/κ_c may be any assigned function of τ, and the integral of (30) or (31) evaluated by quadrature for any $\cos\theta$. This integral is of the form $P + Q\beta$, and if one wishes to obtain it for various β, it suffices to determine P and Q each by one quadrature.

Since $(\sigma/\kappa_c)d\tau = ds$, the expressions for the depths are of Unsöld's type † $D = \int_{\tau=0}^{\infty} g_2(\tau, \theta)ds$, but our weight $g_2(\tau, \theta)$ for the oscillator is naturally more complicated than Unsöld's expression (44) for isotropic scattering.

The foregoing are all formulæ for the case of pure scattering in the line. If, on the other hand, we have the case of pure absorption in the line, with absorption coefficient σ, we have $\epsilon = \sigma\mathcal{J}(\tau) = 2\epsilon_l = 2\epsilon_r$, and the intensity is given by formula (29*a*) in the footnote to (28). Then we may use all the above formulæ (28) to (31) with the K_n terms left out, and the depth from (30) and (31) is of the Unsöld type $D = D_l + D_r = \int_{\tau=0}^{\infty} g_1(\tau, \theta)d\tau_\nu$, with τ_ν the optical depth of line absorption, and $g_1 = \beta e^{-\tau\sec\theta}$, the same as Unsöld's expression (44), with his $\eta = 1$.

For an absorption coefficient $f\sigma$ and scattering coefficient $(1-f)\sigma$ (see section 3), we

* It is easiest to evaluate first the expression without the K_n terms. This part of I_l is, since $\tau = u - s$:

$$\int_{x=0}^{\infty} \tfrac{1}{2}(\kappa_c + \sigma)\mathcal{J}(0)(1+\beta\tau)e^{-u\sec\theta} dx \sec\theta = \tfrac{1}{2}\mathcal{J}(0)\left\{1 + \beta\cos\theta - \beta\int_{u=0}^{\infty} se^{-u\sec\theta} du \sec\theta\right\} = \tfrac{1}{2}\mathcal{J}(0)\left\{1 + \beta\cos\theta - \beta\int_{u=0}^{\infty} \frac{\sigma}{\kappa_c} e^{-u\sec\theta} du\right\}, \quad (29a)$$

in which we have changed over to ds by partial integration, and then put $ds = (\sigma/\kappa_c)du$ (27).

Incidentally it may be remarked that this is also the expression for I_l or I_r for the case of true absorption in the line: $\epsilon_l = \epsilon_r = \frac{1}{2}\sigma\mathcal{J}(\tau)$.

† A. Unsöld, *Zeitschr. f. Astrophys.*, 4, 339, 1932.

can use the above formulæ, merely multiplying the K_n portion by $1-f$. We have seen that in practice $f < 0{\cdot}06$, so that one can practically always leave out absorption influences and use the pure scattering formulæ (28) to (31).

6. *Milne-Eddington Model. Expected Polarisation within Lines.*—For the Milne-Eddington Model, σ/κ_c is independent of τ.* This quantity can then be put before the integral sign in the formulæ of the previous section. Carrying out the integration offers no difficulties. The integrals involving K_n can be found by reversing the order of integration.†

E.g., putting $\sec\theta = a$ and using (24*a*):

$$\int_{\tau=0}^{\infty} K_5 e^{-\tau a} d\tau a = \int_{w=+1}^{\infty} \frac{dw}{w^5} \int_{\tau=0}^{\infty} e^{-\tau(w+a)} d\tau a = \int_{w=+1}^{\infty} \frac{a\,dw}{w^5(w+a)}$$

$$= \int_{w=+1}^{\infty} \left[\frac{1}{w^5} - \frac{1}{a}\frac{1}{w^4} + \frac{1}{a^2}\frac{1}{w^3} - \frac{1}{a^3}\frac{1}{w^2} + \frac{1}{a^4}\left(\frac{1}{w} - \frac{1}{w+a}\right) \right] dw$$

$$= \tfrac{1}{4} - \tfrac{1}{3}\cos\theta + \tfrac{1}{2}\cos^2\theta - \tfrac{1}{1}\cos^3\theta + \cos^4\theta \ln(1+\sec\theta). \qquad (32)$$

In general, for K_n the expression starts with $+1/(n-1)$, and then the sign alternates, so that the ln term has positive sign if n is odd, and negative sign if n is even.

Carrying out the integration for D_r (31), that is (30) without the $\sin^2\theta$ terms, we obtain for the r component of the depth:

$$D_r = \tfrac{3}{8}\frac{\sigma}{\kappa_c}\left[\frac{+\frac{4}{3} - \frac{3}{4}\beta + 4\beta\cos\theta}{1+\beta\cos\theta} - \tfrac{1}{2}\cos\theta + \cos^2\theta - (\cos\theta + \cos^3\theta)\ln(1+\sec\theta) \right]. \qquad (33)$$

The difference between D_l (30) and D_r (31) is the $\sin^2\theta$ terms of (30), and, after integration, we thus obtain for the polarisation effect as defined in section 3:

$$D_l - D_r = \tfrac{3}{8}\frac{\sigma}{\kappa_c}\sin^2\theta\left[\frac{+\frac{1}{4}\beta}{1+\beta\cos\theta} + \tfrac{3}{2}\cos\theta - 3\cos^2\theta - (\cos\theta - 3\cos^3\theta)\ln(1+\sec\theta) \right], \qquad (34)$$

whereas the l component itself

$$D_l = \text{sum of (33) and (34)}. \qquad (35)$$

The depth without polarising device $D = \frac{1}{2}(D_l + D_r) = D_r + \frac{1}{2}(D_l - D_r)$ follows from (33) and (34):

$$D = \tfrac{3}{8}\frac{\sigma}{\kappa_c}\left[\frac{+\frac{4}{3} + \beta(-\frac{5}{8} + 4\cos\theta - \frac{1}{8}\cos^2\theta)}{1+\beta\cos\theta} + \tfrac{1}{4}\cos\theta - \tfrac{1}{2}\cos^2\theta - \tfrac{3}{4}\cos^3\theta + \tfrac{3}{2}\cos^4\theta \right.$$
$$\left. - (\tfrac{3}{2}\cos\theta - \cos^3\theta + \tfrac{3}{2}\cos^5\theta)\ln(1+\sec\theta) \right], \qquad (36)$$

In the lower part of fig. 3 the depths D_r and D_l for the components of polarisation perpendicular to and along the limb, computed from (33) and (35), have been plotted against $\sin\theta$ for $\sigma/\kappa_c = 0{\cdot}3$ and $\beta = 4$, which is approximately that for λ 4227 of neutral calcium on the Sun. The range plotted is $\sin\theta = 0{\cdot}95$ to 1 (lower scale), or distance from the limb 0 to 0·05 (upper scale), but on the left the depth is also given for the centre: $D_r = D_l = 0{\cdot}22$. At the limb, $D_r = -0{\cdot}19$ and $D_l = -0{\cdot}07$, so that the polarisation effect expected is 11 per cent., being the vertical distance between the two lines. At a distance of 2 per cent. from the limb the effect has gone down to 5 per cent., and 5 per cent. from

* The formulæ of the preceding section presuppose both that I is close to I_0, viz. $D \ll 1$, and $\sigma/\kappa_c \ll 1$. Fig. 4, to be discussed in the next section, shows that $D/(\sigma/\kappa_c)$ is always of the order unity, so that the second condition follows from the first, and it is sufficient to assume that I is close to I_0.

† The simpler case of isotropic scattering, involving K_2 and K_3, which Unsöld did by quadrature, can also be solved in the above way, if this be desired.

the limb to 3 per cent. Since D_r and D_l are proportional to σ/κ_c, the curves for $\sigma/\kappa_c = 0{\cdot}1$ would have ordinates one third of those actually drawn for $\sigma/\kappa_c = 0{\cdot}3$, and the polarisation effect is also divided by 3. Though the effect is much smaller than for the Schuster-

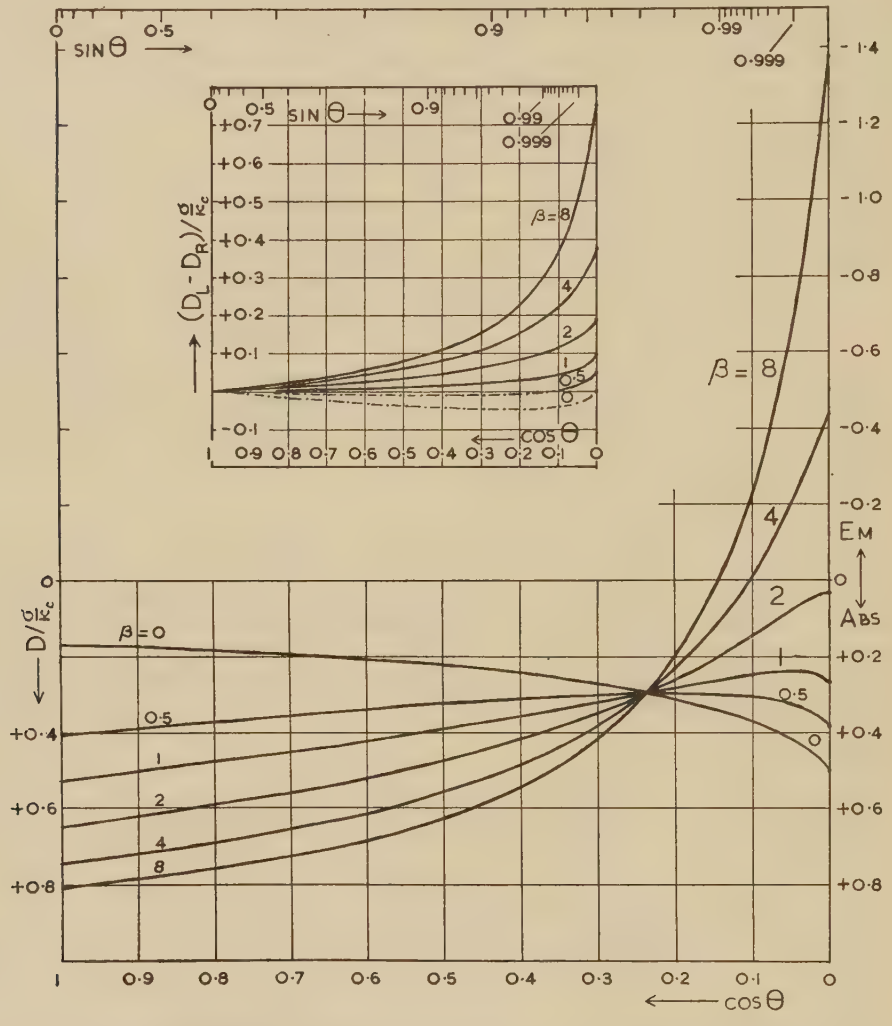

FIG. 4.—*Milne-Eddington Model. For any point on the Sun's disc and any β, the quantity $D/(\sigma/\kappa_c)$ is read off from the large figure, and, after multiplication with σ/κ_c, yields the line depth D without polarising device. Similarly, the small inserted figure yields the polarisation effect $D_l - D_r$.*

Schwarzschild model given in the upper portion of the figure, yet it ought to be quite measurable.

The result of the above formulæ for the limb itself, $\cos\theta = 0$, is quite simple:

$$D_r = \frac{\sigma}{\kappa_c}\left(\tfrac{1}{2} - \tfrac{9}{3\,2}\beta\right), \qquad D_l = \frac{\sigma}{\kappa_c}\left(\tfrac{1}{2} - \tfrac{3}{1\,6}\beta\right),$$

and the polarisation effect $D_l - D_r = \dfrac{\sigma}{\kappa_c}\,\tfrac{3}{3\,2}\beta$. The effect increases therefore with limb darkening, as was expected. For $\sigma/\kappa_c = 1$ these quantities would be the same as for the Schuster-Schwarzschild model at the limb, as is seen from equations (10) to (13) of

section 3. However, such a large value of σ/κ_c is not allowed, since the derivation presupposes it much smaller than 1, and this is the main reason why the Milne-Eddington model gives the much smaller effect of the two.

For other values of $\cos\theta$ the formulæ are rather cumbersome to handle, and for this reason we have made the computations for various β and put the result in fig. 4 (Milne-Eddington Model), which may facilitate future work on the subject. In the main figure, $D/(\sigma/\kappa_c)$ from (36) is plotted against $\cos\theta$, for β ranging from 0 to 8, which latter value is still of practical importance for the Sun (see fig. 2). The upper scale gives $\sin\theta$. In the inserted smaller figure a similar plot is made for $(D_l - D_r)/(\sigma/\kappa_c)$ from (34). For any point of the disc and assigned β one gets the depth without polarising device D and the polarisation effect $D_l - D_r$ by reading the abscissæ and multiplying by σ/κ_c. From these also follow $D_l = D + \frac{1}{2}(D_l - D_r)$ and $D_r = D - \frac{1}{2}(D_l - D_r)$.

A point of some interest is that, for small β, $D_l - D_r$ may become negative, which means that the polarisation effect is reversed. The corresponding portions of the curves in fig. 4 have been drawn as chain lines. The physical reason for this is easily seen by considering the case $\beta = 0$. Then at the boundary there is no limb darkening, and the scattering material there does not contribute to the polarisation effect. Below the photosphere, however, the star, for $\beta = 0$, behaves like a body of uniform temperature. Then the outgoing radiation shows no limb darkening, but the ingoing radiation shows a limb brightening, because the radiating layer gets thicker with increasing θ. The scattering material below the photosphere is therefore subjected to a negative limb darkening, and hence contributes a negative polarisation effect: $D_l < D_r$. As seen from the inserted fig. 4, this negative effect is still important for $\beta = 0{\cdot}5$; at higher β's it is soon destroyed, but nevertheless its tendency is to lessen the effect for the Milne-Eddington model for points away from the limb where these deeper layers become important.

It is seen from fig. 4 that the lines giving $D/(\sigma/\kappa_c)$ as a function of $\cos\theta$ all pass through one point, for which therefore this quantity is independent of β.* Physically this means that, at a certain distance from the limb, the line wings for a given σ/κ_c are independent of β, viz. the same for different spectral regions. This is due to the property of formula (36) that $D/(\sigma/\kappa_c)$ is of the type $(A + \beta B)/(1 + \beta\cos\theta)$ plus a portion independent of β, where A is a constant and B a function of $\cos\theta$ only. The condition that it is independent of β is therefore $A/1 = B/\cos\theta$. This is a quadratic equation which is easily solved and yields $\cos\theta = 0{\cdot}2346$, or $\sin\theta = 0{\cdot}9721$, for the point of intersection for the Milne-Eddington model. Similarly, from formula (12) it follows that for the Schuster-Schwarzschild model D is independent of β for the point $\cos\theta = 0{\cdot}4914$, or $\sin\theta = 0{\cdot}8709$, of the disc.

7. *The Fluxes and Corresponding Line Depths for the Various Models.*—The net flux of radiation πF for a non-rotating spherical star is the same as the light due to the whole disc, which, naturally, is unpolarised. It is given by

$$F = 2\int_{\theta=0}^{\pi/2} I\cos\theta d(-\cos\theta), \tag{37}$$

in which expression I represents the intensity without a polarising device. From the definition of D it follows that $I = I_0(1 - D)$ or, with I_0 from (3),

$$I = \mathcal{F}(0)(1 + \beta\cos\theta)(1 - D). \tag{38}$$

Because of the application to stars, where one generally observes the light due to the whole disc, and for the sake of completeness, the expressions for this flux may now be given for the various models.

* The same is shown in Minnaert's fig. 4, *Zeitschr. f. Astrophys.*, **12**, 321, 1936, for the M.-E. model for isotropic scattering.

For the *Schuster-Schwarzschild Model*, D (12) is substituted in (38), and with this expression for I, the integration (37) leads to

$$F/\mathcal{F}(0) = 1 + \tfrac{2}{3}\beta - s_1(1 + \tfrac{1}{2}\beta). \tag{39}$$

In carrying out this integration, one is entitled to replace $1 - e^{-s_1 \sec\theta}$ by $s_1 \sec\theta$. It is true that for the integrand this approximation breaks down for large $\sec\theta$, but the corresponding portion of the integral can be made arbitrarily small by taking s_1 small enough.

The depth of the line for the integrated light (39) becomes

$$D_F = \frac{F_0 - F}{F_0} = s_1 \frac{1 + \frac{1}{2}\beta}{1 + \frac{2}{3}\beta}. \tag{40}$$

Unsöld's expression for isotropic scattering (*loc. cit.*, eq. (31)) is the same. This is due to the fact that all the energy re-emitted over a hemisphere, which has the same value for oscillator and isotropic scatterer, gets out.

For the *General Model* one may directly substitute $I = I_l + I_r$ from (28) and (29), with $u = \tau$, into (37). Using the definition (24*a*) of K_n, one obtains

$$F/\mathcal{F}(0) = 1 + \tfrac{2}{3}\beta - \int_{\tau=0}^{\infty} [2\beta K_3 + \tfrac{3}{8}(3K_2 - 3\beta K_3 - K_4 + \beta K_5)K_2 + \tfrac{3}{8}(-K_2 + \beta K_3 + 3K_4 - 3\beta K_5)K_4]\frac{\sigma}{\kappa_c} d\tau. \tag{41}$$

For $\sigma/\kappa_c =$ any assigned function of τ, the integral is of the form $R + \beta S$, and R and S can each be determined by one quadrature, or integration.

The depth is of the Unsöld type $D_F = \int_{\tau=0}^{\infty} G_2(\tau) ds$ with $ds = (\sigma/\kappa_c) d\tau$ and the weight $G_2(\tau) =$ the expression in square brackets divided by $1 + \frac{2}{3}\beta$. It is naturally more complicated than Unsöld's expression (*loc. cit.* (29)) for isotropic scattering.

For the *Milne-Eddington Model*, D (36) is substituted in (38), and, with this expression for I, the integration (37) carried out. The procedure is obvious, except for the part involving $\ln(1 + \sec\theta)$. This gives rise to integrals of the type

$$\int_{\theta=0}^{\pi/2} \cos^n\theta \ln(1 + \sec\theta) d(-\cos\theta) = \int_{x=1}^{\infty} \frac{\ln(1+x)}{x^{n+2}} dx = \frac{1}{n+1}\left[\ln 2 + \int_{x=1}^{\infty} \frac{dx}{x^{n+1}} \frac{1}{x+1}\right], \tag{42}$$

the last step by partial integration. The resulting integral is of the type (32) with $a = 1$, and therefore readily evaluated.

The final result of the somewhat laborious but quite straightforward computation is

$$F/\mathcal{F}(0) = 1 + \tfrac{2}{3}\beta - \frac{\sigma}{\kappa_c}(0{\cdot}2081 + 0{\cdot}5378\beta) \tag{43}$$

or

$$D_F = \frac{\sigma}{\kappa_c} \frac{0{\cdot}2081 + 0{\cdot}5378\beta}{1 + \frac{2}{3}\beta}. \tag{44}$$

For $\beta = 2{\cdot}5$, for instance, this leads to $D_F = 0{\cdot}582\sigma/\kappa_c$. Unsöld (*loc. cit.*, eq. (34)), for isotropic scattering, gets $0{\cdot}565\sigma/\kappa_c$, which is not very much different. For the Schuster-Schwarzschild model, D_F for oscillator and isotropic scattering was the same, and it seems safe to conclude that for any model the difference is practically insignificant. From the practical point of view there is but little hope of distinguishing between oscillator and isotropic scattering by measuring the line profile of the total star light for a non-rotating star.

Summary

The scattering of light within a spectral line in a stellar atmosphere is treated under the assumption that the scattering centres behave like classical oscillators. The line depth is assumed to be small (weak lines or line wings), so that a procedure due to Unsöld can be followed.

The three stellar atmospheres treated are: (1) the Schuster-Schwarzschild Model for a given vertical optical depth s_1 of the scattering atmosphere (section 3); (2) the General Model for a scattering coefficient σ per cm. assumed to be a function of the optical depth τ of the general continuous spectrum which has an absorption coefficient κ_c (section 4); and (3) the Milne-Eddington Model for a given ratio σ/κ_c assumed to be independent of τ.

The most important respect in which the classical oscillator differs from an isotropic scatterer is that the light within the line should be polarised, so that the intensity of the polarised component along the radius I_r differs from that parallel to the limb I_l, the plane of polarisation being defined as that perpendicular to the vibration of the electric light vector. The difference $I_r - I_l$, expressed in the intensity of the adjoining continuous spectrum as a unit, is termed the polarisation effect. It depends on the position on the disc and the coefficient of darkening β.

This theoretically expected polarisation effect is sufficiently large to be observed on the Sun. The line λ 4227 of neutral calcium, which should be of the oscillator type (Heisenberg Theory, treated by Öhman) is suggested as suitable. For the Schuster-Schwarzschild Model ($s_1 = 0{\cdot}3$) the expected effect at the limb is 37 per cent. for this line, for the Milne-Eddington Model ($\sigma/\kappa_c = 0{\cdot}3$) it is 11 per cent. At a distance from the limb of 2 per cent. of the solar radius the effect should be 16 per cent. and 5 per cent. in the two cases.

The influence of true absorption within the line is shown to be practically negligible.

The depth of the line without polarising device D at various points of the disc and for various β is also treated. The line depth due to the total light coming from the disc is likewise discussed (section 7).

In the paper following, Dr. Redman has obtained evidence for a polarisation effect for the calcium line λ 4227, which, however, is much smaller than the theoretical one. The probable reason for this is that the effect is disturbed by collisions which also manifest themselves in the abnormally large value of the damping factor for this line. This is to be discussed in another paper by the writer. Meanwhile it is clear that the disturbance can best be dealt with after a clear insight into the undisturbed case which the present paper has aimed to give.

The author is indebted to the late Mr. E. G. Williams for discussions at an earlier stage, to Dr. R. O. Redman for various discussions and suggestions, and to the Radcliffe Observer Dr. H. Knox-Shaw for help in putting the manuscript in its final shape.

Radcliffe Observatory,
Pretoria:
1941 *February.*

OBSERVATIONAL SEARCH FOR POLARISATION IN THE CALCIUM LINE λ 4227 NEAR THE SUN'S LIMB

R. O. Redman

(Received 1941 April 3)

The theory described in the preceding paper by Dr. Zanstra predicts that if the atom producing a spectrum line behaves like a classical oscillator, the line profile near the Sun's limb should show differences of a few per cent. of the continuous spectrum, according as to whether it is measured in light polarised parallel to the limb or perpendicular to the limb. It is not expected that all lines will behave in this manner, and the number of cases appearing favourable for testing the theory is small. Of these, the most suitable from our point of view is the well-known neutral calcium line λ 4227, which we have examined as thoroughly as possible for this effect.

Instrument and Observational Procedure.—The instrument was a spectrograph belonging to the Solar Physics Observatory, Cambridge, and used by the writer at the 1940 eclipse, having three glass prisms of 7·5 cm. aperture, and camera and collimator of 244 cm. focal length. At λ 4227 the dispersion is 3·1 A./mm., and the measured resolving power in the photographed spectrum is at least 38,000. It was set up at the Radcliffe Observatory, Pretoria, in the same manner as at the eclipse, in a pit rather more than 3 metres deep, with the collimator vertical and the slit at ground level, an arrangement found to give very good thermal insulation for the prisms. The remainder of the optical train consisted of a 16-inch (40 cm.) cœlostat feeding a horizontal beam to a 12-inch (30 cm.) concave mirror of focal length 5·5 metres, whence the light returned towards the cœlostat, until intercepted by a small flat, of 10 cm. aperture, held about 1 metre above the spectrograph slit, into which it reflected the beam. The solar image diameter was 4·8 cm. Collimation was checked before every series of observations by inspection from the camera end of the spectrograph. Immediately above the slit a small mounting held a Nicol prism, rotatable and with a long handle to indicate its orientation, and between this and the slit itself was a diaphragm with an aperture 0·8 mm. in diameter. The solar image was set as nearly as possible tangential to this hole, *i.e.* at $\sin\theta = 0{\cdot}985$, with the slit perpendicular to the solar radius at the point of observation. The slit width was about 0·025 mm. Supercoated backed Ilford Process plates were used. Exposure times ranged between $\frac{1}{4}$ and 3 seconds. The general photometric procedure followed that used by the writer in earlier work.*

To calibrate the plates, exposures were made through a neutral tint glass wedge, with a very wide slit, using the Sun as source. For this, a spectacle lens of 1 metre focal length, aperture stopped down to about 1 cm., was placed in the beam so as to focus an image of the concave mirror on to the slit. The small central part of the mirror, whose image falls on the wedge, should be perfectly uniformly illuminated, and should illuminate the wedge similarly. With this arrangement, however, light from each part of the wedge passes through a different part of the collimator and there is some vignetting at the collimator aperture. This was overcome by using another spectacle lens, of about 80 cm. focal length, placed immediately over the wedge, so as to throw an image of the first auxiliary lens on the collimator. The resolving power of the spectrograph is then quite low, owing to the small collimator aperture in use, but this is of no importance, as it is still quite adequate to image the wedge accurately

* *M.N.*, 97, 552, 1937.

on the plate. Wedge exposures were ½ or 1 second. In order to ensure that all parts of the wedge were equally exposed, a simple shutter was used, consisting of a screen pivoted on a long arm so that its edge moved in a direction perpendicular to itself, and when crossing the slit was parallel to the jaws.

Fifteen plates were taken on the early mornings of 1940 December 13, 15 and 16, each having one exposure with light polarised parallel to the limb, a second polarised perpendicular to the limb, and a third calibration exposure through the wedge. The spectrograph transmits about twice as much light when the plane of polarisation is parallel to the slit as in the perpendicular position, so that for all but the first four plates the exposure was adjusted so as to give the two polarised spectra as nearly as possible equal photographic densities, a procedure which should minimise photometric errors. Plates were brush developed in M–Q. Thirteen of the fifteen were measured. Tracings at magnification 100 : 1 were made with the Radcliffe Observatory's microphotometer, and readings from these were taken at plate intervals 0·02 mm., and also at each maximum and minimum. Readings within about 5 per cent. of either clear glass or total blackness were ignored. Reduction and the fitting together of results were done as usual, the two polarisation components being kept independent throughout. The position of the continuous spectrum was determined from separate tracings at magnifications 5 : 1 or 10 : 1, also independently for the two different polarisations.

Results.—Fig. 1 shows the observed points on the two profiles plotted in $\log I$. Reducing the ordinates to intensities, expressed as percentages of the continuous spectrum, the two curves may be superposed as in fig. 2. We see immediately that the differences between the two components are everywhere small; the effect we are seeking is certainly not as great as theoretically predicted and may even be zero. The only differences to which any significance can be attached are at the maxima marked A, B, C, D, E. These lie in the range 45–70 per cent. of the continuous spectrum; their average $\log I$ is 1·770 (continuous at 2·000) when the plane of polarisation is parallel to the Sun's limb, and 1·783 with polarisation perpendicular to the limb, *i.e.* a difference of 1·8 per cent. of the continuous spectrum at intensity about 60 per cent., in the sense predicted by theory, but considerably smaller. We ignore the line centre, for the intensity there may be expected to be rather sensitive to the exact distance from the limb at which one observes, and, furthermore, the theory is valid only for the line wings. (The residual intensity should not be compared with the much lower value the writer has found in other work*, since here we are observing near the limb, not at the centre of the disc, and with a spectrograph of considerably lower resolving power than formerly.) A tendency for a systematically negative effect to show in the wing of longer wave-length is believed to be due to a small error in the position of the continuous spectrum. It could be eliminated without doing violence to the observations, in which case the effect nearer the centre would be slightly increased. We have not made this modification, as it was felt that to determine the two curves from first to last quite independently would be the fairer procedure.

Errors.—The critical reader may at this stage decide, not without justification, that the polarisation effect is zero. There is, however, something to be said in defence of the opposite view.

Let us first consider accidental errors. There is no noticeable difference in quality between the two curves (see fig. 1). For light polarised perpendicular to the limb, the profile between λλ 4224·18 and 4229·78 has 1108 observed points, with an average deviation from the smooth curve of 0·010 in $\log I$. For polarisation parallel to the limb, the corresponding number of points is 952, with average deviation 0·012 in $\log I$. At the maxima A, B, C, D, E, the "perpendicular" spectrum has respectively 11, 11, 10, 10, and 9 readings, while the average deviation for an individual reading from the corresponding mean maximum is 0·011 in $\log I$; for the "parallel" spectrum, the

* *M.N.*, 95, 742, 1935.

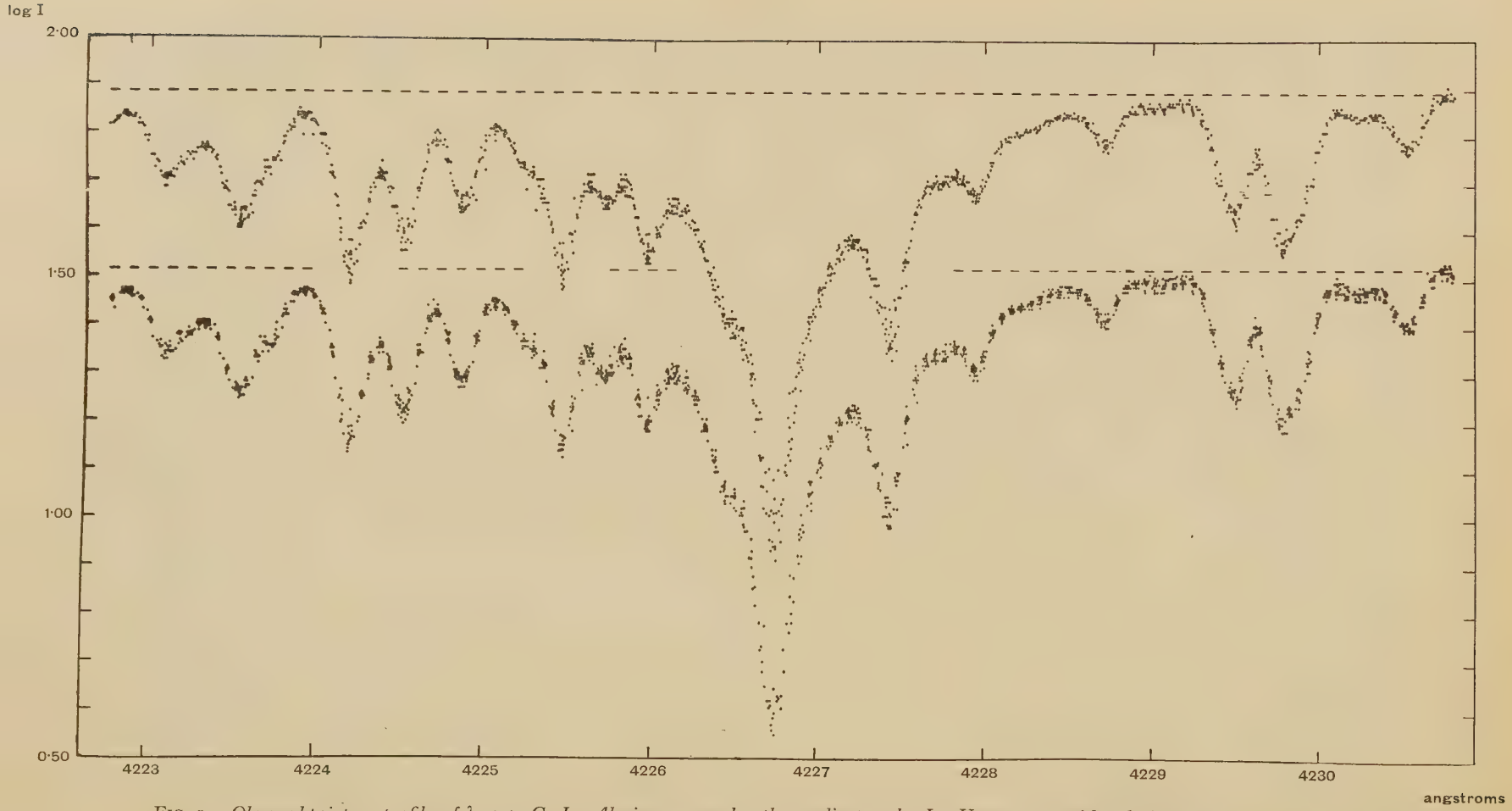

FIG. 1.—*Observed points on profiles of λ 4227, Ca I. Abscissæ: wave-lengths; ordinates: log I. Upper curve with polarisation parallel to Sun's limb; lower curve with polarisation perpendicular to limb. Dotted lines show adopted position of continuous spectrum.*

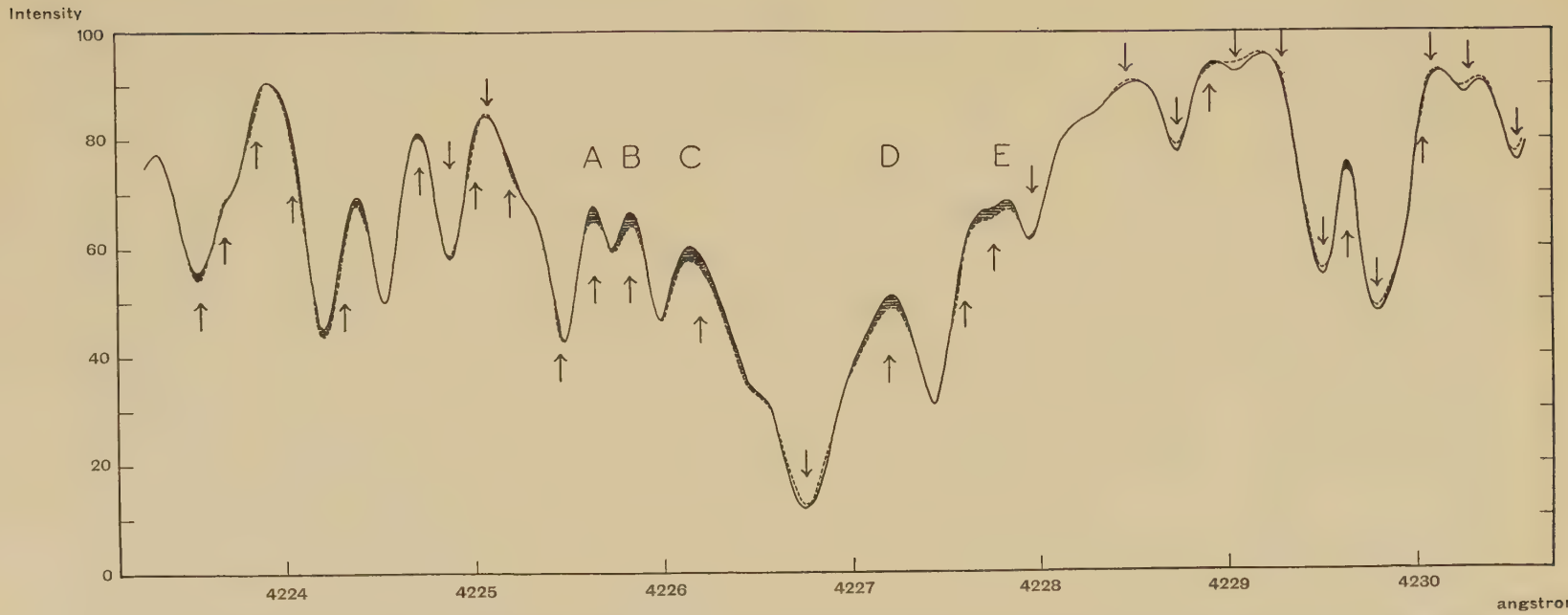

FIG. 2.—*Profiles of λ 4227, Ca I, at sin θ = 0·985, in light polarised perpendicular (——) and parallel (- - - -) to the limb. Arrows indicate the principal differences between the curves; upwards if in the sense theory demands, downwards if* vice versa. *In the former case the space between the curves is shaded.*

equivalent figures are 8, 9, 9, 9, 7, and 0·008. Thus purely accidental errors are quite small, and of themselves are unlikely to be responsible for the observed effect.

Systematic photometric errors are to a large extent nullified by the fact that we are seeking for an effect of a differential nature. Errors arising, for instance, from poor wedge calibration, or non-uniform illumination of the wedge, would in our results be reduced to the second order, provided we were able always to obtain "perpendicular" and "parallel" spectra in pairs of equal photographic density. This ideal was not attained, but we may approximate to it by choosing pairs of spectra, "perpendicular" and "parallel," generally not both on the same plate, but which are of such densities that they have utilised the same part of the wedge in their reduction. Profiles from a short list of seven pairs of spectra mated in this manner were found, however, to give the same result as had been obtained from all plates together; the mean log I at the five maxima A, B, C, D, E, was 0·013 higher on the "perpendicular" than on the "parallel" profile, exactly as before. We conclude that what we observe is not simply the spurious effect of erroneous plate calibration.

There are also a number of possible sources of trouble in the instrument.

(*a*) The three aluminium-coated mirrors to a certain extent de-polarise the light they feed into the spectrograph. It seemed unlikely that at the angles of incidence involved the de-polarisation would be very great, but fortunately it happens that this opinion can be checked by calculation on the basis of known data.* I am indebted to Dr. Zanstra for the rather heavy computation. For the actual angles of reflection and orientation of the spectrograph slit, he found that the effect we seek would be reduced in the least favourable case by only 5 per cent. of itself, a quantity well beyond the power of our present observations to detect.

(*b*) The resolving power of the spectrograph might vary with the plane of polarisation of light passing through it. Measures of the instrumental profile in light polarised parallel and perpendicular to the slit respectively, using a krypton discharge tube as source, showed no variation that we could detect, a result confirmed by the general appearance of the calcium line profiles.

(*c*) Our measures will be affected by light scattered from other points of the Sun's disc into the part where our observations have been made, some by the Earth's atmosphere, but most by the cœlostat and telescope mirrors. If the intensity of this false light is not strongly dependent on the plane of polarisation, all that will happen is that our effect will be slightly diluted. In the unlikely event of a strong dependence on the plane of polarisation, the centre to limb change of profile may come into play. This would give a spurious effect, but quantitatively it should be extremely small, as the centre-limb profile variation is itself not very great. Further, we believe that this error, if present, would reduce the observed effect.

(*d*) The instrument we have used is a "straight" three-prism spectrograph, a type which probably gives less false light from internal reflections and scattering than any other of the same optical performance; the lenses are cemented doublets, the camera is well diaphragmed and also lined with black velvet, while we have used as short a slit as practicable. Thus, although more false light is likely to be present when the plane of polarisation is perpendicular to the slit than when parallel, owing to greater reflection at the prism surfaces, its amount must be still quite small and very unlikely to be sufficient to produce the effect we observe. Added weight is given to this conclusion by the fact that we find a negative effect at the line centre, where false light arising in the spectrograph would show its presence most. To achieve greater certainty on this point we would need to use a monochromator.

(*e*) We have examined the possibility of the Nicol prism, as it is rotated, throwing the spectrograph off collimation with the mirror system, and are satisfied that no trouble arises from this cause.

* Born, *Optik*, p. 261, § 68, 1933.

None of these factors, indeed, seems capable of introducing any appreciable systematic error, and it seems possible, therefore, to argue that the observed effect, while certainly small, is probably not zero. But the observations do not encourage excessive optimism, and at the moment we can only grant small odds in favour of the existence of a positive effect; more investigation will be necessary before it can be taken as established beyond question, while accurate determination of its size would require a considerable amount of very precise observation.

Comparison of Observation with Theory.—For the sake of argument we will consider the observations at their face value. To maintain conformity with Dr. Zanstra's paper we shall now refer to line *depths*, the continuous spectrum being at zero and total absorption at unity.

First, in the line wings the effect appears to be undetectable. For instance, at the maximum between λλ 4227·946 and 4228·398 A., at line depth 0·20, fig. 2 shows an effect less than 0·005. Were we to adjust the continuous spectrum so as to minimise the residuals in the line wing of longer wave-length (see above), the effect at the point just mentioned would be increased slightly, but would still be less than 0·01. In estimating σ/k_c or s_1 we use the line depth D_c at the same wave-length, but from the centre of the disc. From *M.N.*, **95**, 742, 1935, figs. 2 and 3, $D_c = 0{\cdot}133$. (We ignore the fact that we are using results from two spectrographs of considerably different resolving power.) For the Milne-Eddington model, fig. 3 of Dr. Zanstra's paper gives, for $\sigma/k_c = 0{\cdot}3$, $D_c = 0{\cdot}22$ at $\sin\theta = 0$, and $D_l - D_r = 0{\cdot}05$ at $\sin\theta = 0{\cdot}985$. These quantities all vary together in the same ratio, and since we have $D_c = 0{\cdot}133$, our $\sigma/k_c = 0{\cdot}18$ and the theoretical effect $D_l - D_r = 0{\cdot}03$, which is more than three times the observed amount. Similarly, for the Schuster-Schwarzschild model, equation (12) gives $s_1 = 0{\cdot}219$ and then from equation (13) $D_l - D_r = 0{\cdot}155$, which is greater than fifteen times the observed value. In view of these figures it would have been better to assume isotropic scattering when evaluating σ/k_c and s_1, but the difference is inconsiderable.

Secondly, as mentioned earlier, the average effect for the maxima A, B, C, D, E is $D_l - D_r = 0{\cdot}018$ at depth 0·40. We estimate roughly that the unblended calcium line would have this depth at the point where the centre of the line λ 4227·442 now is, and that the depth at the centre of the disc D_c would likewise be 0·40 (figs. 2 and 3, *loc. cit.*) for the unblended line. The line depth is no longer small and we cannot estimate σ/k_c and s_1 directly from Dr. Zanstra's paper. In the case of the M–E model, with isotropic scattering, formulæ for finite line depth are given in Unsöld's *Physik der Sternatmosphären*, p. 242, equation (65·34), from which, with $\beta = \beta_0 = 4$ and $\cos\theta = 1$, the auxiliary quantity $\alpha = 0{\cdot}404$ and $\sigma/k_c = 1/3\alpha^2 - 1 = 1{\cdot}04$. As above, $D_l - D_r = \frac{1}{6}\,\sigma/k_c = 0{\cdot}173$, ten times the observed value. For the S–S model, equation (64·10) and Table 48, p. 232, *loc. cit.*, yield $s_1 = 0{\cdot}930$, and Zanstra's equation (13) then gives $D_l - D_r = 0{\cdot}214$, twelve times the observed value. But since the theory of the polarisation effect has been derived for σ/k_c or s_1 small, these theoretical values have been overestimated. We have then that for the M–E model the theoretical effect lies between 3 and 10 times that observed, while for the S–S model it is greater than 15 and less than 12 times that observed! This last contradiction can be attributed to errors of observation, to inapplicability of the S–S model to observations near the limb, or to variation with atmospheric depth of the agency responsible for destroying the polarisation we expect.

This comparison between theory and observation glides over a good many difficulties and its results cannot be regarded as more than a rough approximation. We may conclude, however, that, granted the small differences we measure are real, the observed effect is smaller than that predicted by theory by a factor of the order of ten.

The writer wishes to express his thanks to Dr. Zanstra for valuable assistance in this work.

Summary

Profiles of the neutral calcium line λ 4227 have been measured near the limb of the Sun, at $\sin\theta = 0{\cdot}985$, in light polarised respectively parallel and perpendicular to the limb. For the most part the profiles are indistinguishable, but there is a small difference amounting to about 1·8 per cent. of the continuous spectrum at line intensity 60 per cent. Examination of likely sources of error suggests that this may be real. The ratio of theoretical to observed effect is of the order of ten.

ON THE WEAKENING OF THE POLARISATION EFFECT BY COLLISION DAMPING

H. Zanstra
(Radcliffe Travelling Fellow in Astronomy)

(Received 1941 April 7)

1. *Redman's Observations of Polarisation for Ca λ 4227 suggesting Disturbing Fields.*—In the previous paper, Dr. Redman has discussed his observations of polarisation for the resonance line λ 4227, $4^1S_0 - 4^1P_1$, of neutral calcium on the Sun. On the assumption that a calcium atom polarises the incident light in the same way as a classical oscillator, the writer has shown, in the paper preceding that of Dr. Redman, that the light within this Fraunhofer line should be polarised when observed near the Sun's limb, in such a way that the component with plane of polarisation perpendicular to the limb (electrical vibration parallel to the limb) should have the strongest intensity. Now indeed Dr. Redman has found evidence of such a polarisation effect, but, though its sense is the same as predicted by theory, its magnitude falls far below the theoretical expectation, being too low by a factor of the order ten. In the following, the probable reason for this large discrepancy will be discussed, and a way opened for dealing with it quantitatively.

There is little doubt that under normal conditions the calcium line under consideration should polarise like a classical oscillator. Heisenberg's * theoretical criterion for this, viz. that the inner quantum numbers j of the two states have the values zero and one, is satisfied. Though experiments have not been done on the calcium line, the polarisation of light in the similar mercury resonance line, λ 2537, $6^1S_0 - 6^3P_1$, has been investigated in the laboratory, and its oscillator character confirmed.* It is therefore likely that the smallness of the effect observed by Dr. Redman is due to disturbing fields of electrons, ions or atoms in the Sun, acting upon the vibrating atom, which were not taken into account in the theory of the polarisation effect as presented thus far.

2. *Collision Damping for Ca λ 4227* (Unsöld).—One of the most important of such disturbances is that manifesting itself in the abnormally large value of the damping factor γ. For an oscillator of strength f and damping factor γ, the absorption coefficient is

$$\alpha = f\frac{\pi e^2}{mc}\,\frac{\gamma}{(\omega-\omega_0)^2+(\gamma/2)^2}, \qquad (1)$$

where e and m are the charge and mass of the electron, and c the velocity of light. In this expression, ω represents the frequency of the incident light, and ω_0 the natural frequency of the oscillator, viz. of the centre of the line (angular frequencies $\omega = 2\pi\nu$ are used throughout). For the greater part of a strong absorption line, $\omega - \omega_0 >> \gamma$, and the absorption coefficient is proportional to γ, so that an abnormally large absorption might be interpreted by an abnormally large γ.

Without going into details as regards the literature of this subject, we may at once turn to the line under consideration. Comparing it with the other calcium line λ 6527 in the Sun, which is so weak that its total absorption does not depend on its γ, but only on its f, Unsöld † concludes that the total absorption of λ 4227 is abnormally large and may be accounted for by a value of the damping constant $\gamma_{obs} = 16{\cdot}3 \times 10^8$ sec.$^{-1}$, whereas

* *Cf.* Y. Öhman, *M.N.*, **89**, 479, 1929.
† A. Unsöld, *Physik der Sternatmosphären* (Springer, 1938), p. 276.

one would theoretically expect an oscillator strength of about 1·2, resulting in a radiation damping constant $\gamma_0 = 1{\cdot}48 \times 10^8$.

This abnormally large γ_{obs} he explains by sudden changes in phase in the emitted wave train by the quadratic Stark effect due to close approaches ("collisions") of electrons and ions, which results in a temporary change in natural frequency $\Delta\omega_0$ (Weisskopf and Lenz's quantum theory of collision damping).

Only those collisions are taken into account for which the change in phase $\int \Delta\omega_0 dt$ (see section 5 (*c*)) is appreciable, viz. exceeds unity, and, in so far as this quantity soon becomes large, the resulting changes in phase may be considered arbitrary. On the other hand, the oscillator is appreciably affected by such a collision only during very few vibrations (see section 5 (*c*)), so that the energy radiated during the encounter is negligible. Nor is any energy imparted or lost in the form of kinetic energy, since the amount $h\Delta\omega_0/(2\pi)$ added by the quadratic Stark effect during the first half of the collision is again freed during the second half, the process being considered adiabatic.* The energy of the radiating atom is therefore not changed by the collision. Let there be z of such effective collisions per second. The result is then that the wave train of the emitting oscillator is cut up into a number of separate trains, each starting after one of these z collisions with an arbitrary phase † but without change in amplitude. Expansion into a Fourier series ‡ then leads to a distribution of frequencies of the same type as would occur for an undisturbed oscillator with damping constant

$$\gamma_1 = 2z = 2/\bar{\tau}, \tag{2}$$

which may therefore be termed the collision damping constant. The reciprocal of z is $\bar{\tau}$, the mean time between collisions.

The same derivation for an oscillator damped by radiation damping γ_0 leads to a distribution corresponding to a damping constant $\gamma_1 + \gamma_0$. §

For the derivation of this equation it is assumed that the collisions suffered by one atom occur at random as regards the time ||, a condition which is fulfilled if the atom is at rest. For instance, this applies to collisions with electrons or even protons, whose thermal velocity is always large compared with that of the radiating atom. Then the probability that the time interval between subsequent collisions is between τ and $\tau + d\tau$ is

$$\frac{dz}{z} = \frac{1}{\bar{\tau}} e^{-\tau/\bar{\tau}} d\tau, \tag{3}$$

where dz is the number of collisions of this type per second.¶ In the derivation below, equation (3) will be made use of, whereas (2) will merely be looked upon as the definition of γ_1.

Unsöld then proceeds on the assumption that, when a radiation field is present also, the oscillator disturbed by the sudden changes in phase may be replaced by an undisturbed one of normal strength, but with damping constant $\gamma_1 + \gamma_0$. For the electron and ion concentrations and temperature representative of the Sun, he then calculates the theoretical $\gamma_1 + \gamma_0$ if the changes in phase are due to the quadratic Stark effect (*loc. cit.*, p. 279), and finds that this theoretical value is about 11 times γ_0, agreeing with the above

* W. Lenz, *Zeitschr. f. Phys.*, **80**, 426, 1933.

† V. Weisskopf, *Phys. Zeitschr.*, **34**, 12, 1933.

‡ *Cf.* M. Born, *Optik* (Springer, 1933), p. 437. Born's final formula (12) for the square of the Fourier coefficient should contain the factor N (the total number of terms) on the right-hand side if one wishes absolute values (Born, p. 424).

§ V. Weisskopf, *loc. cit.*, p. 11.

|| H. A. Lorentz, *Proc. Amsterdam Ac.*, **8**, 595, 1906.

¶ The formula is readily obtained if one remembers that the fraction $z d\tau$ is eliminated by collisions within $d\tau$, and looks upon z or $1/\bar{\tau}$ as the "absorption coefficient" and upon τ as the "length."

γ_{obs} (*loc. cit.*, p. 281). For the calcium line, as also for other lines, the theory of combined radiation and collision damping is therefore confirmed. In one respect, however, Unsöld's views require modification, as will be seen in the next section.

3. *Oscillator with Incident Radiation. Combined Action of Radiation Damping and Collisions. Emission of Two Frequency Groups, ω and ω_0.*—The present section deals with the absorption and re-emission of an oscillator undergoing the sudden disturbances of phase discussed in section 2, when placed in an incident radiation field of frequency ω. The result of the treatment will be that the average absorption is the same as for an oscillator of damping constant $\gamma_1+\gamma_0$, as anticipated by Unsöld. The re-emission, however, takes place in two groups of frequencies, one close to the incident frequency ω, and the other close to the natural frequency ω_0. Thus the re-emission turns out to be quite different from that for an oscillator of damping constant $\gamma_1+\gamma_0$, which would merely re-emit the incident frequency ω.

Consider one atom suffering a series of collisions in a radiation field of frequency ω and constant intensity. The behaviour of this one atom is pursued over a very long time, in which many collisions occur, so that the average quantities obtained are representative of any atom. The long-wave train for this one atom is cut up into a number of separate trains, each starting at one collision and ending in the next. We shall consider the case of a *resonance line*, the only case which allows description in terms of one oscillator. During the time between two collisions only the radiation field acts on the atom, and it will be assumed that this interaction can be described in an entirely classical manner, so that we can replace the atom by an oscillator of strength f and radiation damping constant γ_0. During the very brief time of collision, the behaviour of the oscillator cannot be described in a classical manner, but this stage is taken care of by the abrupt arbitrary change in phase at constant energy. (Just like the energy radiated, the energy absorbed from the radiation field during the short time of collision is negligible.)

In between two collisions, the equation of motion of this oscillator is

$$\ddot{x}+\gamma_0\dot{x}+\omega_0^2x=\sqrt{f}\,.\,eE_0\cos(\omega t+\phi), \tag{4}$$

where the time t will be reckoned from the moment of the last collision, when a new train starts. We take the incident light wave to be plane polarised, with electric vector $E=E_0\cos(\omega t+\phi)$, viz. amplitude E_0 and initial phase angle ϕ.* The displacement x is in the direction of this vector.

The general solution of this equation is the sum of the stationary solution for the given radiation field (particular solution) and that without radiation field (right-hand side zero), viz.

$$x=C\cos(\omega t+\phi')+Ae^{-\frac{1}{2}\gamma_0 t}\cos(\omega_0 t+\delta), \tag{5}$$

where

$$C^2=f\frac{e^2E_0^2}{m^2}\,\frac{1}{(\omega^2-\omega_0^2)^2+\gamma_0^2\omega^2}, \tag{5a}$$

and

$$\phi'=\phi+\psi, \qquad \tan\psi=\frac{\gamma_0\omega}{\omega^2-\omega_0^2}. \tag{5b}$$

From (5*a*) one sees that the influence of the factor $\sqrt{f}$ in (4) is such as to make the scattered energy f times that for a vibrating electron, which is what is meant by an oscillator of strength f.

This solution (5) is most easily discussed by a vector diagram (figs. 1*a*, 1*b*), in which the vector C (5*a*) makes the initial phase angle ϕ' (5*b*) with the axis of x and rotates with

* The incident wave is $E=E_0\cos(\omega t_0)$, if t_0 is the ordinary time. Thus $\phi=\omega t_{0i}$, where t_{0i} is the ordinary time at which the last collision occurred. The phase ϕ is therefore different for the different trains, and it can of course be made smaller than 2π by subtracting an integral multiple of 2π.

an angular velocity ω, whereas for the vector of slowly changing magnitude $Ae^{-\frac{1}{2}\gamma_0 t}$ the initial phase angle is δ and the angular velocity ω_0. Both vectors are projected on the axis of x, the projections representing the two terms of (5). The resultant of the two vectors is the vector B, which also represents the slowly changing amplitude of the oscillator. The vector diagram at the initial time, $t=0$, is given in fig. 1*a*, and at any time $t \leqslant \tau$ in fig. 1*b*. At the time $t=\tau$ the train ends.

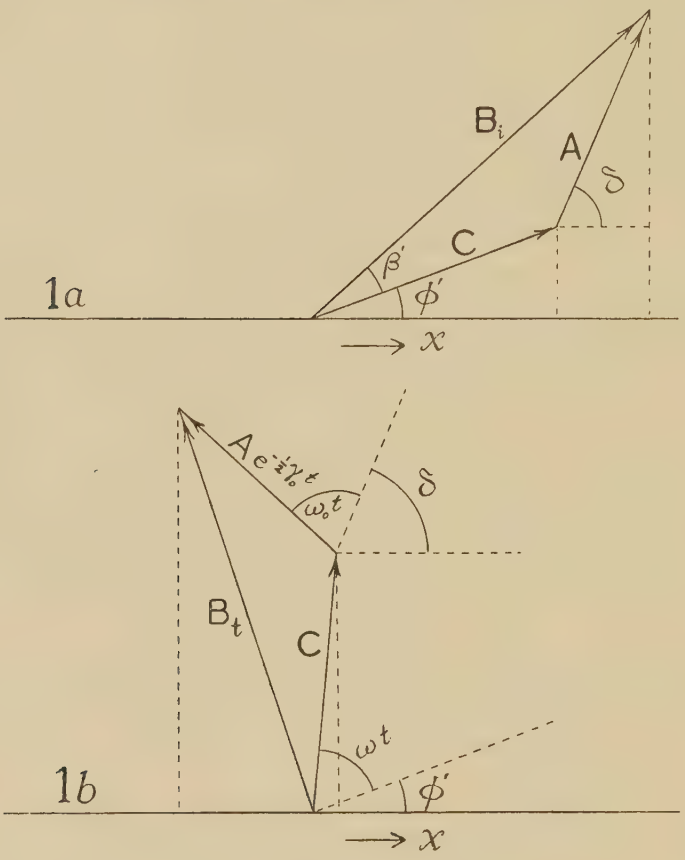

FIGS. 1*a*, 1*b*.

From the *condition that the energy just before and just after the collision is the same*, viz. the size of the amplitude B is unaltered, it follows that the statistical distribution of the amplitude magnitudes B is the same at the beginning and at the end of the trains, so that

$$\overline{B_i^2} = \overline{B_f^2}, \tag{6}$$

where i refers to the initial, and f to the final states of the separate trains, and the average indicated by the bar is taken over all wave trains succeeding one another during some time very much larger than $\bar{\tau}$, which we can conveniently take to be one second.

From the vector triangle ABC in the initial state (fig. 1*a*),

$$A^2 = B_i^2 + C^2 - 2B_i C \cos \beta', \tag{7}$$

if β' is the angle between the vectors B_i and C, which is related to the phase angle β of B_i by $\beta' = \beta - \phi'$.

During the very short time of collision the influence of the radiation field is negligible, and the oscillator behaves therefore as if there were no radiation field (see section 5 (*c*)).

The *condition that the phase changes in an arbitrary manner by collision* refers therefore to the vector B, which represents the momentary amplitude and phase of the oscillator. The initial phase angles β of B_i are therefore equally probable, but at this ordinary time t_{0i}, the ϕ' can only have one value (viz. $\omega t_{0i}+\psi$), so that the angles $\beta'=\beta-\phi'$ are likewise equally probable, and $\overline{\cos\beta'}=0$. Since the arbitrary changes in phase occur for atoms of any energy, which itself remains unchanged, this result applies to any energy group, viz. any group of amplitude magnitudes between B_i and B_i+dB_i.

Averaging for this group, one obtains, from (7),

$$\overline{A^2}=\frac{1}{2\pi}\int_{\beta'=0}^{2\pi}A^2d\beta'=B_i^2+C^2.$$

Then, averaging over all values of B_i, one obtains the $\overline{A^2}$ over all initial states

$$\overline{A^2}=\overline{B_i^2}+C^2. \tag{8}$$

At any time t, the vector diagram (fig. 1*b*) gives

$$B_t^2=C^2+A^2e^{-\gamma_0 t}+2CAe^{-\frac{1}{2}\gamma_0 t}\cos[\delta-\phi'-(\omega-\omega_0)t]. \tag{9}$$

The time interval elapsing between an initial and a final state is τ. Consider all final states characterised by the interval τ to $\tau+d\tau$. The average over such states gives

$$\overline{B_\tau^2}=C^2+\overline{A^2}e^{-\gamma_0\tau}+2Ce^{-\frac{1}{2}\gamma_0\tau}\{\overline{A\cos(\delta-\phi')}\cos[(\omega-\omega_0)\tau] + \overline{A\sin(\delta-\phi')}\sin[(\omega-\omega_0)\tau]\}. \tag{10}$$

It would be conceivable that the distribution of A and $\delta-\phi'$ of the various trains would be different for different τ. This, however, is not the case: the condition $\int\Delta\omega_0 dt>1$, characterising the collision which cuts off the train at τ, is entirely determined by the quadratic Stark effect $\Delta\omega_0$, and is not dependent on the values of A and $\delta-\phi'$. Hence the collisions at smaller τ do not change the distribution of those quantities for the remaining trains of larger τ, and, for any τ, this distribution is the same as for the total. The quantities $\overline{A\cos(\delta-\phi')}$, $\overline{A\sin(\delta-\phi')}$ and $\overline{A^2}$ in (10) are therefore the same as the total averages, and the $\overline{A^2}$ is given by (8).

Multiplication by the probability (3) and integration yields the average B^2 in the final state:

$$\overline{B_f^2}=\int_{\tau=0}^{\infty}\overline{B_\tau^2}e^{-\tau/\bar\tau}d\tau/\bar\tau=C^2+A^2\frac{1}{\gamma_0\bar\tau+1} + 2C\overline{A\cos(\delta-\phi')}\int_{\tau=0}^{\infty}e^{-(\frac{1}{2}\gamma_0+1/\bar\tau)\tau}\cos[(\omega-\omega_0)\tau]d\tau/\bar\tau + 2C\overline{A\sin(\delta-\phi')}\int_{\tau=0}^{\infty}e^{-(\frac{1}{2}\gamma_0+1/\bar\tau)\tau}\sin[(\omega-\omega_0)\tau]d\tau/\bar\tau. \tag{11}$$

The solar absorption line λ 4227, as many others of astrophysical interest, is much broader than either the width of radiation damping γ_0 or the width of collision damping γ_1.* That means that only incident frequencies $\omega-\omega_0>>\gamma_1$ or γ_0 are of importance, and we shall only consider this case; in our inequalities for the orders of magnitude, the absolute values of the quantities are meant. The average value of $(\omega-\omega_0)\tau$ under the integrals of (11) is, by (2), $2(\omega-\omega_0)/\gamma_1>>1$, and hence the quantity under the cos or the sin changes by very many units, without affecting the value of the factor in front of

* See section 5. It is also much greater than the Doppler width (section 5 (*b*)), which is really necessary for our application to this line in section 4. The derivation in this section has been given for an oscillator at rest.

it, $\tau/\bar{\tau}$ remaining sensibly the same. The integrals therefore vanish. Substituting (8) for A^2, and from (2) $\frac{1}{2}\gamma_1$ for $1/\bar{\tau}$, equation (11) reduces to

$$\overline{B_i^2} = \overline{B_f^2} = C^2(1 + \gamma_1/\gamma_0), \tag{12}$$

and therefore, by (8),

$$\overline{A^2} = C^2(2 + \gamma_1/\gamma_0). \tag{13}$$

The work against the radiation force $-m\gamma_0\dot{x}$ in (4) is transferred into radiation. From this it follows that the energy radiated per second by a vibration of frequency ω is $\frac{1}{2}m\gamma_0\omega^2$ times the square of the amplitude. Since $\omega - \omega_0 >> \gamma_0$ or γ_1, the phase difference between the undamped and the damped wave of the wave train (5), $0 < t < \tau$, reaches a very high value, before either the amplitude $Ae^{-\frac{1}{2}\gamma_0 t}$ has gone down appreciably or the train ends. Hence the two waves may be considered incoherent, and the rate at which energy is radiated is

$$\tfrac{1}{2}m\gamma_0 C^2\omega^2 + \tfrac{1}{2}m\gamma_0 A^2 e^{-\gamma_0 t}\omega_0^2. \tag{14}$$

The first term has a frequency very close to ω, viz. an inappreciable width (the subsequent C trains have no jump in phase), the second term a frequency close to the line centre ω_0, the width being of the order $\gamma_1 + \gamma_0$, the width γ_1 resulting from the finite length of the trains.

The average total energy emitted for a train τ is

$$\int_{t=0}^{\tau} \{\tfrac{1}{2}m\gamma_0 C^2\omega^2 + \tfrac{1}{2}m\gamma_0\overline{A^2}\omega_0^2 e^{-\gamma_0 t}\}dt = \tfrac{1}{2}m\gamma_0 C^2\omega^2\tau + \tfrac{1}{2}m\gamma_0\overline{A^2}\omega_0^2\frac{1}{\gamma_0}[1 - e^{-\gamma_0\tau}], \tag{15}$$

where, as in (10), the $\overline{A^2}$ is the same as for all trains.

Multiplying this by the number of trains dz in one second for the interval $d\tau$ from (3) and (2),

$$dz = (\tfrac{1}{2}\gamma_1)^2 e^{-\frac{1}{2}\gamma_1\tau}d\tau, \tag{16}$$

and integrating over the range of τ from zero to ∞, the average energy R re-emitted per second is obtained,

$$R = \tfrac{1}{2}m\gamma_0 C^2\left\{\omega^2 + \frac{\gamma_1}{\gamma_0}\omega_0^2\right\}, \tag{17}$$

where also (13) was substituted before integration. The first term in the brackets represents the energy of the ω wave, and the second term that of the ω_0 wave. Since γ_0 in (4) has been treated as a constant, whereas it actually should be proportional to ω^2, we might as well put ω_0^2 for ω^2 in (17), to which it is very close (section 5 (*a*)), our approximation being no better. The energy of the ω_0 wave is therefore γ_1/γ_0 times that of the ω wave. Although the individual oscillators may store and lose energy over short times, the state is statistically stationary, and, there being no dissipation, the average energy absorbed per second is likewise given by (17). Hence we may consider the energy as scattered, but only in the statistical sense, there being a re-emission of different frequencies.

Dividing (17) by the incident energy per sec. per cm.^{2}, the average Poynting vector, $\frac{1}{4\pi}\overline{cE \times H} = \frac{1}{4\pi}c\overline{E^2} = \frac{1}{8\pi}cE_0^2$, we obtain, after substitution of (5*a*), remembering that $\omega_0 >> \omega - \omega_0 >> \gamma_0$, the absorption coefficient per atom

$$a = f\frac{\pi e^2}{mc}\frac{\gamma_0 + \gamma_1}{(\omega - \omega_0)^2}, \tag{18}$$

where the γ_0 portion is re-emitted in a frequency band very close to the incident frequency ω, and the γ_1 portion in another frequency band about the line centre ω_0.

Comparing (18) with (1), for $\omega - \omega_0 >> \gamma$, it is seen that the oscillator under collisions

absorbs, on the average, like an undisturbed oscillator of the same strength and with damping constant $\gamma_0+\gamma_1$. The re-emission, however, is quite different.

4. *Weakening of the Polarisation Effect by Collision Damping.*—Consider now the case of a broad absorption line λ 4227 of neutral calcium in the Sun. For this line we may adopt Unsöld's value $(\gamma_0+\gamma_1)/\gamma_0=\gamma_{obs}/\gamma_0=11$ (section 2) as giving the right order of magnitude.

For practically all portions of such a broad line, the condition $\omega-\omega_0>>\gamma_0+\gamma_1$ holds. A frequency ω is then absorbed with the absorption coefficient α (18), *but only the fraction* $\gamma_0/(\gamma_0+\gamma_1)=1/11$ *is re-emitted in the same frequency* ω as the γ_0 portion of (18). The remaining 10/11ths go into re-emission about the line centre with a width $\gamma_0+\gamma_1$.* This radiation might either get out as a frequency close to ω_0 (for the Schuster-Schwarzschild model), or it might be absorbed by the general continuous absorption, or finally, some of it might get back into the line wings, as the wing of the emission line of width $\gamma_0+\gamma_1$, if its density becomes very high, which requires many subsequent scatterings. (If this line is re-emitted only once, the fraction of it re-emitted outside $\omega-\omega_0$ is $\pi(\gamma_0+\gamma_1)/|\omega-\omega_0|$ for one-half of the line, and therefore negligible.)

Leaving it an open question which of the three processes is predominant, we may now consider the polarisation. Since the atom under consideration polarises, in between collisions, like a classical oscillator, both the ω wave and the ω_0 wave show the same polarisation as for classical scattering. The ω_0 wave is either lost near the centre, or part of its energy comes back in the wings, but only after many scatterings, so that then it is unpolarised. The result for the line wings is that, of the radiation absorbed in the frequency ω, only the fraction $\gamma_0/(\gamma_0+\gamma_1)=1/11$ is directly re-emitted in the same frequency, showing the classical polarisation. If any other light is re-emitted in this frequency, it must have been scattered many times, as explained above, and is therefore unpolarised. *The polarisation effect for a given absorption is therefore cut down by a factor of the order 11*, due to collision damping. This seems to explain the result found by Dr. Redman that the polarisation effect observed is too small by a factor of the order ten. However, it should be kept in mind that what he found is the polarisation effect for a given line depth, and that a complete discussion still requires the relation between absorption and line depth. This relation, for the type of absorption and re-emission developed, is a good deal different from that for undisturbed scattering. Another point is that the quadratic Stark effect for λ 4227 is not simply a line shift, but involves two somewhat different line shifts for two components. But this may well be deferred to a future investigation, which also might cover questions such as the centre-limb variation over the Sun's disc, which for the new type of scattering may be a good deal different from that given by current theory.

5. *Numerical Values. Justification of the Assumptions.*—In the following, some numerical data for the calcium line λ 4227 will be considered, providing a justification of the assumptions made as regards the various orders of magnitude in sections 2 and 3.

(*a*) The centre of the line, $\lambda_0=4227$ A., corresponds to $\omega_0=4{\cdot}4566\times10^{15}$ sec.$^{-1}$. Allowing for superimposed absorption lines, the absorption has gone down to one-half of that at the line centre for $\lambda-\lambda_0=0{\cdot}52$ A. (R. O. Redman, *M.N.*, 95, 749, 1935, fig. 3), or $\omega-\omega_0=5{\cdot}5\times10^{11}$, which is therefore the order of this quantity for the main portion of the line which interests us. Hence $\omega-\omega_0<<\omega_0$. Since, according to Unsöld (see section 2), $\gamma_0=1{\cdot}48\times10^8$ and $\gamma_{obs}=\gamma_1+\gamma_0=16{\cdot}3\times10^8$, we have $\omega-\omega_0>>\gamma_1$ or γ_0. The average time between collisions is $\bar{\tau}=2/\gamma_1=1{\cdot}35\times10^{-9}$ sec.

(*b*) With $T=5600°$, the Doppler half-width for which the intensity has gone down by one-half is (Unsöld, *loc. cit.*, p. 158) $\Delta'\omega=1{\cdot}85\times10^{10}$. Hence $\omega-\omega_0\simeq30\Delta'\omega>>\Delta'\omega$.

* For the sake of simplicity, the reasoning is carried out for Doppler width zero. If the Doppler width is taken into account, the re-emission still occurs close to the line centre, since this width is $<<\omega-\omega_0$ (section 5 (*b*)).

(*c*) *Time during which a Collision is Effective.*—Let an electron with thermal velocity v pass the vibrating calcium atom, and introduce a change in phase by the quadratic Stark effect. Only such collisions are considered effective for which the total change in phase is larger than unity (section 2). Let ρ be the distance of closest approach if a collision introduces a change of phase of unity. The time during which the collision is effective is then of the order $\tau_{\text{coll}} = \rho/v$. If the approach is closer, the same expression still holds, because the criterion is always that, over the parts of the orbit where the distance from electron to atom is $>> \rho$, the total change in phase introduced is $<< 1$, and this leaves only the part of the orbit, the length of which is of the order ρ, as effective.

We have (Unsöld, *loc. cit.*, pp. 279–281)

$$v \simeq \sqrt{\frac{8}{\pi}\frac{RT}{\mu_e}} = 4{\cdot}67 \times 10^7 \text{ cm./sec.},$$

with $T = 5600°$ and $\mu_e = 1/1838$, also

$$\rho = \left(\pi^2 \frac{C'}{v}\right)^{\frac{1}{3}}, \qquad C' = \frac{0{\cdot}0615}{\lambda^2}\frac{\Delta\lambda}{F^2} \qquad \text{and} \qquad \frac{\Delta\lambda}{F^2} = \frac{0{\cdot}35}{160^2}$$

from the observed quadratic Stark effect $\Delta\lambda$ for the field F. From this follows $\tau_{\text{coll}} = \rho/v = 0{\cdot}46 \times 10^{-14}$ sec., which is very much smaller than the average time between collisions obtained under (*a*). Since $1/\nu_0 = 2\pi/\omega_0 = 1{\cdot}41 \times 10^{-15}$ sec., the change in phase is only effective for 3·3 vibrations. This corresponds to an average shift in wave-length $\Delta\lambda/\lambda_0 > 1/(2\pi \times 3{\cdot}3)$ or $\Delta\lambda > 204$ A. $>> \lambda - \lambda_0$. For this reason the change in phase may be calculated as if $\lambda = \lambda_0$, and is given by $\int \Delta\omega_0 dt$.

The train (5) consists of many beats between minimum amplitude $C - Ae^{-\frac{1}{2}\gamma_0 t}$ and maximum amplitude $C + Ae^{-\frac{1}{2}\gamma_0 t}$, each beat lasting the time $2\pi/(\omega - \omega_0) = 1{\cdot}14 \times 10^{-11}$ sec. The time of collision is therefore only 1/2500 of the time of one beat. Since the incident radiation only manifests itself in a time comparable with one beat, the oscillator, during the short time of collision, should behave as if there were no radiation field.

Summary

Though the calcium atom, in the wave-length λ 4227, should theoretically polarise light in the same way as a classical oscillator, Dr. Redman found that the polarisation of the light within this line near the Sun's limb is no more than about one-tenth of that predicted by the author on this assumption. It is now shown that the large collision damping attributed to this line is the probable cause of this weakening of the polarisation, because of the hitherto unnoticed circumstance that it converts much of the light absorbed in the line wing to light of a frequency close to that of the line centre.

Radcliffe Observatory, Pretoria:
1941 *February.*

POLARISATION OF THE CORONA

C. W. Allen, D.Sc.

(Communicated by the Director, Commonwealth Solar Observatory)

(Received 1941 July 7)

1. *Introduction.*—The following paper contains the polarisation observations made on the Solar Corona by the Australian Eclipse Expedition to South Africa on 1940 October 1. The main aim was to determine to what extent the polarisation of the corona varied with colour. This was done by obtaining standardised photographs of the corona through a "polaroid" screen and blue and red colour filters.

2. *Equipment.*—The camera was fitted with a 6-inch Dallmeyer lens of focal length 36 inches, and fed from an 8-inch cœlostat with silvered mirror and gramophone motor drive. Both cœlostat and camera were mounted on brick piers. A $2\frac{1}{2}$-inch disc of polaroid was placed about 1 inch in front of the plate in such a way that it could be rotated through 90°. It was oriented to rotate from a polar to an equatorial direction. Interchangeable blue and red filters were mounted between the plate and the polaroid.

The plates used were Kodak (Australian) "Panatomic X" for the red, and "Ordinary" for the blue. They were developed with Kodak "Simplex" developer at 65° F. for 5 minutes. Two exposures of the corona were made on each plate, one with the polaroid oriented in a polar direction and the other with equatorial polaroid.

The 6-inch camera was stopped down to 2 inches for some exposures, and for others full aperture was used but with a cardboard disc mounted just before the polaroid to cut off the light from the bright central part of the corona. This eliminated scattered light from the polaroid and filters, and halation from the plate.

3. *Eclipse Photographs.*—For three complete sets of photographs it was necessary to obtain 6 plates and 12 exposures during the 230 seconds of totality. Each plate contained a pair of photographs that were similar except for the polaroid orientation. All pairs of images showed evidence of considerable polarisation. No obvious differences between the red and the blue polarisations could be detected by a visual examination of the plates.

A certain amount of fogging by extraneous light was expected with the long exposures, and it is the correction for this that is perhaps the chief difficulty in corona photometry. At great distances from the Sun on the long exposures it was quite evident that the extraneous light was much brighter than the corona. There was a certain amount of fogging near the edges of the plates due to leakage at the plateholder. In general this fogging was not close enough to the images to be serious.

4. *Calibration.*—Calibration of the photographic plates was effected by the use of a platinum step wedge placed in contact with the plate. Exposure was made inside the camera and with the same colour filters, polaroid, and plates as used for the eclipse. By exposing on sunlit paper with reduced aperture a similar exposure time was also obtained.

Several such plate calibrations were made before the eclipse, but it was found that some of these (including one developed with the eclipse plates themselves) had to be discarded as a result of extraneous light. The characteristics of the eclipse plates were averaged from plates developed a few days before the eclipse but with similar development conditions. As the main observation was dependent on the relative contrast of the blue and red plates the characteristics of these were redetermined in the laboratory

shortly after the return of the Expedition. It was then found that the small difference in contrast shown by the field calibrations was not real, and that, in fact, the blue and red plates had almost exactly the same contrast. A small amendment to the original reductions had to be made to account for this.

The regions of transmission of the filters (Wratten 26 and 47) were measured with a spectrograph and are shown in Table I.

TABLE I

Filter	Maximum Transmission	Approximate Region
Red	6250 A.	6000–6500 A.
Blue	4600 A.	4300–4900 A.

5. *Photometry.*—The photographs were measured with the photoelectric microphotometer of the Radcliffe Observatory at Pretoria. The coronal photographs were studied by making diametric tracings at every 15°. From these tracings measurements were made of density, and hence intensity, at every $1\frac{1}{2}'$ from the Moon's limb. The estimates of polarisation were made by comparing the intensities at identical positions for the image pairs.

The step-wedge exposures were studied with the same microphotometer, and the plate characteristics drawn in the usual way. For testing the plate contrasts after the return of the Expedition a thermo-electric microphotometer was used, but this was merely to detect a small differential effect. The calibration exposures of the eclipse photographs were remeasured and showed the same contrast difference as with the photoelectric photometer.

6. *Corrections.*—A small correction was made to allow for the incompleteness of the polarisation of the polaroid. Viewing unpolarised light, it was found that the intensity of light transmitted by two crossed polaroids was 0·006 of that transmitted by parallel polaroids. This figure was the same for both blue and red. The polarisation measurements in both blue and red would thus be underestimated. To allow for this, the degree of polarisation was increased by 0·6 per cent. of the measured value.

Corrections for scattered light were applied to the measured intensities of all images of the corona. In the medium exposures the general scatter was just sufficient to be detectable on the plate, but its intensity influenced the results considerably. For the short exposures there was nothing to show the presence of scattered light, but its intensity could be judged from the stronger exposures. Even for the short exposures the correction for scattered light increased the polarisation by about 2 per cent. and made the results much more consistent.

For the long exposures with full aperture the values obtained depend mainly on the scattering corrections. The amount of correction was judged from the amount of scattering appearing in full Moon photographs taken under the same conditions. High accuracy for the outer parts of the corona is not possible.

Further corrections of the order of 1 per cent. in the polarisation were also made to allow for later plate-contrast measurements mentioned in section 4.

The polarisation produced by a silvered mirror when the angle of incidence is 15° is negligible; moreover, it cancels out when the degree of polarisation is determined from an average of all orientations.

7. *Results of Polarisation Measurements.*—The results showed at once that there was no great change of polarisation with distance from the Sun's limb. Consequently for each plate the intensity ratios were averaged for all distances from the Sun. From the ratios the degrees of polarisation were determined for each 15° of the Sun's azimuth, and the results were then weighted as in Table II to give the weighted mean value for each plate. The results are shown in Table III.

TABLE II

Pole and Equator	2 azimuths	weight 3
15° from Pole and Equator	4 azimuths	weight 5
30° from Pole and Equator	4 azimuths	weight 1

TABLE III

Degree of Polarisation

(*i.e.* percentage of total light that is completely polarised)

Plate Colour and Exposure Time	Pole and Equator	15° from P. and E.	30° from P. and E.	Weighted Mean
Red 2 sec.	41·7	39·1	47·0	40·8
Blue 3 sec.	44·7	42·6	45·1	43·7
Red 6 sec.	38·9	41·0	42·3	40·4
Blue 10 sec.	41·4	42·6	44·1	42·4
Red 12 sec.	50	46	34	46
Blue 20 sec.	47	45	41	45

Mean Red (small weight to long exposure) 41·0 per cent.

Mean Blue (small weight to long exposure) 43·2 per cent.

Averaging the values for selected distances from the Sun gave the results in Table IV for the change of polarisation with limb distance. Apparently the degree of polarisation is almost constant except for the decrease always found close to the limb. On account

TABLE IV

Polarisation as a Function of Distance from the Sun's Limb

Distance from Sun's limb	3′·9	5′·5	7′·0	8′·6	10′	12′	13′	15′	16′	24′	32′	40′
Percentage polarisation (mean red and blue)	35	37	42	41	41	45	46	47	44	49	41	43

of the scattered light the accuracy of the polarisation measurements became very poor beyond a distance of about 16′ from the limb, where the results are only provisional. However, there is quite good evidence that the degree of polarisation is about 40 or 50 per cent. to distances of 60′ from the Sun's limb, which is the limit of our photographs. On both the red and blue long exposures equatorial streamers can be seen extending to 60′ when the polaroid is in an equatorial position, while the same streamers can only be traced to 40′ when the polaroid is oriented towards the pole.

Conclusion

The polarisation of the corona at the 1940 Eclipse was almost independent of colour from 4600 A. to 6250 A., and almost independent of limb distance from 7′ to 40′. The degree of polarisation was 41 per cent. for red and 43 per cent. for blue light.

Discussion, comparison, photographs and acknowledgments connected with the above work will be given later in a *Memoir of the Commonwealth Solar Observatory*.

Canberra:
1941 *May*.

THE DERIVATION OF THE VELOCITY ELLIPSOID FROM PROPER MOTIONS

Archibald Brown, M.A.
(*Carnegie Research Scholar*)

(Communicated by the Director, Cambridge Observatory)

(Received 1941 June 5)

1. *Introduction.*—In the discussion of the distribution of peculiar motions in his *Stellar Dynamics* Smart suggests a method * of obtaining the characteristics of the (general) velocity ellipsoid from proper motions without the use of statistical parallaxes or other assumptions as to the distance of the stars considered. His method falls into two parts :

(i) From the distribution of the directions of the proper motions of stars in a small region of the sky coefficients P, Q, S, which define the velocity ellipse of the region, are obtained.

(ii) From the values of P, Q, S in a number of regions, the velocity ellipsoid is deduced.

The present paper considers in greater detail the second part, the solution for the velocity ellipsoid, and assumes throughout that each region is analysed by Smart's method.

2. *Notation.*—Let

$$F(\mathrm{U}, \mathrm{V}, \mathrm{W}) \equiv A\mathrm{U}^2 + B\mathrm{V}^2 + C\mathrm{W}^2 + 2F\mathrm{VW} + 2G\mathrm{WU} + 2H\mathrm{UV} = 1 \qquad (2.1)$$

be the equation of the velocity ellipsoid referred to the usual equatorial axes, *i.e.* OU is directed toward the vernal equinox, OV toward the point ($\alpha = 90°$, $\delta = 0°$), and OW to the North Pole.

When referred to a second set of rectangular axes Ou, Ov, Ow which have direction cosines (l_1, m_1, n_1), (l_2, m_2, n_2), (l_3, m_3, n_3) with respect to OU, OV, OW, the equation of the ellipsoid (2.1) becomes

$$au^2 + bv^2 + cv^2 + 2fvw + 2gwu + 2huv = 1, \qquad (2.2)$$

where

$$\left.\begin{aligned} a &= Al_1^2 + Bm_1^2 + Cn_1^2 + 2Fm_1n_1 + 2Gn_1l_1 + 2Hl_1m_1, \\ f &= Al_2l_3 + Bm_2m_3 + Cn_2n_3 + F(m_2n_3 + m_3n_2) + G(n_2l_3 + n_3l_2) + H(l_2m_3 + l_3m_2), \end{aligned}\right\} \qquad (2.3)$$

with similar expressions for b, c, g, h.

If A_0, B_0, C_0, F_0, G_0, H_0 are the co-factors † of A, B, C, F, G, H respectively in the determinant

$$\Delta = \begin{vmatrix} A & H & G \\ H & B & F \\ G & F & C \end{vmatrix},$$

and a_0, b_0, c_0, f_0, g_0, h_0 are the co-factors of a, b, c, f, g, h in

$$\Delta_1 = \begin{vmatrix} a & h & g \\ h & b & f \\ g & f & c \end{vmatrix}$$

* W. M. Smart, *Stellar Dynamics*, 177–185, 1938.

† *E.g.*, $H_0 = FG - CH$, $F_0 = GH - AF$.

it is easily proved * that

$$\Delta = \Delta_1 \tag{2.4}$$

and

$$a_0 = A_0 l_1^2 + B_0 m_1^2 + C_0 n_1^2 + 2F_0 m_1 n_1 + 2G_0 n_1 l_1 + 2H_0 l_1 m_1, \tag{2.5}$$

$$f_0 = A_0 l_2 l_3 + B_0 m_2 m_3 + C_0 n_2 n_3 + F_0(m_2 n_3 + m_3 n_2) + G_0(n_2 l_3 + n_3 l_2) + H_0(l_2 m_3 + l_3 m_2), \tag{2.6}$$

with similar equations for b_0, c_0, g_0, h_0.

3. *Definition of Smart's Coefficients P, Q, S.*—If R (α, δ) is the centre of a small region on the celestial sphere and

$$\left.\begin{array}{lll} l_1 = -\sin\alpha, & l_2 = -\cos\alpha\sin\delta, & l_3 = \cos\alpha\cos\delta, \\ m_1 = \cos\alpha, & m_2 = -\sin\alpha\sin\delta, & m_3 = \sin\alpha\cos\delta, \\ n_1 = 0, & n_2 = \cos\delta, & n_3 = \sin\delta, \end{array}\right\} \tag{3.1}$$

then Ow is the line of sight to R, Ov is parallel to the tangent at R to the meridian through

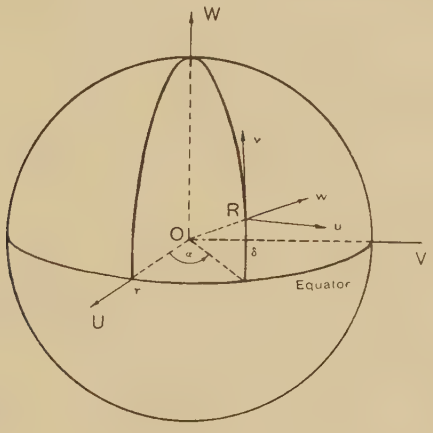

FIG. 1.

R (in the direction of δ increasing) and Ou is perpendicular to the meridian plane through R (see fig. 1).

The equation of the velocity ellipse for the region can be written †

$$pu^2 + 2suv + qv^2 = 1, \tag{3.2}$$

where

$$p = b_0/c, \qquad s = -h_0/c, \qquad q = a_0/c. \tag{3.3}$$

If X denotes the speed of the solar motion with respect to the stars considered and λ the angular distance RA′ from the centre of the region to the solar apex A′ (A_0', D_0'), then the three coefficients P, Q, S are defined by the relations

$$\left.\begin{array}{lll} P = Kp, & Q = Kq, & S = Ks, \\ 1/K = (pq - s^2)X^2 \sin^2\lambda. & & \end{array}\right\} \tag{3.4}$$

The analysis ‡ of the observed proper motions in the region gives P, Q, S and the position angle, θ_0, of the direction to the solar apex. From the values of θ_0 obtained for a number of regions, the direction to the solar apex can be found by Bessel's method, and the angular distance, λ, of each region from A′ can then be calculated.

* Either by matrix algebra or by direct substitution from (2.3).

† *Cf.* Smart, *op. cit.*, p. 172.

‡ Details of the method of analysis are given by Smart, *op. cit.*, pp. 181–185.

4. The relations between P, Q, S and the coefficients of the velocity ellipsoid are found as follows:—

$$P \sin^2 \lambda = \frac{p}{pq - s^2} \cdot \frac{1}{X^2} \qquad \text{from (3.4)}$$

$$= \frac{b_0}{c} \cdot \frac{c^2}{a_0 b_0 - h_0^2} \cdot \frac{1}{X^2} \qquad \text{from (3.3)}$$

$$= b_0 / \Delta X^2$$

since

$$a_0 b_0 - h_0^2 = c\Delta.$$

Similarly,

$$Q \sin^2 \lambda = a_0/\Delta X^2 \quad \text{and} \quad S \sin^2 \lambda = -h_0/\Delta X^2. \tag{4.1}$$

Putting

$$A_1 = A_0/\Delta X^2, \qquad B_1 = B_0/\Delta X^2, \quad \ldots \quad H_1 = H_0/\Delta X^2,$$

and substituting for a_0 from (2.5),

$$Q \sin^2 \lambda = A_1 l_1^2 + B_1 m_1^2 + C_1 n_1^2 + 2F_1 m_1 n_1 + 2G_1 n_1 l_1 + 2H_1 l_1 m_1. \tag{4.2}$$

Similarly,

$$P \sin^2 \lambda = A_1 l_2^2 + B_1 m_2^2 + C_1 n_2^2 + 2F_1 m_2 n_2 + 2G n_2 l_2 + 2H_1 l_2 m_2, \tag{4.3}$$

$$-S \sin^2 \lambda = A_1 l_1 l_2 + B_1 m_1 m_2 + C_1 n_1 n_2 + F_1(m_1 n_2 + m_2 n_1) + G_1(n_1 l_2 + n_2 l_1) + H_1(l_1 m_2 + l_2 m_1). \tag{4.4}$$

Also, from (4.1),

$$(PQ - S^2) \sin^4 \lambda = \frac{a_0 b_0 - h_0^2}{\Delta^2 X^4} = \frac{c}{\Delta X^4}$$

$$= \frac{1}{\Delta X^4}\{A l_3^2 + B m_3^2 + C n_3^2 + 2F m_3 n_3 + 2G n_3 l_3 + 2H l_3 m_3\}. \tag{4.5}$$

From (3.3), (4.1), and (4.5)

$$\frac{P}{PQ - S^2} = \frac{b_0}{\Delta X^2 \sin^2 \lambda} \cdot \frac{\Delta X^4 \sin^4 \lambda}{c} = p \,.\, X^2 \sin^2 \lambda,$$

$$p = \frac{P}{PQ - S^2} \cdot \frac{1}{X^2 \sin^2 \lambda}. \tag{4.6}$$

Similarly,

$$q = \frac{Q}{PQ - S^2} \cdot \frac{1}{X^2 \sin^2 \lambda}; \qquad s = \frac{S}{PQ - S^2} \cdot \frac{1}{X^2 \sin^2 \lambda}.$$

Thus when P, Q, S, λ are known, the equation of the velocity ellipse can be calculated (in terms of X as unit of velocity).

5. *Methods of Solution for Velocity Ellipsoid.*—Smart suggested that (4.5) be used as equation of condition in a least-squares solution to give A, B, C, F, G, H * when P, Q, S, λ have been found for a number of regions. When A, B, C, F, G, H have been evaluated, it is a simple matter to obtain the lengths and directions of the principal axes of the ellipsoid (2.1). Objections to this procedure are:

(i) $PQ - S^2$ is independent of the orientation of the velocity ellipse, so that the available information is not used fully;

(ii) in at least one case of practical interest a least-squares solution based on equation (4.5) will not be completely determinate. (This is explained in section 6.)

(iii) It would be preferable to use a linear function of P, Q, S, $\sin^2 \lambda$ rather than the quadratic form $(PQ - S^2) \sin^4 \lambda$, which will exaggerate the effect of errors in P, Q, S.

* The values obtained will be in terms of X as unit of velocity.

To avoid these objections the group of equations (4.2), (4.3), (4.4) could be used to determine $A_1, B_1, C_1, F_1, G_1, H_1$, which again permits the evaluation * of the lengths † and directions of the axes of the velocity ellipsoid. If a large number of regions are available, the corresponding normal equations might be combined, in order to reduce the computation required.

6. *Special Cases.*—If the centres of the regions considered lie on a small circle on the celestial sphere a least-squares solution by means of equation (4.5) will not be completely determinate.

For, consider the set of equations

$$a_{1r}x_1 + a_{2r}x_2 + \ . \ . \ . \ a_{mr}x_m = l_r, \tag{6.1}$$

in which $r = 1, 2, 3, \ . \ . \ . \ n$, $(n > m)$, the a's and l's being observed (or known) coefficients and the x's linearly independent unknowns. If, for all values of r, there exists a relation

$$\alpha_1 a_{1r} + \alpha_2 a_{2r} + \ . \ . \ . \ \alpha_m a_{mr} = 0, \tag{6.2}$$

where the α's are constants which are not all zero, say $\alpha_k \neq 0$, then (6.1) can be written

$$a_{1r}\left(x_1 - \frac{\alpha_1}{\alpha_k}x_k\right) + a_{2r}\left(x_2 - \frac{\alpha_2}{\alpha_k}x_k\right) + \ . \ . \ . \ a_{mr}\left(x_m - \frac{\alpha_m}{\alpha_k}x_k\right) = l_r, \tag{6.3}$$

an equation which is now linear in the $(m-1)$ independent variables

$$x_1 - \frac{\alpha_1}{\alpha_k}x_k, \qquad x_2 - \frac{\alpha_2}{\alpha_k}x_k, \qquad . \ . \ ., \qquad x_m - \frac{\alpha_m}{\alpha_k}x_k.$$

Hence the application of the method of least squares to equation (6.1) would give only $(m-1)$ independent normal equations.‡

Now suppose that the centres of the regions considered are distributed on the celestial sphere in such a manner that a second degree cone of vertex O can be drawn to pass through the centre of each region. Referred to any set of rectangular axes through O the equation of this cone will be of form

$$\alpha_1 x^2 + \alpha_2 y^2 + \alpha_3 z^2 + 2\alpha_4 yz + 2\alpha_5 zx + 2\alpha_6 xy = 0, \tag{6.4}$$

where the α's are constants which are not all zero.

If the direction-cosines of the centre of the r^{th} region, S_r, are (l_{3r}, m_{3r}, n_{3r}) then, since OS_r is a generator of the cone,

$$\alpha_1 l_{3r}^2 + \alpha_2 m_{3r}^2 + \alpha_3 n_{3r}^2 + 2\alpha_4 m_{3r}n_3 + 2\alpha_5 n_{3r}l_{3r} + 2\alpha_6 l_{3r}m_{3r} = 0 \tag{6.5}$$

for all values of r. Comparing (4.5) with (6.1) it is seen that (6.5) constitutes a relation between the coefficients of A, B, C, F, G, H in (4.5) analogous to the relation given by (6.2) between the coefficients of $x_1, x_2, \ . \ . \ . \ x_m$ in (6.1). Hence if the centres of the regions are distributed as stated, the method of least squares will not give a completely determinate solution.

This will occur, for example, if the regions are part of a narrow zone of declination, in which case their centres will lie on a small circle and a right circular cone of vertex O can be found to pass through each.

7. *Reduced Solutions.*—Analytically, the method of solution given at the end of section 5 provides a complete solution of the problem, although, as A, B, C, F, G, H are assumed to be constant, or sensibly constant, the material used should be restricted to stars of a single spectral type. In many practical cases, however, paucity of material

* *Cf.* Smart, *op. cit.*, p. 173.

† The values obtained will be in terms of X as unit of velocity.

‡ *Cf.* D. Brunt, *Combination of Observations*, p. 79, Cambridge, 1923.

makes it desirable to combine data for more than one spectral type. With an additional assumption, that the ratios and directions of the axes of the velocity ellipsoid are the same but the scale of the ellipsoid varies from type to type *, Smart's coefficients P, Q, S can still be used to determine the ratios and directions of the axes. For, with this assumption, variations in the spectral composition from region to region will not alter the eccentricity or orientation of the corresponding velocity ellipse, while variations in scale can be eliminated by using equations involving only the ratios $P : Q : S$ and not the absolute values.

Even for material of a single spectral type, the use of the ratios of P, Q, S presents one important advantage. From (4.2), (4.3), (4.4), the values of P, Q, S are inversely proportional to $(X \sin \lambda)^2$. Hence any accidental or systematic errors of the proper motions of stars in a particular region which produce a deviation of the (effective) projected solar motion from the theoretical value, $X \sin \lambda$, will introduce a scale error in P, Q, S as computed for the region. This scale error should be most pronounced when $\sin \lambda$ is small, *i.e.* near the solar apex or antapex; in these areas the scale of P, Q, S will be practically indeterminate. Indeed, since empirical considerations (see sections 11, 14) suggest that the method of analysing each region gives a much less reliable estimate of the scale of the velocity ellipse than of the other characteristics, it appears advisable to use only the ratios $P : Q : S$ in obtaining the directions and ratios of the axes of the velocity ellipsoid.

8. Let ϵ be the eccentricity of the velocity ellipse $pu^2 + 2suv + qv^2 = 1$ and ϕ_0 the angle between Ou and the major axis. Then, in choosing a function of the ratios $P : Q : S$ from which to form an equation of condition for each region,

(i) the function chosen should depend on both ϵ and ϕ_0; if possible it should be capable of a simple interpretation in terms of ϵ and ϕ_0 so that exceptional values of these can be recognised and discussed,

(ii) any weight given to the derived equation should depend on the accuracy with which the ratios $P : Q : S$ are determined and not on the values of ϵ and ϕ_0, *e.g.* the equation should not vanish where the velocity ellipse is almost circular nor at other special points on the celestial sphere.

The most suitable functions appear to be

$$\mu = \frac{Q-P}{Q+P} = \frac{q-p}{q+p} = \frac{\epsilon^2}{2-\epsilon^2} \cos 2\phi_0 \tag{8.1}$$

and the corresponding function

$$\nu = \frac{2S}{Q+P} = \frac{2s}{q+p} = \frac{\epsilon^2}{2-\epsilon^2} \sin 2\phi_0. \tag{8.2}$$

Substituting for P, Q, S from equations (4.2), (4.3), (4.4) we get, as equations of condition for each region,

$$\begin{aligned} &A_1\{l_1^2(\mu-1) + l_2^2(\mu+1)\} + B_1\{m_1^2(\mu-1) + m_2^2(\mu+1)\} + C_1\{n_1^2(\mu-1) + n_2^2(\mu+1)\} \\ &\quad + 2F_1\{m_1n_1(\mu-1) + m_2n_2(\mu+1)\} + 2G_1\{n_1l_1(\mu-1) + n_2l_2(\mu+1)\} \\ &\quad + 2H_1\{l_1m_1(\mu-1) + l_2m_2(\mu+1)\} = 0 \end{aligned} \tag{8.3}$$

and

$$\begin{aligned} &A_1\{\nu(l_1^2 + l_2^2) + 2l_1l_2\} + B_1\{\nu(m_1^2 + m_2^2) + 2m_1m_2\} + c_1\{\nu(n_1^2 + n_2^2) + 2n_1n_2\} \\ &\quad + 2F_1\{\nu(m_1n_1 + m_2n_2) + (m_2n_1 + m_1n_2)\} + 2G_1\{\nu(n_1l_1 + n_2l_2) + (n_1l_2 + n_2l_1)\} \\ &\quad + 2H_1\{\nu(l_1m_1 + l_2m_2) + (l_2m_1 + l_1m_2)\} = 0. \end{aligned} \tag{8.4}$$

* For O- and B-type stars the preferential motion is much less pronounced than in later types. As the proportion of O and B stars, especially among faint stars, is usually small, they can be omitted in many cases.

Solving these equations by the method of least squares gives the ratios

$$A_1 : B_1 : C_1 : F_1 : G_1 : H_1 ,$$

from which the ratios and directions of the velocity ellipsoid can be obtained.

9. Fleming, who derived * the analytical relations on which Smart's method is based, gives an equation of condition for each region of the form †

$$h_0h_1A_0 + j_0j_1B_0 + k_0k_1C_0 + (j_0k_1 + j_1k_0)F_0 + (k_0h_1 + h_0k_1)G_0 + (h_0j_1 + h_1j_0)H_0 = 0, \quad (9.1)$$

where

$h_0 \equiv h(\theta_0) \equiv -\sin\alpha\cos\theta_0 + \cos\alpha\sin\theta_0\sin\delta,$
$j_0 \equiv j(\theta_0) \equiv \cos\alpha\cos\theta_0 + \sin\alpha\sin\theta_0\sin\delta,$
$k_0 \equiv k(\theta_0) \equiv -\sin\theta_0\cos\delta,$
$h_1 \equiv h(\theta_1), \quad k_1 \equiv k(\theta_1), \quad j_1 \equiv j(\theta_1),$
θ_0 = Position angle of direction from centre of region R(α, δ) to solar apex,
θ_1 = Position angle of conjugate diameter of velocity ellipse
$= \tan^{-1}\{-(S\sin\theta_0 + Q\cos\theta_0)/(P\sin\theta_0 + S\cos\theta_0)\}.$

Equation (9.1) involves only the ratios $P : Q : S$ and thus is free from the effects of scale errors. On the other hand, if the equation of the velocity ellipse is known ‡ for the region, the choice of the direction to the solar apex and the conjugate direction rather than any other pair of conjugate diameters is extremely arbitrary. In particular, for regions near the solar apex (or antapex), where the projected solar motion is small, θ_0 will be badly determined although the velocity ellipse may be well defined.

10. *Application to Observations.*—As a test of its practical value, Smart's method of analysis was applied to a number of regions. The proper motions used were taken from those published by the Royal Observatory, Cape of Good Hope, for almost 20,000 stars lying in the zone between declination $-40°$ and $-52°$. § The zone was divided into 16 regions of equal area, bounded by the meridians of R.A. 0^h, $1\frac{1}{2}^h$, 3^h, . . . $22\frac{1}{2}^h$. For the distribution in position angle of the proper motions in these regions I am indebted to Prof. W. M. Smart and Mr. T. R. Tannahill, who placed at my disposal the tables prepared during their analysis of the same material on the two-stream theory. ‖ Table I gives the right ascension, number of stars used ¶, galactic co-ordinates, and the values of P, Q, S, θ_0, λ for each region. From the values of θ_0, the position of the solar apex was found to be in

Right Ascension, $A_0' = 270°{\cdot}6 \pm 0{\cdot}6$ (p.e.).
Declination, $D_0' = 26°{\cdot}0 \pm 0{\cdot}4$ (p.e.).

Using this position, λ was calculated for each region.

The position found for the solar apex by Jackson **, who used Schwarzschild's automatic method (spheroidal hypothesis) to analyse the motions, was $A_0' = 266°{\cdot}9$, $D_0' = 28°{\cdot}3$. As the same criterion is used to find θ_0, the small difference in the actual result must be due to the different division of the zone into regions. Independent

* J. Fleming, *M.N.*, **97**, 173, 1937.

† This corresponds to Fleming's equation (10.3), *loc. cit.*, p. 180. The coefficient of $\bar{F}$ in his equation should be $2(l_2l_3 + \sigma\lambda m_2m_3) - (\sigma + \lambda)(l_2m_3 + l_3m_2)$ and similar corrections are required in the coefficients of $\bar{G}$ and $\bar{H}$.

‡ Fleming gives a graphical method of determining θ_0 and θ_1, and thus proceeds to the velocity ellipsoid without evaluating the velocity ellipse for each region explicitly.

§ *Proper Motions of Stars in the Zone Catalogue of 20,843 Stars*, 1936.

‖ W. M. Smart and T. R. Tannahill, *M.N.*, **100**, 30, 1939. Details of the apparent magnitudes, reduction of observations, etc., are given in this paper and by Dr. J. Jackson in his introduction to the *Proper Motions Catalogue.*

¶ Smart and Tannahill, *loc. cit.*, p. 31, note.

** J. Jackson, introduction to *Cape Proper Motions Catalogue*, p. xxxiii.

confirmation of the low declination * is provided by Smart and Tannahill's analysis † which gave $A_0' = 265°{\cdot}1$, $D_0' = 26°{\cdot}1$.

Table I

Region	R.A. of Centre	No. of Stars	Galactic Co-ordinates		P	Q	S	θ_0	λ
			Long.	Lat.					
	h m		°	°				°	°
I	0 45	638	267·1	−72·2	4·41	11·49	0·57	100	115·5
II	2 15	564	229·9	−64·2	14·08	39·69	−16·75	86	131·1
III	3 45	706	218·9	−49·7	10·38	10·27	− 5·67	56	146·2
IV	5 15	819	218·3	−34·0	40·99	34·32	−13·64	3	158·0
V	6 45	1112	222·6	−18·8	9·49	5·09	+ 1·15	324	158·3
VI	8 15	2000	230·2	− 5·1	3·09	3·05	+ 1·05	294	146·9
VII	9 45	1538	241·0	+ 6·2	1·29	1·85	+ 0·64	274	131·8
VIII	11 15	1179	254·9	+13·7	1·09	3·22	+ 0·53	262	116·3
IX	12 45	1271	270·9	+16·2	0·68	2·12	− 0·06	248	101·5
X	14 15	1382	286·8	+13·1	0·93	1·72	− 0·30	231	88·5
XI	15 45	1773	300·4	+ 5·1	0·89	1·34	− 0·27	212	78·4
XII	17 15	1817	310·8	− 6·5	1·01	0·71	− 0·11	191	72·8
XIII	18 45	1172	318·1	−20·5	1·47	1·04	− 0·06	176	72·6
XIV	20 15	872	321·9	−35·8	2·29	2·49	+ 0·55	154	78·0
XV	21 45	760	320·6	−51·4	2·90	5·53	− 0·15	144	87·9
XVI	23 15	746	307·6	−65·5	4·84	6·21	+ 0·48	134	100·8

Table II

Region	$(P+Q)\sin^2\lambda$		$(PQ-S^2)\sin^4\lambda$		$\frac{\sqrt{(PQ-S^2)}}{P+Q}$		$\frac{Q-P}{Q+P}$
	Observed	Calculated	Observed	Calculated	Observed	Calculated	
I	12·96	4·00	33·43	3·22	0·45	0·45	+0·453
II	30·60	3·97	90·16	3·20	0·31	0·45	+0·476
III	6·38	3·81	7·07	3·02	0·42	0·46	−0·005
IV	10·62	3·68	24·41	2·87	0·46	0·46	−0·089
V	2·00	3·67	0·89	2·86	0·47	0·46	−0·302
VI	1·83	3·81	0·74	3·01	0·47	0·46	−0·007
VII	1·75	3·97	0·61	3·19	0·45	0·45	+0·178
VIII	3·46	4·00	2·08	3·23	0·37	0·45	+0·494
IX	2·69	3·80	1·33	3·01	0·43	0·46	+0·514
X	2·65	3·41	1·51	2·57	0·46	0·47	+0·298
XI	2·14	2·97	1·03	2·08	0·47	0·49	+0·202
XII	1·57	2·68	0·59	1·75	0·49	0·49	−0·174
XIII	2·28	2·67	1·27	1·74	0·49	0·49	−0·170
XIV	4·57	2·96	4·94	2·07	0·49	0·49	+0·042
XV	8·41	3·40	15·96	2·55	0·30	0·47	+0·312
XVI	10·65	3·79	27·71	3·00	0·49	0·46	+0·124

* Attributed by Jackson to the introduction of a correction for galactic rotation in reducing the proper motions.

† Smart and Tannahill, *loc. cit.*, p. 40.

11. For comparison $(P+Q)\sin^2\lambda$ and $(PQ-S^2)\sin^4\lambda$ were computed for each region for an assumed velocity ellipsoid

$$\frac{x^2}{\sigma_1^2}+\frac{y^2}{\sigma_2^2}+\frac{z^2}{\sigma_3^2}=1, \tag{11.1}$$

such that Ox, Oy lie in the galactic plane in the direction of galactic longitudes 340° and 70° respectively, Oz is toward the Galactic Pole, $\sigma_2=\sigma_3=\frac{5}{8}\sigma_1$ and $\frac{\sigma_1}{X}=1{\cdot}7$. This corresponds, roughly, to Jackson's solution for all spectral types * ; the computed values of $(P+Q)\sin^2\lambda$ and $(PQ-S^2)\sin^4\lambda$ may be regarded as corresponding to the average spectral distribution over the whole zone. Table II shows that for high galactic latitudes the observed values are greater and for low galactic latitudes less than the computed values.

With the assumption made in section 7, this effect agrees qualitatively with expectation, since $(P+Q)\sin^2\lambda$ is then proportional to $\bar{r}^2/X^2$, where $\bar{r}$ is the mean peculiar velocity of the stars considered. Table III, which is taken from an analysis of radial

Table III

Spectral Type	B	A	F	G	K	M
r (kms./sec.)	8·7	9·9	12·5	14·8	15·3	16·1
X (kms./sec.)	22·7	18·6	19·7	18·6	18·0	22·1
$(r/X)^2$	0·15	0·28	0·40	0·63	0·72	0·53

velocities by Campbell and Moore †, indicates that for low galactic latitudes, where the percentage of early-type stars is a maximum, the value of $\bar{r}^2/X^2$ will be smaller than the average and in high galactic latitudes it will be above average. As Campbell and Moore's figures are for stars brighter than visual magnitude $5^m{\cdot}51$, the increased percentage of G, K and M-type dwarfs among fainter stars might make the change of $\bar{r}/X$ with latitude even more marked.

On taking the ratios $\sqrt{PQ-S^2}/(P+Q)$ for each region, the agreement between observed and computed values appears more satisfactory (see Table II, cols. 6, 7). It should be noted, however, that $\sqrt{PQ-S^2}/(P+Q)$, which is a function ‡ of the eccentricity ϵ of the velocity ellipse, varies very slowly with ϵ, when ϵ is small.

12. *Evaluation of Velocity Ellipsoid.*—Instead of applying the method of section 8 as it stands, advantage was taken of the constant declination of the centres of the regions to use a variant method applicable to this special case. Using equations (5.1), (5.2) and (3.1),

$$\frac{Q-P}{Q+P}=\frac{a_1+a_2\cos\alpha+a_3\sin\alpha+a_4\cos 2\alpha+a_5\sin 2\alpha}{b_1+b_2\cos\alpha+b_3\sin\alpha+b_4\cos 2\alpha+b_5\sin 2\alpha}, \tag{12.1}$$

where

$$\left.\begin{aligned} a_1&=\tfrac{1}{2}(A_1+B_1-2C_1)\cos^2\delta,\\ a_2&=G_1\sin 2\delta,\\ a_3&=F_1\sin 2\delta,\\ a_4&=\tfrac{1}{2}(B_1-A_1)(1+\sin^2\delta),\\ a_5&=-H_1(1+\sin^2\delta). \end{aligned}\right\} \tag{12.2}$$

$$\left.\begin{aligned} b_1&=\tfrac{1}{2}(A_1+B_1)(1+\sin^2\delta)+C_1\cos^2\delta,\\ b_2&=-G_1\sin 2\delta,\\ b_3&=-F_1\sin 2\delta,\\ b_4&=\tfrac{1}{2}(B_1-A_1)\cos^2\delta,\\ b_5&=-H_1\cos^2\delta. \end{aligned}\right\} \tag{12.3}$$

* J. Jackson, introduction to *Cape Proper Motions Catalogue*, p. xxxiii.

† W. W. Campbell and J. H. Moore, *Publ. Lick Obs.*, **16**, Introd., xxviii, 1928.

‡ Actually $\frac{\sqrt{1-\epsilon^2}}{2-\epsilon^2}=\frac{1}{2}-\frac{\epsilon_4}{16}+$higher powers of ϵ.

Hence

$$\left.\begin{aligned} a_2 &= -b_2, & a_4 &= \beta b_4, \\ a_3 &= -b_3, & a_5 &= \beta b_5, \end{aligned}\right\} \quad \text{where} \quad \beta = \frac{1+\sin^2\delta}{\cos^2\delta}. \tag{12.4}$$

For the Cape regions, $\delta = -45^\circ\,45'$, and thus $a_1, a_2, \ldots a_5, b_1, b_2, \ldots b_5, \beta$ are constants. For the k^{th} region, $\alpha = \dfrac{2k-1}{16}\pi$.

Now consider the expression

$$\Phi \equiv [(b_1 + b_2\cos\alpha + b_3\sin\alpha + b_4\cos 2\alpha + b_5\sin 2\alpha)$$
$$\times \{c_0 + \sum_{r=1}^{7} 2(c_r\cos r\alpha + s_r\sin r\alpha) + s_8\sin 8\alpha\}]$$
$$- [a_1 + a_2\cos\alpha + a_3\sin\alpha + a_4\cos 2\alpha + a_5\sin 2\alpha],$$

in which the a's and b's are assumed to be known and $c_{0,1,2,\ldots 7}$, $s_{1,2,3,\ldots 8}$, which will be denoted collectively by $\Gamma(c, s)$, are constants.

If $\alpha = \dfrac{2k-1}{16}\pi$, where $k = 1, 2, 3, \ldots$, then

$$\cos 8\alpha = \cos\frac{2k-1}{2}\pi = 0,$$

$$\cos 9\alpha = \cos\{(2k-1)\pi - 7\alpha\} = \cos(\pi + 7\alpha) = -\cos 7\alpha.$$

Similarly,

$$\cos 10\alpha = -\cos 6\alpha, \qquad \sin 9\alpha = \sin 7\alpha, \qquad \sin 10\alpha = \sin 6\alpha.$$

Hence, if $\alpha = \dfrac{2k-1}{16}\pi$, $k = 1, 2, 3, \ldots$, Φ can be written in the form

$$\Phi = L_0 + \sum_{r=1}^{7}\{L_r\cos r\alpha + M_r\sin r\alpha\} + M_8\sin 8\alpha, \tag{12.5}$$

where the L's and M's are linear functions of $\Gamma(c, s)$ and are independent of k, *i.e.*

$$\left.\begin{aligned} L_0 &\equiv b_1c_0 + b_2c_1 + b_3s_1 + b_4c_2 + b_5s_2 - a_1, \\ L_1 &\equiv 2b_1c_1 + b_2(c_0 + c_2) + b_3s_2 + b_4(c_1 + c_3) + b_5(s_1 + s_3) - a_2, \\ M_1 &\equiv 2b_1s_1 + b_2s_2 + b_3(c_0 - c_2) + b_4(s_3 - s_1) + b_5(c_1 - c_3) - a_3, \\ L_2 &\equiv 2b_1c_2 + b_2(c_1 + c_3) + b_3(s_3 - s_1) + b_4(c_0 + c_2) + b_5s_4 - a_4, \\ M_2 &\equiv 2b_1s_2 + b_2(s_1 + s_3) + b_3(c_1 - c_3) + b_4s_4 + b_5(c_0 - c_4) - a_5. \\ &\ldots\ldots\ldots\ldots\ldots\ldots\ldots\ldots\ldots\ldots\ldots\ldots \end{aligned}\right\} \tag{12.6}$$

In general, if we solve the 16 equations $L_0 = 0$, $L_1 = 0$, $M_1 = 0$, $\ldots$ $M_8 = 0$, unique values of the 16 constants $\Gamma(c, s)$ will be obtained. With these values of $\Gamma(c, s)$

$$\Phi = 0, \quad \text{for } \alpha = \frac{2k-1}{16}\pi, \quad k = 1, 2, 3, \ldots$$

and

$$\mu(k) = \frac{a_1 + a_2\cos\alpha + a_3\sin\alpha + a_4\cos 2\alpha + a_5\sin 2\alpha}{b_1 + b_2\cos\alpha + b_3\sin\alpha + b_4\cos 2\alpha + b_5\sin 2\alpha}$$
$$= c_0 + \sum_{r=1}^{7} 2(c_r\cos r\alpha + s_r\sin r\alpha) + s_8\sin 8\alpha. \tag{12.7}$$

Thus, in general, coefficients $\Gamma(c, s)$ can be found to satisfy (12.7) for the given values of α.

13. From (12.7), if $\alpha = \frac{2k-1}{16}\pi$, $t = 0, 1, 2, \ldots 8$,

$$\sum_{k=1}^{16} \mu(k) \cos t\alpha = c_0 \sum_{k=1}^{16} \cos t\alpha + 2 \sum_{k=1}^{16} \sum_{r=1}^{7} \{c_r \cdot \cos r\alpha \cos t\alpha + s_r \sin r\alpha \cos t\alpha\}$$
$$+ s_8 \cdot \sum_{k=1}^{16} \sin 8\alpha \cos t\alpha = 16 c_t,$$

since

$$\sum_{k=1}^{16} \cos r\alpha \cos t\alpha \begin{cases} = 8, & \text{if } r = t \\ = 0, & \text{if } r \neq t \end{cases}$$

and

$$\sum_{k=1}^{16} \sin r\alpha \cos t\alpha = 0.$$

Similarly,

$$\sum_{k=1}^{16} \mu(k) \sin t\alpha = 16 s_t.$$

Conversely, if the a's and b's are not known explicitly, but $\mu(k)$ is known for $k = 1, 2, 3, \ldots 16$, and coefficients $\Gamma(c, s)$ are found by means of the equations

$$c_r = \frac{1}{16} \sum_{k=1}^{16} \mu(k) \cos r\alpha; \qquad s_r = \frac{1}{16} \sum_{k=1}^{16} \mu(k) \sin r\alpha, \tag{13.1}$$

where $r = 0, 1, 2, 3, \ldots 8$, then these coefficients will satisfy (12.7) and, consequently, the equations $L_0 = 0$, $L_1 = 0$, $M_1 = 0$, . . .

This suggests the following practical procedure:—

(i) tabulate $\mu(k) = \frac{Q-P}{Q+P}$ for each region (*cf.* Table II),

(ii) evaluate c_0, c_1, c_2, c_3, c_4, s_1, s_2, s_3, s_4 by means of equations (13.1),

(iii) use relations (12.4) to express L_1, M_1, L_2, M_2 in terms of b_1, b_2, b_3, b_4, b_5,

(iv) solve the equations $L_0 = 0$, $L_1 = 0$, $M_1 = 0$, $L_2 = 0$, $M_2 = 0$ for the ratios $a_1 : b_1 : b_2 : b_3 : b_4 : b_5$,

(v) use equations (12.2) and (12.3) to evaluate the ratios $A_1 : B_1 : C_1 : F_1 : G_1 : H_1$ from the ratios $a_1 : b_1 : b_2 : b_3 : b_4 : b_5$.

14. The above method gave

$$A_1 = 4{\cdot}69, \quad C_1 = 3{\cdot}15, \quad G_1 = 0{\cdot}29,$$
$$B_1 = 10{\cdot}32, \quad F_1 = 0{\cdot}22, \quad H_1 = -0{\cdot}72,$$

the values being in terms of an arbitrary unit. This solution corresponds to a velocity ellipsoid having its

longest * axis in direction	$\alpha = 97°{\cdot}0$,	$\delta = 3°{\cdot}0$,	or	$G = 355°{\cdot}9$,	$g = 1°{\cdot}2$,
shortest axis in direction	$\alpha = 194°{\cdot}0$,	$\delta = 78°{\cdot}2$,	or	$G = 88°{\cdot}9$,	$g = 39°{\cdot}6$,
and intermediate * axis in direction	$\alpha = 6°{\cdot}8$,	$\delta = 10°{\cdot}9$,	or	$G = 265°{\cdot}0$,	$g = 51°{\cdot}0$.

The ratios of the shorter axes to the longest are 0·54 and 0·67 respectively.

It is doubtful how much significance can be attached to the observed difference in intensity of streaming along the two shorter axes. As their directions bear no distinct relation to the galactic plane, it appears probable that the distribution of velocities perpendicular to the principal axis of star-streaming is practically random and that the distribution in three dimensions is represented sufficiently by a spheroidal frequency-law.

* The equatorial and galactic co-ordinates given correspond to opposite ends of the axis.

Jackson's solution * (for spectral types A5 – M) gave for the direction of preferential motion ($\alpha = 90°{\cdot}2$, $\delta = 13°{\cdot}4$) or ($G = 343°{\cdot}6$, $g = 2°{\cdot}1$) and for the ratio of the shorter axes to the greatest 0·62. The position of the vertex found by Smart and Tannahill by analysing the present material on the two-stream theory † agrees closely with that found by Jackson, being ($\alpha = 91{\cdot}5$, $\delta = 14{\cdot}5$), *i.e.* ($G = 343{\cdot}2$, $g = 0{\cdot}5$).

The outstanding discrepancy between the above results and those of the present investigation is the difference in galactic longitude of the positions found for the vertex, This difference, which corresponds almost entirely to the difference in declination, may be due to the disposition of the regions on a small circle of declination which makes them more suitable for a determination of right ascension than of declination. This difficulty appears also from the longitudes of the regions, which lie within a range of 105 degrees.

Summary

On the basis of a particular method of analysing the proper motions of stars in a small region of the sky, the eccentricity, orientation and scale of the velocity ellipse for the region can be obtained. The paper discusses the problem of combining such determinations of the velocity ellipse in different parts of the sky into a determination of the velocity ellipsoid.

It is found that little reliance can be placed on the value obtained for the scale of the velocity ellipse, which is determined in terms of the projected solar motion for the region. (Near the solar apex it will become completely indeterminate.) It is preferable therefore to use only the eccentricity ϵ of the ellipse and the orientation angle ϕ_0 of the major axis. Further, in choosing the quantities to be given equal weight in the solution, it is to be noticed that ϕ_0 becomes indeterminate when $\epsilon = 0$. The most suitable quantities to use in deriving the velocity ellipsoid appear to be

$$\mu = \frac{\epsilon^2}{2 - \epsilon^2} \cos 2\phi_0 \quad \text{and} \quad \nu = \frac{\epsilon^2}{2 - \epsilon^2} \sin 2\phi_0.$$

The corresponding equations of condition are given in section 8.

The results of applying the analysis to regions in the Cape Astrographic Zone ($-40°$ to $-52°$) are given and by means of a variant method, applicable to this particular case, the corresponding velocity ellipsoid is deduced.

In conclusion, I should like to thank Prof. Sir A. S. Eddington and Prof. W. M. Smart for their advice, suggestions, and encouragement during the course of this work.

17 *Murdieston Street,*
Greenock:
1941 *June* 5.

* Jackson, *loc. cit.*, p. xxxiii.
† Smart and Tannahill, *loc. cit.*, p. 40.

XZ AURIGÆ: AN N-TYPE VARIABLE

G. Alter and D. L. Edwards

(Received 1941 June 6)

An accidental comparison of a photovisual plate of a star field with the corresponding Franklin-Adams chart showed the surprising fact that XZ Aur (R.A. $5^h\ 56^m\ 59^s$, Dec. $+47°\ 17'{\cdot}3$, 1900·0), recorded by Prager * and Schneller † as possibly a β Lyræ star, is not present on the F.-A. chart (limiting magnitude about 15), while it appeared on the Sidmouth photovisual plate as a rather bright star of about 10^m. Some further exposures were therefore taken (both photographic and photovisual) before the region disappeared in the twilight, but unsatisfactory weather conditions prevented continuous observations, especially when it was clear that XZ Aur had a colour index of about $+4^m$, so that the exposure-time for photographic magnitudes had to be fairly long to get a star image at all with the Mond Astrograph.

Thirty-four comparison stars were chosen in the surrounding region, and Table I gives their co-ordinates and magnitudes, the latter being determined with the help of the

TABLE I

Comparison Stars of XZ Aur

Unit = 1′·0 X = West, Y = North Zero = Star 27

Star	X	Y	m_p	m_{pv}	Star	X	Y	m_p	m_{pv}
1	+25·7	+41·7	10·35	10·75	18	+8·2	+15·4	12·78	12·90
2	+24·9	+44·3	10·61	10·45	19	+8·5	+ 7·2	12·74	12·62
3	+24·2	+39·4	9·82	9·62	20	+7·0	+ 3·5	10·27	9·94
4	+22·3	+42·9	10·47	10·42	21	+4·7	+16·1	12·06	12·03
5 *	+21·1	+42·2	7·09	6·68	22	+4·8	+ 4·7	12·50	12·56
6	+16·6	+ 6·8	11·01	11·16	23	+3·8	+11·1	12·40	12·48
7	+15·9	+ 9·7	11·79	11·48	24	+3·2	+11·6	13·29	13·40
8	+14·7	+ 0·3	10·76	9·56	25	+2·2	+ 7·4	12·16	10·50
9	+14·4	+ 4·5	13·19	13·19	26	+1·3	+10·4	11·99	12·67
10	+13·7	− 0·7	11·85	10·54	27 †	0·0	0·0	8·64	8·26
11	+12·1	+ 8·3	12·02	12·22	28	−0·8	+14·4	12·48	12·06
12	+11·6	+14·7	12·05	12·54	29	−1·5	+15·1	12·53	12·86
13	+11·6	+ 7·7	11·22	11·23	30	−1·8	+16·2	12·13	12·50
14	+11·8	+ 1·4	12·23	12·70	31	−2·2	+12·4	12·56	12·78
15	+10·0	+ 8·8	12·85	12·89	32	−2·4	+10·3	11·62	11·65
16	+ 9·6	+13·9	11·02	10·66	33	−2·2	+ 4·3	12·02	12·36
17	+ 9·3	+16·8	13·28	13·60	34	−2·9	− 9·3	dist.	12·48

* Star 5 = H.D. 40650 = B.D. 47° 1236. † Star 27 = H.D. 40995 = B.D. 47° 1242.

N.B.—The stars 8, 10, 25 are red stars, and are therefore specially suitable for visual comparisons in this magnitude range.

North Polar Sequence.‡ The magnitude range of these comparison stars is large enough to exceed that of XZ Aur in the photovisual scale; it is, however, not large enough to secure the extension for the fainter photographic magnitudes, because the available

* *G.u.L.*, 114, 1934. † *Kl. Ver. Berlin-Bab.*, **20**, 27, 1938. ‡ *M.N.*, **100**, 387, 1940.

apertures are too small. The mean error of the photographic magnitudes for stars fainter than 13 is ± 0·20, for the photovisual magnitudes ± 0·10; the mean error of the colour index is therefore ± 0·22.

The results for XZ Aur are given in Table II. As will be seen, we were able to secure both photographic and photovisual magnitudes on three occasions only. On

TABLE II

XZ Aur

Date 1941	J.D. 240000 +	m_p	m_{pv}	CI	Date 1941	J.D. 240000 +	m_p	m_{pv}	CI
Jan. 3	2998		9·9		Feb. 21	3047		10·2	
9	3004		9·8		24	3050		9·9	
10	3005		10·1		Mar. 19	3073	14·9	9·9	+5·0
Feb. 1	3027	14·9	10·9	+4·0	30	3084	14·3	10·5	+3·8

February 1 the photographic exposure had to be cut short because of cloud. On March 19 the photographic exposure was extended to 2^h to secure sufficient intensity. The exposures of March 30 were used for the magnitude determinations of the comparison stars.

In view of the large colour index of this star, an attempt was made to obtain its spectrum with the 12-inch McClean objective prism, using Ilford Hypersensitive Panchromatic plates. Owing to poor weather conditions and the faintness of the star (near the limiting magnitude obtainable with this instrument) it was impossible to get good photographs. The best, taken on March 30 with 3^h exposure, was very narrow and of poor definition. It was, however, sufficient to show the following features: (1) The spectrum was not visible in wave-lengths shorter than 5290 A., though stars of similar, or fainter, magnitudes on the same plate showed much greater extension to the violet. (2) The region of maximum density (quite pronounced) was at approximately 6000–6600 A. (3) Broad absorption lines or bands were detected at approximately the following wave-lengths (accurate measures were not possible): 5640, 5890, 5970, 6060, 6120; the first two of these being the most prominent. Although somewhat crude, these observations indicate that the spectrum is probably of type N. A remark by Merrill * that "In advanced N-type variables . . . it is properly said that there is almost no blue and violet light," and the H.D. description of the typical Nc star S Cep "there is little or no light below Hβ," is in accordance with (1) above, while the additional H.D. remark that the most brilliant portion of the spectrum is from 5900–6800 is in good agreement with (2). Three of the absorption bands mentioned in (3) correspond reasonably well with the more prominent "Swan" bands of carbon in this region, viz. those with heads at 5636, 6060, 6122. These are described by Shane † as "the most striking features of the class N spectra," with 5636 more conspicuous than the other two. The observed absorption at 5890 is almost certainly the sodium [D] lines, described by Shane as "very broad and heavy" in N-type stars. "In no other known spectral type do the sodium lines have nearly the intensity shown in the class N stars." No origin can be suggested for 5970, but it appears fainter than the others and may possibly be spurious.

It therefore seems reasonably certain that the spectrum of XZ Aur is of late N type, and this is supported by the large colour index, concerning which Merrill has said (*loc. cit.*) "As far as I am aware, every star in the sky with a measured colour index exceeding 2·5 has a spectral class N or R."

* *Spectra of Long-period Variable Stars*, p. 29, 1940. † *L.O.B.*, No. 329, 85, 1920.

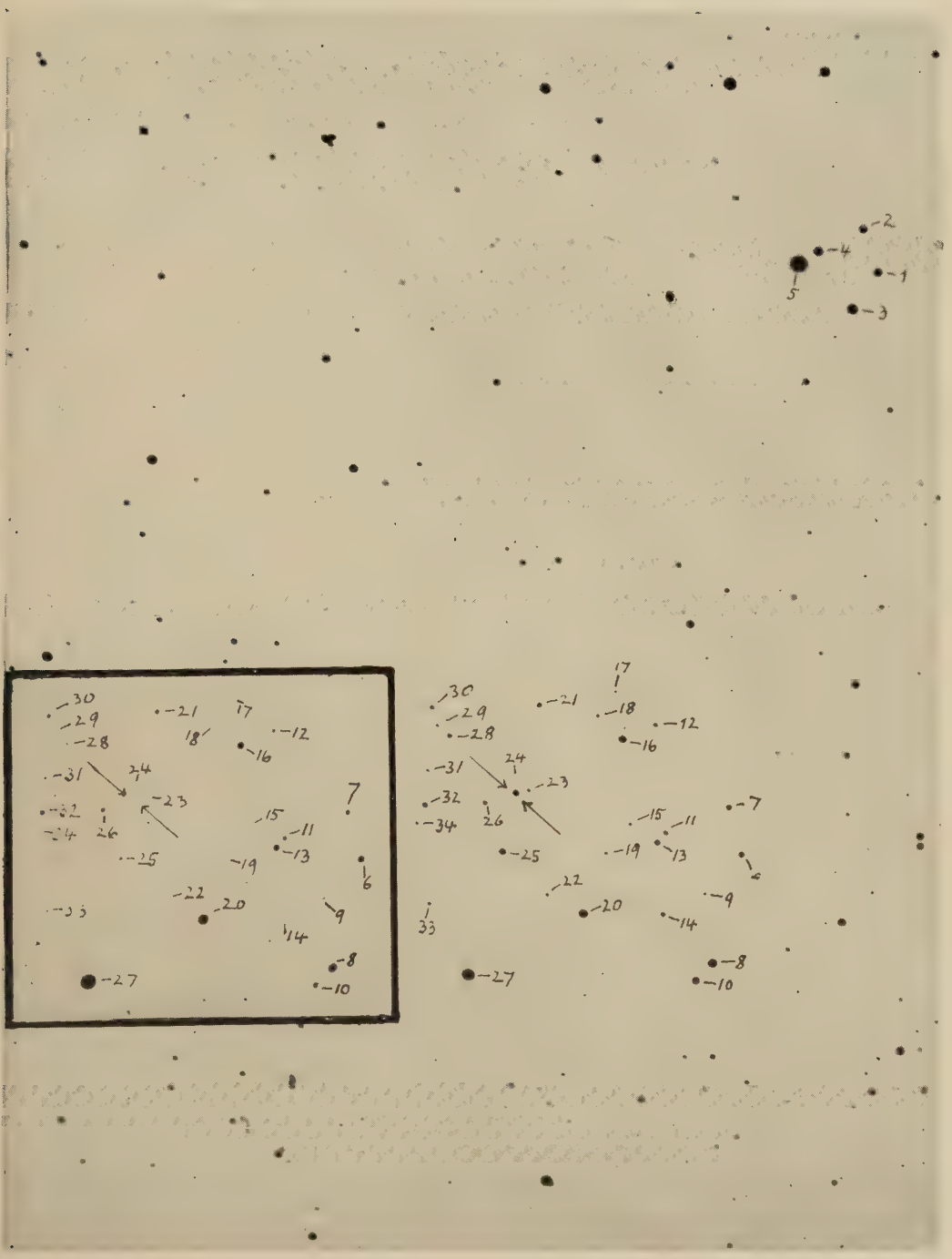

XZ Aurigæ.

Photovisual plate of region with 1^h exposure. Inset: central part of photographic plate of same region, 2^h exposure. XZ Aur indicated by arrows.
Magnitudes of XZ: $m_{pv}=10{\cdot}9$; $m_p=14{\cdot}9$ (probably not visible in reproduction).

G. Alter and D. L. Edwards, XZ Aurigæ: An N-Type Variable.

Summary

Observations of XZ Aurigæ show that this star is not a β Lyræ type as previously suggested, but has a very large colour index of +4 to +5, and spectral type N. There is no evidence of a 5-day period, and the star is probably a typical irregular or long-period red variable.

The photographic magnitude was about 14·5, in agreement with Wolf's * observations. The photovisual magnitude varied from about 10 to 11 during three months but never reached the values (12 to 13·2) found by Parenago.† A remarkable feature is the change of colour index by about one magnitude in 10 days.

Photovisual and photographic magnitudes of 34 comparison stars have been measured, and are given for the benefit of other observers, together with a photograph of the region.

Larger instruments would be necessary to investigate the star more thoroughly.

Norman Lockyer Observatory,
Sidmouth:
1941 *June* 4.

* *A.N.*, 204, 429, 1917.

† *N.N.V.S.*, 41, 1933.

A PHOTOGRAPHIC SURVEY OF GALACTIC CLUSTERS: III. N.G.C. 103, 129, 133, 136, 146, 225, Anonymous $0^h\ 26^m.2$, $+62°\ 36'$

George Alter, D.Sc.

(Communicated by the Director, Norman Lockyer Observatory)

(Received 1941 July 5)

The method of this investigation was described in two earlier papers * (the second designated later on as A II). The photographs of this group of clusters were taken on a clear night with little haze and stars unusually steady. Order of exposures: NPS, cluster. The magnitude deviations of the NPS give a mean deviation of $\pm\ 0^m.02$ on the photographic scale and of $\pm\ 0^m.10$ on the photovisual scale. The mean error of the CI is therefore $\pm\ 0^m.10$. The reduction of cluster star magnitudes to the NPS-scale for extinction and fog effect is given by:

	p Plate	pv Plate
	m	m
Extinction coefficient	0·12	0·06
Fog effect	−0·09	−0·24
Reduction	0·03	−0·18

The cluster group lies within a very richly populated region of Cassiopeia (see also Ross Calvert's *Milky Way Atlas*, Plate 20, $4\frac{1}{2}$ in., right and below upper left corner), except N.G.C. 225 which is situated outside and in front of a dark patch. The position of the six clusters suggests that no absorption is present. The absence of absorption cannot, however, be proved at present because no spectral types of the cluster stars are available and no agreement of the observed CI with the true one can be established. The same is unfortunately true of N.G.C. 225 where an absorbing cloud is indicated by its position in a dark patch, and by the $(m - M)$ range which is larger than the CI suggests. (On this relation see A II, page 90.)

There was also another uncertainty which can now be cleared up. It is concerned with the identification and the co-ordinates of N.G.C. 133 and 146. (It may be mentioned that Shapley † gives in his catalogue, by mistake, the same galactic co-ordinates for the two clusters.) Collinder ‡ remarks in the notes to his cluster catalogue, *re* N.G.C. 146, that it forms a double cluster with N.G.C. 133, but that its co-ordinates seem to be erroneous in N.G.C.; that, however, to judge from d'Arrest's description, "the present object should be N.G.C. 146." This object is actually N.G.C. 146, but the error does not lie in its co-ordinates. These are correct and the error is based on a false identification of N.G.C. 133.

N.G.C. 146 was observed by John Herschel (No. 28 of his catalogue) and his description includes the presence of a double star which is identical with H 1033 = Burnham 281 = Aitken 460. (Burnham quotes "In a cluster of 8th class.") The cluster co-ordinates, given for 1860·0, correspond to its position and to the respective values for 1900·0, used by Collinder and Shapley.

N.G.C. 133 was first observed by d'Arrest, and his data were included by Dreyer in his supplementary catalogue to the G.C. under No. 5103. Now, d'Arrest also mentions

* *M.N.*, **100**, 387, 1940; *M.N.*, **101**, 89, 1941.
† *Star Clusters*, p. 228, 1930.
‡ *Lund Annals*, **2**, B23, 1931.

in his description a double star ("Stella duplex in cumulo dispersarum") which can be easily identified with Burnham 247 = Aitken 423 = B.D. 62° 93 because the co-ordinates of cluster and double star coincide perfectly.

Thus the co-ordinates both of N.G.C. 146 and 133 are found to be correct. What, however, Collinder is treating as N.G.C. 133 is not this cluster but the cluster, called in this paper Anonymous, which does not contain any known double star, and this may be the reason for his suspicion that the co-ordinates of N.G.C. 146 are false, assuming the co-ordinates of Anonymous to be those of N.G.C. 133. The reason for the mistake in identification, shared apparently by Shapley (according to the data on star number and diameter), may be found in the fact that N.G.C. 133 does not seem to be a cluster at all, as will be seen later, but only an accidental grouping of a few bright stars, while Anonymous appears on visual comparison as a cluster very similar to its neighbour N.G.C. 146. It is rather surprising that it has not been found worth mentioning by Herschel and d'Arrest, although the latter noticed in his remark "huic haud dissimiles non adeo rari in eis partibus." The situation is obvious when we inspect the Franklin-Adams charts. The clusters can be found on plate 182 around the cross point of the lines 6/32. The three clusters correspond to the three corners of a small triangle: N.G.C. 133 lies in the right upper corner, N.G.C. 146 in the left upper corner and Anonymous on line 32 just below the cross point.

The distances in the present paper are in general smaller than those found by earlier investigations. This may be fully explained by the fact that the latter were determined by mere inspection of photographs, without knowledge of spectral types or CI, but with various assumptions as to cluster diameters and magnitudes. A more detailed explanation is given in the case of the Anonymous cluster.

The differences in the measured distances found in the previous papers of this series were smaller because the stars in these clusters were of earlier type and agreed more closely with the above-mentioned assumptions on magnitude.

N.G.C. 103

R.A. = $0^h\ 19^m.8$, Dec. = $+60°\ 47'$ (1900·0)

This cluster is mentioned in the catalogues of Shapley, Trumpler * and Collinder, who remarks that he could not identify it on the Franklin-Adams charts and quotes a note of Lundmark's (Franklin-Adams plates): "Somewhat dubious object." The cluster can, however, be found on the charts: its position is 9 mm. right of line 32 and 1 mm. above line 8, on plate 182.

The star counting gave 65 stars as the total number within the region. The distribution of stars within the cluster region and its surroundings results in a background density of 4800 stars per square degree and 33 cluster stars within a cluster region of $5'.5$ diameter. Fig. 1 (p. 300) gives the diagram of the star density per square degree within the cluster region and its surroundings.

Table I gives the distribution of $m - M$. The mean distance modulus of the cluster group is 10·878 corresponding to

$$r = 1500 \pm 70 \text{ parsecs}, \qquad d = 5'.5 = 2.4 \text{ parsecs}.$$

The results of the previous investigations were:

	Distance Parsecs	Diameter	
		′	Parsecs
Shapley	2400–3800	13	14·4
Trumpler	2580	4	2·9
Collinder	4800	5 × 4	6·2

* *L.O.B.*, 14, 170, 1930.

The diameter given by Shapley is certainly a mistake because the number of stars, mentioned to be 35, is far too small to account for even the brighter stars alone within 13′ diameter.

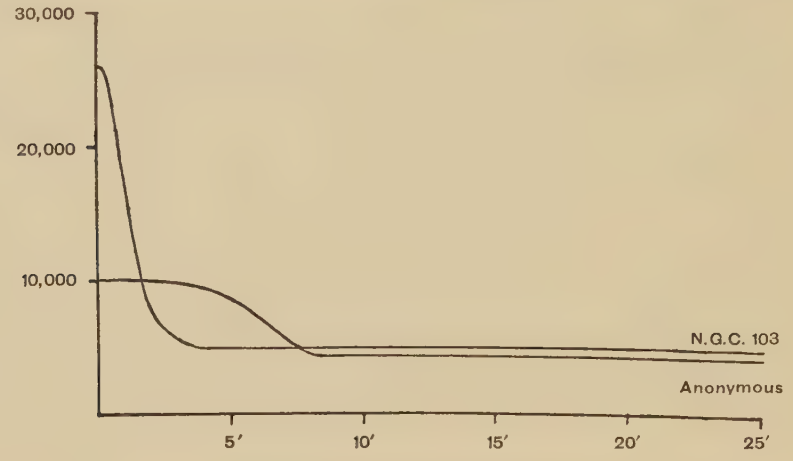

FIG. 1.—*Star density per square degree.*

TABLE I

Co-ordinates, Magnitudes and Distance Moduli of 33 Stars (N.G.C. 103)

Zero point = H.D. 190030 = B.D. 60° 47, unit = 1′·0, X = east, Y = south
Co-ordinates of the assumed cluster centre $X = +8{\cdot}5$, $Y = +11{\cdot}3$

Star	X	Y	m_p	m_{pv}	$m-M$	Star	X	Y	m_p	m_{pv}	$m-M$
36	+ 8·5	+10·7	13·72	12·27	4·7	64	+10·7	+12·9	13·21	12·99	11·1
51	9·3	10·5	12·13	11·05	4·8	15	7·1	11·3	12·70	12·64	11·3
50	9·1	11·6	14·10	12·99	6·6	30	8·3	12·4	12·25	12·29	11·3
65	10·7	12·5	12·14	11·47	6·8	10	6·8	9·0	12·89	12·85	11·6
26	8·0	13·0	13·17	12·43	7·5	20	7·6	13·9	13·55	13·37	11·6
19	7·6	8·8	12·21	11·80	8·7	8	6·7	11·9	13·18	13·09	11·7
60	10·2	11·8	12·79	12·36	9·1	40	8·6	11·7	13·21	13·09	11·7
24	8·0	10·0	12·94	12·52	9·3	29	8·2	11·1	13·48	13·37	12·0
41	8·6	11·2	11·79	11·53	9·3	53	9·6	11·9	14·39	14·14	12·0
47	9·0	9·0	13·21	12·75	9·3	14	7·2	9·1	13·48	13·43	12·1
32	8·4	12·0	13·51	13·05	9·6	5	6·4	9·5	13·43	13·43	12·2
46	8·9	11·4	13·25	12·84	9·7	9	6·8	12·2	13·48	13·46	12·3
56	9·8	10·7	11·48	11·36	10·0	63	10·5	11·8	13·79	13·80	12·7
59	10·1	9·0	12·45	12·21	10·2	23	8·0	12·5	13·84	13·94	13·6
21	7·6	13·2	11·76	11·75	10·6	33	8·3	11·0	12·74	12·98	14·7
48	9·0	11·0	12·21	12·13	10·7	25	+8·0	+12·2	13·69	13·95	16·0
17	+ 7·3	+10·9	12·21	12·13	10·8						

The number of cluster stars, after correction for the background stars, is 33, by chance exactly the same number as that got statistically. The magnitude distribution is given in the following table:—

m_{pv}	12	13	> 13·5
Number of stars	8	13	12

N.G.C. 129

R.A. = $0^h\ 24^m{\cdot}3$, Dec. = +59° 40′ (1900·0)

This cluster is mentioned in the catalogues of Shapley, Trumpler and Collinder.

The star counting gave 52 stars as the total number within the region. The distribution of stars within the cluster region and its surroundings results in a background density of 3531 stars per square degree, and in 29 cluster stars within a cluster region of 5′·5 diameter. The star counting in the southern part of the surroundings was restricted to a little narrower area than usual because farther out there seems to be a suspicion of some absorbing matter; the whole area used for star counting is in any case large enough to permit this restriction: It usually exceeds the cluster region 10 to 30 times.

TABLE II

Co-ordinates, Magnitudes and Distance Moduli of 26 Stars (N.G.C. 129)

Zero point = H.D. 260026, unit = 1′·0, X = west, Y = north
Co-ordinates of the assumed cluster centre $X = +1{\cdot}2$, $Y = +13{\cdot}2$

Star	X	Y	m_p	m_{pv}	$m-M$	Star	X	Y	m_p	m_{pv}	$m-M$
7	+2·9	+14·2	9·74	8·88	3·8	39	−0·1	+11·0	14·40	13·85	9·8
31	+0·1	+12·6	9·55	9·01	5·0	45	−0·5	+12·7	12·68	12·36	9·8
13	+1·9	+10·6	9·42	9·00	5·8	4	+3·5	+14·0	11·89	11·69	9·9
43	−0·4	+11·7	11·30	10·59	5·8	5	+3·4	+12·0	12·99	12·69	10·3
8	+2·8	+10·9	11·90	11·09	6·1	17	+1·5	+12·6	12·81	12·56	10·5
14	+1·7	+13·7	11·26	10·66	6·3	27	+0·3	+11·2	14·23	13·86	11·0
6	+3·2	+12·7	12·56	11·84	7·0	50	−1·2	+12·5	13·14	13·16	11·1
1	+4·1	+13·7	13·08	12·22	7·1	15	+1·6	+11·7	12·25	12·26	11·2
24	+0·8	+10·4	11·90	11·35	7·2	10	+2·6	+12·9	13·99	13·70	11·4
46	−0·6	+13·8	13·76	13·13	8·5	48	−0·7	+13·0	13·30	13·15	11·6
49	−0·9	+15·0	11·40	11·15	8·9	3	+3·6	+12·3	13·32	13·27	12·0
40	−0·2	+15·2	13·09	12·69	9·6	21	+0·9	+15·4	13·37	13·49	13·4
42	−0·4	+13·8	12·29	11·99	9·6	11	+2·3	+15·0	13·70	13·80	13·5

Table II gives the distribution of $m-M$. The mean distance modulus of the cluster group is 10·347 corresponding to

$$r = 1170 \pm 60 \text{ parsecs}, \qquad d = 5'{\cdot}5 = 1{\cdot}9 \text{ parsecs}.$$

The results of the previous investigations were:

	Distance Parsecs	Diameter	
		′	Parsecs
Shapley	1260–2000	11	6·4
Trumpler	2090	13	8·0
Collinder	2900	10	8·4

The difference in the diameter between the present and the previous results was investigated by measuring 24 more stars within twice the cluster diameter and it was found that only 4 of them belong to the $(m-M)$ range of the cluster group. This does not exceed the number of background stars within this $(m-M)$ range and the same area so that the stars cannot be considered as cluster stars. The larger diameter in the previous papers is perhaps caused by the "chains going outwards from the centre," mentioned by Collinder, an accidental grouping of some brighter stars.

The number of cluster stars, after correction for the background stars, is 26 against

29 got statistically, the dispersion is $\sigma = \pm 5$. The magnitude distribution is given in the following table:—

m_{pv}	11	12	13	> 13·5
Number of stars	1	4	5	16

N.G.C. 133

R.A. = $0^h\ 25^m{\cdot}5$, Dec. = $+62°\ 48'$ (1900·0)

This object is mentioned in the catalogues of Shapley and Collinder (by mistake, as mentioned above). As a matter of fact, it is conspicuous only by 5 bright stars situated pretty close, so that there may be an impression of clustering, given a suitable optical equipment; but a photographic exposure does not show any condensation of stars besides these 5 bright stars. It was therefore not necessary to investigate the distribution of star density in the region and its surroundings. This view was supported by the results of the $(m - M)$ distribution (given in Table III) of the 5 bright stars plus 8 additional

TABLE III

Co-ordinates, Magnitudes and Distance Moduli of 13 Stars (N.G.C. 133)

Zero point = B.D. 62° 105, unit = 1′·0, X = west, Y = north

Star	X	Y	m_p	m_{pv}	$m - M$	Star	X	Y	m_p	m_{pv}	$m - M$
6 *	+17·8	+15·3	10·71	9·73	4·1	1	+19·6	+16·2	12·70	12·10	7·7
8	17·6	13·4	10·31	9·50	4·4	5	18·3	16·0	9·70	9·53	7·9
9	17·4	14·6	10·20	9·47	4·7	2	19·1	15·5	13·38	12·74	8·2
10	17·2	12·4	12·84	11·69	5·1	15	15·8	13·0	13·92	13·17	8·3
16	15·5	14·2	11·60	10·68	5·4	3	18·6	15·2	14·50	13·70	8·7
11	17·2	15·2	13·09	12·32	7·3	12	17·0	14·0	13·09	12·59	8·9
14	+16·4	+14·9	14·08	13·13	7·6						

* = B.D. 62° 93 = β107 = Burnham 247 = Aitken 423.

stars in their region. The table shows that 4 of the bright stars are at an average distance of about 100 parsecs, while almost all fainter stars are distributed between 300 and 600 parsecs. It may, however, be noticed that the data of star 6 may be falsified by the fact that it is a double star which the Mond astrograph is unable to separate. Thus the recorded magnitudes of this double star are due to the sum of the star intensities, and the CI and consequently the distance modulus may change the given values.

Burnham and Aitken give the positions of the bright stars relatively to the double star. It was possible in the present investigation to re-measure the respective distances with the help of the micrometer, but a determination of the position angles was not possible, no suitable device being available. The mean error of the distance determination is $\pm$ 0″·15. The following table gives the respective values and the resulting relative motion. (A = star 6, C = 5, D = 9, E = 8, F = 16.)

Date	A–C (336°)	A–D (147°)	A–E (171°)	A–F (115°)
	″	″	″	″
1898·7	46·95	50·27	113·78	150·44
1899·8	46·83	50·30	113·48	150·32
1900·7	46·78	50·32	113·55	100·49
1902·9	46·70	...	...	...
1917·8	...	...	...	151·96
1940·9	45·52	52·95	114·94	154·25
1940–1898	−1·43	+2·68	+1·16	+3·81

The difference in sign between the motion *A–C* and the other three motions (which take place, in the average, in the opposite position angle) suggests the possibility of a proper motion of *A* in the direction of *C*. *C* is situated on the side of *A* nearly opposite to *D*, *E* and *F*, and a motion of *A* towards *C* decreases their distance but increases the three others, as the signs indicate. A yearly motion of *A* of 0″·03 towards *C* would give apparent yearly motions of about 0″·03 for *D* and about 0″·06 for *F*, both in the opposite direction.

N.G.C. 136

R.A. = $0^h\ 25^m.9$, Dec. = +60° 58′ (1900·0)

This cluster is mentioned in Trumpler's and Collinder's catalogues. It is described in N.G.C. as a small and extremely concentrated globular cluster, but Trumpler finds from a Crossley plate that it is a small loose open cluster of 40 to 50 stars, 13^m to 18^m. The Sidmouth photograph shows a well detached and concentrated small group of 11 stars. The concentration of the star images on the photographic and photovisual plates C and B makes it almost impossible to determine the image diameters and consequently the CI and distance moduli. It was, however, possible to use the HSP-plate A, taken with the largest of the Mond telescopes, for the measurements of diameters on the photovisual scale. Since there was no NPS on this plate this had to be done by the use of the stars of the neighbouring N.G.C. 103 which yielded the reference scale, because the magnitudes of these stars had been found in the normal way. The results are given in Table IV.

TABLE IV

Co-ordinates and Photovisual Magnitudes of 11 *Stars* (*N.G.C.* 136)

Zero point = B.D. 60° 63, unit = 1′·0, *X* = east, *Y* = north

Co-ordinates of the assumed cluster centre *X* = +4·0, *Y* = +4·3

Star	*X*	*Y*	m_{pv}	Star	*X*	*Y*	m_{pv}
1	+3·6	+4·3	13·2	7	+4·1	+4·1	13·8
2	3·6	4·1	13·6	8	4·1	4·8	13·2
3	3·7	4·0	13·9	9	4·2	3·9	14·0
4	3·7	5·0	14·3	10	4·3	4·1	14·0
5	3·9	4·6	13·4	11	4·3	4·3	13·6
6	+4·0	+4·3	13·5				

The angular cluster diameter is 1′·2. The results of the previous investigations were :

	Distance Parsecs	Diameter	
		′	Parsecs
Trumpler	5320	2·2	3·4
Collinder	8300	2·0	4·8

(Collinder quotes in his Remarks, page B 24, Trumpler's classification by mistake as II 1 *r*: it is instead II 2 *p*.)

Anonymous

R.A. = $0^h\ 26^m.2$, Dec. = +62° 36′ (1900·0)

This cluster is mentioned (by mistake under N.G.C. 133, as mentioned above) in the catalogues of Shapley and Collinder.

The star counting gave 101 stars as the total number within the region. The distribution of stars within the cluster region and its surroundings results in a background density of 4015 stars per square degree and 54 cluster stars within a cluster region of

7′·3 diameter. Fig. 1 gives the diagram of the star density per square degree within the cluster region and its surroundings.

TABLE V

Co-ordinates, Magnitudes and Distance Moduli of 41 Stars (Anonymous)

Zero point = B.D. 62° 105, unit = 1′·0, X = west, Y = north
Co-ordinates of the assumed cluster centre $X = +13·1$, $Y = +1·7$

Star	X	Y	m_p	m_{pv}	$m-M$	Star	X	Y	m_p	m_{pv}	$m-M$
27	+14·5	+3·5	13·63	12·26	4·9	53	+13·5	+1·5	13·90	13·24	8·5
94	+10·5	−0·6	11·20	10·30	5·0	76	+12·0	−0·6	14·36	13·60	8·6
41	+14·0	+3·3	13·39	12·24	5·6	16	+15·8	+0·2	12·91	12·41	8·7
98	+10·3	+0·3	11·76	11·00	6·0	72	+12·3	−1·1	13·02	12·51	8·7
74	+12·1	+1·2	10·62	10·09	6·1	24	+15·0	+2·3	11·29	11·05	9·1
85	+11·4	+4·8	10·97	10·44	6·5	55	+13·4	+1·8	14·60	13·91	9·1
81	+11·7	+2·8	11·26	10·70	6·6	100	+10·1	+2·3	12·55	12·16	9·2
15	+15·8	+2·4	12·25	11·54	6·7	63	+12·7	−0·7	14·03	13·46	9·3
87	+11·3	+2·8	12·25	11·54	6·7	46	+13·8	+1·3	11·19	11·04	9·5
42	+14·0	+3·1	13·62	12·63	6·9	101	+10·0	+2·6	13·10	12·72	9·8
34	+14·2	+2·9	12·70	11·97	7·1	6	+16·4	+2·2	14·50	13·98	10·2
68	+12·5	+2·3	12·98	12·14	7·1	23	+15·1	+3·7	12·41	12·17	10·2
9	+16·0	0·0	13·52	12·59	7·2	26	+14·7	+0·8	14·50	13·98	10·2
10	+16·0	+2·6	12·91	12·20	7·4	49	+13·7	+4·7	13·21	12·92	10·6
69	+12·5	−0·4	13·50	12·65	7·5	11	+16·0	+3·0	14·14	13·79	11·1
51	+13·6	−0·1	13·50	12·68	7·6	62	+12·7	−1·1	13·59	13·48	12·1
36	+14·2	+0·7	13·60	12·81	7·8	20	+15·3	+3·1	13·44	13·40	12·2
50	+13·6	−0·6	13·71	12·90	7·8	84	+11·5	+3·5	11·18	11·38	12·5
60	+12·7	+2·1	12·91	12·30	7·8	82	+11·6	−1·1	13·99	13·97	12·8
4	+16·6	+2·6	14·60	13·62	8·0	93	+10·6	+1·1	13·57	13·64	13·0
25	+15·0	+0·2	13·30	12·71	8·4						

Table V gives the distribution of $m-M$. The mean distance modulus of the cluster group is 7·872 corresponding to

$$r = 375 \pm 20 \text{ parsecs}, \qquad d = 7'·3 = 0·8 \text{ parsec.}$$

The results of the previous investigations were:—

	Distance Parsecs	Diameter	
		′	Parsecs
Shapley	1740–2750	7	5·6
Collinder	2830	8 × 5	5·5

The difference between the distances in the present investigation and the previous ones may be due to the spectral classification of the cluster. Collinder supposed the cluster to be of the Pleiades type, *i.e.* consisting of B-type stars, while the table above indicates instead, by the average CI of about $+0^m·60$, the Hyades type. The spectral classification, together with the apparent magnitudes, affects the deduced values of distances. The difference in absolute magnitude between a CI of $+0^m·60$ ($M = 4·4$) and $-0^m·10$ ($M = 0·3$) is $4^m·1$. About the same difference appears for Shapley, whose distances are determined with $M = +0·5$ or $M = -0·5$ respectively. If M were decreased by $4^m·1$ in the present paper, the average $m-M$ of this cluster would be increased to 11·972, corresponding to a distance of about 2500 parsecs. This explains entirely the difference in the distances.

The number of cluster stars, after correction for the background stars, is 47 against 54 got statistically; the dispersion $\sigma = \pm 7$. The magnitude distribution is given in the following table:—

m_{pv}	10	11	12	13	> 13·5
Number of stars	1	2	7	10	27

N.G.C. 146

R.A. = $0^h\ 27^m{\cdot}5$, Dec. = $+62°\ 44'$ (1900·0)

This cluster is mentioned in the catalogues of Shapley and Collinder.

The star counting gave 62 stars as the total number within the region. The distribution of stars within the cluster region and its surroundings results in a background density of 3992 stars per square degree, and in 19 cluster stars within a cluster region of $7'{\cdot}0$ diameter.

TABLE VI

Co-ordinates, Magnitudes and Distance Moduli of 34 Stars (N.G.C. 146)

Zero point = B.D. 62° 105, unit = $1'{\cdot}0$, X = west, Y = north

Co-ordinates of the assumed cluster centre $X = +6{\cdot}3$, $Y = +11{\cdot}0$

Star	X	Y	m_p	m_{pv}	$m-M$	Star	X	Y	m_p	m_{pv}	$m-M$
4	+9·0	+12·8	12·30	11·32	5·7	46	+5·1	+11·7	12·86	12·55	10·1
36	5·8	9·1	13·11	12·14	6·5	50	4·5	11·0	12·82	12·52	10·1
8	8·1	13·2	13·67	12·63	6·6	33	5·8	14·2	14·09	13·66	10·4
2	9·2	12·4	13·16	12·26	7·0	20	6·9	11·4	13·42	13·10	10·5
52	4·3	9·1	13·19	12·36	7·3	18	7·1	12·4	14·40	13·98	10·8
6	8·4	11·7	14·05	13·30	8·4	28	6·0	13·2	13·29	13·08	11·2
7	8·4	8·6	9·67	9·64	8·4	61	3·2	12·3	11·29	11·40	11·2
17	7·4	12·0	12·91	12·37	8·4	53	4·2	8·8	13·21	13·05	11·5
25	6·3	14·0	14·16	13·41	8·5	44	5·1	10·1	13·89	13·68	11·8
10	8·0	10·6	11·64	11·30	8·6	15	7·7	7·8	13·57	13·49	12·1
24	6·4	9·4	13·49	12·93	8·8	54	4·1	10·0	12·78	12·86	12·4
11	7·8	11·3	14·65	13·94	9·1	55	4·1	11·1	12·97	13·04	12·4
12	7·8	8·4	14·29	13·66	9·4	51	4·4	12·5	14·09	13·95	12·5
19	7·0	9·8	13·37	12·94	9·6	38	5·6	11·7	13·94	14·01	13·0
59	3·5	12·8	11·21	11·13	9·8	56	4·1	12·0	12·86	13·01	13·3
27	6·0	11·2	11·54	11·40	9·9	57	3·8	9·2	13·14	13·38	15·1
23	+6·5	+10·8	11·18	11·16	10·0	42	+5·4	+10·7	13·76	14·02	16·0

Table VI gives the distribution of $m-M$. It does not contain the double star mentioned above (star 48 = H 1033, co-ordinates $X = +4{\cdot}6$, $Y = +10{\cdot}3$) because the lenses could not separate the two stars and thus no CI and $m-M$ was available. The mean distance modulus of the cluster group is 9·375 corresponding to

$$r = 750 \pm 35 \text{ parsecs}, \qquad d = 7'{\cdot}0 = 1{\cdot}5 \text{ parsecs}.$$

The results of the previous investigations were:

	Distance Parsecs	Diameter ′	Diameter Parsecs
Shapley	910–1450	6	2·5
Collinder	3160	6	5·5

The number of cluster stars, after correction for the background stars, is 20 against 19

got statistically; the dispersion is $\sigma = \pm 4$. The magnitude distribution is given in the following table:—

m_{pv}	11	12	13	> 13·5
Number of stars	3	2	5	10

N.G.C. 225

R.A. = $0^h\ 37^m.6$, Dec. = $+61°\ 14'$ (1900·0)

This cluster is mentioned in the catalogues of Trumpler and Collinder, and was investigated by Lee.*

The cluster lies within a small patch of dark background almost empty of stars. This patch is not large enough to permit the usual method of establishing the background density for the statistical determination of the number of cluster stars; it is not even large enough to find an area of cluster size outside the cluster region to use this method in a restricted way. The shape of the dark area is quite irregular and some dark bands extend into the rich surrounding region. So it appears as if the cluster is connected by one or two narrow tongues of normal star density with the surroundings.

The star counting resulted in 44 as the total star number within a region of 12′·5 diameter. The scarcity of stars in the dark region and the unusually small relative number of faint stars in the cluster group make it very probable that the obscuring cloud is pretty near and that its absorption coefficients are fairly large. The question of the position of the cluster with regard to the cloud, *i.e.* if it is in front of, within, or behind the cloud, and of its distance, can be answered only by the knowledge either of the spectral types and the total absorption (formula (2) in a recent paper †), or of the CI, the CE and

Table VII

Co-ordinates, Magnitudes and Distance Moduli of 36 Stars (N.G.C. 225)

Zero point = star 41 = B.D. 61° 163, unit = 1′·0, X = west, Y = south
Co-ordinates of the assumed cluster centre $X = +5·0$, $Y = +3·3$
L = Lee's star number

Star	L	X	Y	m_p	m_{pv}	$m-M$	Star	L	X	Y	m_p	m_{pv}	$m-M$
13	35	+ 6·8	+3·0	11·38	10·19	3·4	27	...	+ 3·7	+6·1	13·67	13·02	8·4
5	29	+ 9·7	+3·6	10·51	9·64	4·4	2	...	+11·0	+0·9	14·60	13·72	8·5
31	...	+ 3·3	+3·4	13·36	12·00	4·6	41	43	0·0	0·0	9·12	9·19	8·6
24	33	+ 5·6	+4·7	10·43	9·71	4·9	22	31	+ 5·8	+8·6	11·00	10·77	8·8
25	...	+ 5·5	+6·0	12·83	11·74	5·4	39	41	+ 1·1	+2·0	9·15	9·24	8·8
33	40	+ 3·0	−1·9	12·45	11·41	5·4	37	...	+ 2·5	+8·0	14·17	13·52	8·9
34	...	+ 3·0	+8·7	12·91	11·83	5·6	23	34	+ 5·7	+3·6	11·93	11·60	9·0
20	37	+ 6·0	−1·1	10·62	10·12	6·4	4	...	+ 9·8	+4·8	14·50	13·91	9·5
7	30	+ 8·7	+3·0	10·11	9·69	6·5	11	...	+ 7·1	+0·3	13·90	13·37	9·8
26	38	+ 4·4	−0·2	10·69	10·22	6·8	9‡	28	+ 8·6	+1·1	10·67	10·68	9·9
43	...	− 0·6	−2·2	12·82	12·00	6·9	40	42	+ 0·1	+3·6	9·80	9·94	10·1
3	25	+10·7	+2·0	10·01	9·69	7·1	35	...	+ 2·7	+8·7	13·97	13·53	10·2
32	...	+ 3·2	+6·6	13·00	12·15	7·1	44	...	− 1·0	+4·1	13·49	13·11	10·2
21	36	+ 5·8	+1·8	10·93	10·48	7·3	1	...	+11·1	+2·9	13·70	13·35	10·6
12	32	+ 7·1	+5·4	10·99	10·57	7·4	38	...	+ 1·7	+2·4	13·17	13·05	11·7
36	...	+ 2·5	−0·9	13·06	12·30	7·4	42	...	0·0	+4·5	13·10	13·06	11·9
6	26	+ 9·0	+0·3	11·26	10·83	7·5	17	...	+ 6·4	+3·7	13·83	13·94	13·7
28	39	+ 3·5	−2·1	11·19	10·80	7·8	15	...	+ 6·6	+6·1	13·26	13·72	17·8

* *M.N.*, **86**, 645, 1926. † *M.N.*, **101**, 84, 1941.
‡ = H1046 = Burnham 378 (= *A*, 10 = *B*, 6 = *C*); not registered by Aitken.

the total absorption (formula (5) in the same paper). There are no spectral types available for the cluster stars, but Table VII yields some indication of the presence of absorption. It gives the distribution of $m - M$, and the mean distance modulus is 8·38. The range of the distance moduli is, however, 4·2, and this is not what should be expected for a star group with an average CI of $+0^m.42$ and a mean error of CI of $\pm 0^m.10$. Stars of this true CI would yield a range of about 2·0 to 2·5, and the range of 4·2 corresponds to that of B stars (as shown more in detail in A II). Thus the irregularity in the range indicates that the stars are reddened and if we assume it to be entirely the result of absorption, a CE of about $0^m.50$ would represent the shift between the observed CI and that of B stars. This CE corresponds, on the proper place of the $M - CI$ curve, to an M-change of $2^m.6$, and the average distance modulus of 8·38 will increase by this amount to 10·98. To find the true distance we have also to assume a value of the total absorption. We adopt here $a_{pv} = 0^m.35$, the same value as in A II, for the same reasons. Thus our assumptions on CE and a_{pv}, together with the observed CI, give a probable answer to the distance question; we have to plot the distance on the curve, mentioned in A II, with the corrected $m - M$. A comparison of the results is given below:

	Distance Parsecs	Diameter	
		′	Parsecs
No absorption	475 ± 20	12·5	1·7
Absorption	1275 ± 50	12·5	4·7

The results of the previous investigations were:

Trumpler	1100	14	4·5
Collinder	524	15 × 10	1·9

The question of the position with regard to the obscuring cloud is, under the above assumptions, partially answered. The final decision whether the cluster lies within or behind cannot be given because there are not enough stars available within the cloud to investigate the behaviour of their distance moduli.

The number of cluster stars, after correction for background stars, is 17. The magnitude distribution is given in the following table (without and with absorption):—

m_{pv}	9	10	11	12	13	14
Number of stars	2	4	3	2	3	3
	2	5	6	4	...	...

Lee's investigation on proper motions is extended over a larger area than the cluster region of this paper, but it does not cover the region of "the whole cluster," supposed by Lee to be a pear-shaped structure of about 44′ length and a maximum width of 36′. It is, further, restricted to the brighter stars scattered along the contour of this pear-shaped figure, except in the real cluster region. Even if an extension of his investigation of proper motions to the remaining part of the larger group should yield the final part of the average proper motions in the direction north-south, thus completing the peculiar appearance of an elliptical movement of this star group, it seems difficult to construct a dynamical explanation of these motions in a comparatively small star group of brighter stars. Besides, N.G.C. 225, situated in the east end of the supposed larger structure, does not show any average motion at all. The cluster is represented by the central dense group of Lee's graph and includes besides the stars of the fourth group (except 19 and 21) enumerated on the following page of Lee's paper, the nearby stars 31 and 32 of group 1. The motion of these two stars nearly cancels the very small average motion of this group. Thus the proper motion is a further proof of the cluster quality of N.G.C. 225.

Nevertheless, an attempt was made to find out if Lee's stars outside the cluster region do or do not belong to the cluster group. Besides these 34 stars 10 fainter stars were included, and the resulting 44 stars were treated as the cluster stars. But on neither

assumption (obscured or not obscured cluster) does the number of stars within the respective $(m - M)$ range exceed the number of background stars. It can therefore be assumed that Lee's stars outside the proper cluster region are not physically connected with the cluster itself.

Summary

The cluster investigation of the present paper deals with 7 further clusters situated, with one exception, in a rich Cassiopeia region, the exception being N.G.C. 225, where an absorbing cloud is indicated not only by a dark background but by an irregularity in the range of distance moduli.

An uncertainty in the identification and co-ordinates of two clusters is explained and it is shown that N.G.C. 133 does not seem to be a cluster at all, while the data given for it by previous investigations correspond to a cluster not named up to date and designated here as Anonymous; its co-ordinates are given.

Tables showing co-ordinates, photographic and photovisual magnitudes of all measurable stars within the above cluster regions have been prepared, but owing to shortage of paper it is regretted that these cannot be printed. Copies can be supplied on request to those specially interested.

Norman Lockyer Observatory,
Sidmouth:
1941 *June* 23.

OBSERVATIONS OF OCCULTATIONS AT SYDNEY OBSERVATORY DURING 1940

(Received 1941 June 10)

The following observations of occultations were made and reduced in duplicate by H. W. Wood (H. W.) and E. E. Adderley (E. A.). The observations were made with a six-inch equatorial telescope, using a tapping key to record the times on a chronograph, no correction for personal effect being allowed in reading off. The reductions were made by Comrie's method (Supplement to the *Nautical Almanac*, 1938), $0^h.00076$ being added to the time.

The observational material is given in Table I, and the results of the reductions in Table II. In each case the phase observed was disappearance at the dark limb. The lunation number and occultation number were taken from the *Nautical Almanac*.

TABLE I

No.	Date	Star	Mag.	U.T.	Observer
				h m s	
62	Jan. 22	B.D. +19° 1110	6·0	10 07 51·2	E. A.
430	June 11	B.D. +9° 2262	5·9	8 41 47·0	E. A.
448	June 14	B.D. −3° 3329	7·0	7 45 25·5	E. A.
491	July 8	*o* Leonis	3·8	8 51 33·2	H. W.
586	Aug. 11	49 Libræ	5·5	10 53 58·6	H. W.
608	Aug. 14	B.D. −17° 5310	7·1	8 21 16·8	H. W.
615	Aug. 15	54 Sgtr	5·4	9 18 52·4	H. W.
616	Aug. 15	55 Sgtr	5·1	10 19 24·8	H. W.
651	Sept. 6	B.D. −12° 4134	6·4	11 20 17·4	H. W.
655	Sept. 7	η Libræ	5·6	10 31 12·2	H. W.
665	Sept. 9	B.D. −17° 4903	7·5	13 26 23·5	H. W.
757	Oct. 6	B.D. −17° 4773	6·0	9 56 38·5	H. W.
866	Nov. 4	B.D. −17° 5347	6·8	9 01 59·9	H. W.

TABLE II

No.	Lunation	p	q	p^2	pq	q^2	$\Delta\sigma$	$p\Delta\sigma$	$q\Delta\sigma$	Coefficient of $\Delta\alpha$	Coefficient of $\Delta\delta$
62	211	+ 84	+55	70	+46	30	−1·4	−1·2	−0·8	+11·9	+0·53
430	216	+ 99	+14	98	+14	2	+0·3	+0·3	0·0	+14·6	−0·15
448	216	+100	− 9	99	− 9	1	+0·5	+0·5	0·0	+13·8	−0·39
491	217	+ 76	−65	58	−49	42	+2·2	+1·7	−1·4	+ 8·2	−0·84
586	218	+ 96	−28	92	−27	8	+0·8	+0·8	−0·2	+13·2	−0·41
608	218	+ 95	+31	90	+29	10	−1·5	−1·4	−0·5	+13·2	+0·38
615	218	+ 57	−82	32	−47	68	−0·3	−0·2	+0·2	+ 9·8	−0·73
616	218	+ 91	−41	83	−37	17	−0·4	−0·4	+0·2	+13·8	−0·28
651	219	+ 89	+46	79	+41	21	−2·5	−2·2	−1·2	+14·1	+0·26
655	219	+100	− 8	99	− 8	1	+0·2	+0·2	0·0	+14·1	−0·24
665	219	+ 78	+62	61	+49	39	−2·6	−2·0	−1·6	+11·2	+0·62
757	220	+ 96	+27	93	+26	7	−1·2	−1·2	−0·3	+13·9	+0·23
866	221	+ 88	+47	78	+41	22	−2·7	−2·4	−1·3	+12·0	+0·54